Towards Conformal Antennas

for miniaturized Autarchic Distributed Systems

Eingereicht durch

Dipl.-Ing.

Nchewah Angwafo

Von der
Fakultät IV - Elektrotechnik und Informatik -
der Technischen Universität Berlin

Zur Erlangung des akademischen Grades

Doktor der Ingenieurwissenschaften

Dr.-Ing.

genehmigte Dissertation

Berlin 2006
D 83

Towards Conformal Antennas

for miniaturized Autarchic Distributed Systems

Eingereicht durch

Dipl.-Ing.

Nchewah Angwafo

Von der
Fakultät IV - Elektrotechnik und Informatik -
der Technischen Universität Berlin

Zur Erlangung des akademischen Grades

Doktor der Ingenieurwissenschaften

Dr.-Ing.

genehmigte Dissertation

Promotionsausschuß:

Vorsitzender:	Prof. Dr.-Ing. Herbert Reichl	Technische Universität Berlin
Gutachter:	Prof. Dr.-Ing. Gerhard Mönich	Technische Universität Berlin
	Prof. Dr.-Ing. Friedrich Landstorfer	Universität Stuttgart

Tag der wissenschaftlichen Aussprache: Freitag, den 2. Juni 2006

Berlin 2006
D 83

Alumbe a bonghe la nu nging tschi.
Mafo Angwafo III

Je n'ai fait celle-ci plus longue que parceque je n'ai pas eu le loisir de la faire plus courte.
Blaise Pascal dans 'Lettres Provinciales'

Acknowledgements

MY GOOD FORTUNE it has been to meet many people who have given me more of their time, companionship, assistance, and above all patience than I could possibly justify.

I would like to express profound gratitude to,

Herr Prof. Mönich

from whom I received more scientific support and invaluable advice than a graduate student can customarily expect. His unique brand of enthusiasm extended my Einsteinufer experience well beyond the confines of electromagnetic field theory.

Herr Prof. Landstorfer

for delivering that initial spark that lit the world of RF Technology for me. His co-supervision of this effort confers on me the singular distinction of being a *Meinkeenkel* in two respects.

Herr Prof. Reichl

whose brainchild the AVM Project is for his chairmanship of the committee.

A list featuring, alas, far too many names to mention separately is that of all the co-workers and members of staff, teachers and mates with whom I have interacted from my days of infancy. My gratitude goes out to my colleagues and ex-colleagues at the Institut für Hochfrequenz- und Halbleiter-Systemtechnologien especially Dipl.-Ing. Sherko Zinal.

My appreciation goes as well to the German Federal Ministry of Education and Research (BMBF) which supported the work reported herein through grant 16SV1658. I'd also like to mention the entire AVM consortium. The project is now over but memories of some stimulating and exciting sessions remain a lasting treasure — special mention to Julian Haberland, Herr Schulz and Björn Döring.

I would like to *transmit* a big packet of thanks to be *received* by all my family and friends[1] for their unflinching support and encouragement on all fronts. I can no other answer make, but, thanks, and thanks.

♔ *Nchewah Angwafo* ♔

Berlin, June 2006

[1] here and in the hereafter, known and unknown

Contents

Nomenclature

Symbol	Quantity	Unit
A_e	effective aperture of antenna	m^2
A_{em}	maximum effective aperture of antenna	m^2
α	attenuation constant	dB m^{-1}
B	magnetic flux density	Tesla (Wb m^{-2})
β	phase constant	rad m^{-1}
c	velocity of light *in vacuo* $\frac{1}{\sqrt{\mu_0 \epsilon_0}} \approx 2.998$ x 10^8	ms^{-1}
D	Dielectric Displacement	C m^{-2}
d	array inter-element spacing	m
dB	decibel, $10\log_{10} \cdot$(power ratio)	
D	directivity of antenna	dB
χ_0	skin depth	m
E	electric field intensity	V m^{-1}
ϵ_r	relative permittivity constant of medium	
ϵ_0	permittivity of free space $\approx \frac{1}{36\pi}$ x 10^{-9}	F m^{-1}
f	frequency	Hz
F	receiver noise Figure	dB
G	gain of antenna	dB
γ	propagation constant	m^{-1}
H	magnetic field intensity	A m^{-1}
P, P_T, P_R	power, transmitted, received	W
R_{in}	real part of input impedance	Ω
R_{rad}	radiation resistance	Ω
$R_\square$	surface resistance	Ω
J	electric current density	A m^{-2}
ρ	electric charge density	C m^{-2}
k	wavenumber	m^{-1}
η	radiation efficiency factor	
λ	wavelength	m
μ_r	relative permeability constant of medium	
μ_0	permeability of free space 4πx10^{-7}	Hm^{-1}
σ	conductivity	S
S	Poynting vector $\mathbf{S} = \frac{\mathbf{1}}{\mathbf{2}}\mathbf{E} \times \mathbf{H}^*$	Wm^{-2}
R	signal range	m
$\Delta\rho_s$	surface roughness	
k_B	Boltzmann constant 1.38065 x 10^{-23}	m^2 kg s^{-2} K^{-1}
T_N	System noise temperature	K
X_{in}	imaginary part input impedance	Ω
Z_0	intrinsic impedance of free space $\sqrt{\frac{\mu_0}{\epsilon_0}} = 120\pi$	Ω

Continued on next page

Symbol	Quantity	Unit
Z_F	intrinsic impedance of a medium $\sqrt{\frac{\mu}{\epsilon}}$	Ω
Z	characteristic impedance of a line	Ω
Z_{in}	antenna input impedance $Z_{in} = R_{in} + jX_{in}$	Ω

List of Abbreviations

ABC	Absorbing Boundary Conditions
AVM	Autarke Verteilte Mikrosysteme
BEM	Bounded Element Method
CPU	Central Processing Unit
CDMA	Code Division Multiple Access technique
CST	Computer Simulation Technology
CEM	Computational Electromagnetics
DUT	Device Under Test
ESA	Electrically Small Antenna
FDTD	Finite Difference Time Domain method
FEM	Finite Element Method
FIT	Finite Integration Technique
GPS	Global Positioning System
GTEM	Gigahertz Transverse Electromagnetic (Cell)
ITS	Intelligent Transportation System
IEEE	Institute of Electrical and Electronics Engineers
IEE	Institution of Electrical Engineers
MML	Microstrip Miniloop (Antenna)
MPA	Microstrip Patch Antenna
MAC	Media Access Control
MMIC	Microwave Monolithic Integrated Circuit
MM	Moment Method

OOK	On-Off-Keying
PML	Perfectly Matched Layer
PCS	Personal Communication Systems
RFID	Radio Frequency Identification Systems
SNR	Signal to Noise Ratio
SPFD	Scalar Potential Finite Difference Method
TE	Transverse Electric
TM	Transverse Magnetic
TLT	Transmission Line Theory
TEM	Transverse Electromagnetic
UMTS	Universal Mobile Telecommunications System
UWB	Ultra-Wideband
VSWR	Voltage Standing Wave Ratio

Zusammenfassung

DIE TENDENZ ZUR MINIATURISIERUNG wirft die Frage danach auf, welche Antenne(n) für energetisch Autarke Verteilte Mikrosysteme (AVM) kleinen Volumens angemessen ist/sind. Solche Mikrosysteme werden für den Einsatz in Sensornetzwerken z.B. in der Logistik, Raumüberwachung und Inventarisierung usw. angestrebt. Ein komplettes Mikrosystem samt Energieversorgung soll gemäß der AVM-Vision in einem Würfel dessen Volumen 1 cm^3 nicht überschreitet untergebracht werden. Die Raumknappheit bedeutet aber auch ein knappes Energiebudget. Die Kleinheit der AVM-Module und ihr anvisierter engmaschiger Einsatz machen weder das Auswechseln noch Wiederaufladen der Batterien durchführbar. Somit ist Energiesparen hinsichtlich einer brauchbaren Lebenszeit als Quintessenz des Systemkonzepts unerläßlich. Neben einem Energie-effizienten RF-Frontend-Entwurf empfiehlt sich für relativ lange Zeiträume, in denen keine Übertragungsoperationen anfallen, ein Versetzen des Mikrosystems in einen Schlummerzustand verschwindenden Energieverbrauchs.

Bei Kommunikation in wachem Zustand ist gerichtete Strahlung anstrebenswert. Dies ist sowohl der Energieeffizienz als auch der Interferenzminimierung dienlich. Darüber hinaus kann bei gerichteter Strahlung von einer erhöhten Übertragungssicherheit ausgegangen werden, da das Signal nicht in unerwünschte Richtungen gesendet wird. Da Richtwirkung direkt proportional zur elektrischen Größe der Antennen ist, scheint es zunächst angebracht, höhere Frequenzen zu verwenden. Auf Grund der damit verbundenen höheren Freiraumdämpfung muss ein Kompromiß zwischen Reichweite und Gewinn getroffen werden.

Diese Arbeit bietet in Gestalt von Schlitzanordnungen und Patches Antennenstrukturen, welche bei den vorgegebenen Abmessungen eine hinreichende Strahlungsbündelung dahingehend erzielen, dass sowohl im Sende- als auch im Empfangsfall ein adäquates SNR zur Überbrückung der Funkstrecke vorliegt. Da es sich um eine dynamische Netzwerk-Topologie handelt, wird dahingehend bewertet, ob die Strahlungsbündelung der Antennen abhängig von der momentanen räumlichen Orientierung der kommunizierenden Module einstellbar ist. Die begrenzte Möglichkeiten zur Ausrichtung des Hauptstrahls jedoch, welche von der Einschränkung der erlaubten Antennenabmessungen herrühren, führen zu dem Kompromiß einer weniger ausgeprägten Strahlungsbündelung, die aber die Abdeckung eines größeren Raumwinkels ermöglicht. Dies gestattet ein hohes Maß an Funktionssicherheit, da kommunizierende AVM-Module nicht stets fest aufeinander ausgerichtet sind.

Kapitel 1 setzt ein mit einigen Meilensteinen der elektromagnetischen Feldtheorie mit dem Schwerpunkt auf Entstehung und Entwicklung der drahtlosen Kommunikation und endet mit einer Schilderung des AVM-Szenarios. Kapitel 2 beschäftigt sich mit der Diskretisierung und Implementierung der Maxwellschen Gleichungen, einer sich lohnenden Vorleistung in

Anbetracht der ernormen Fortschritte, die die Rechentechnik zu verzeichnen hat.
In Kapitel 3 werden in Frage kommende Strukturen als Kandidaten betrachtet. Dann werden diese auf ihre Eignung bezüglich Wirkungsgrad, Vor-Rück-Verhältnis, Polarisationseigenschaften, Oberflächenkonformität und Herstellungsaufwand für das AVM untersucht. Als ein vielversprechender Kandidat erweist sich die Mikrostrip-Antenne. Sie wird in Kapitel 4 theoretisch behandelt. Es erfolgt eine Untersuchung der Auswirkungen von Geometrie- und Materialparametern auf die Strahlungseigenschaften. Auf die Empfindlichkeit der Strahlungscharakteristik in den Hauptebenen bezüglich der Speisestelle und der Größe des strahlenden Patchs wird in Kapitel 5 eingegangen. Dies eröffnet die Möglichkeit zu Antennenoptimierungen. Das Miniaturisierungsziel des AVM-Projekts verfolgend, wird in Kapitel 6, basierend auf der Miniloop-Antenne die Theorie und Funktionsweise einer neuen elektrisch kleinen Antenne vorgestellt. Die gute Übereinstimmung zwischen analytischem Modell, Simulationsmodell und Messungen belegt die Funktionstüchtigkeit dieser Antenne, welche sowohl für Kommunikation als auch Wake-Up Verwendung finden kann.

Only when lions have historians will hunters cease being heroes.
African Proverb

1 Historical Survey and Perspectives

1.1 Prologue

THE ADVENT OF MICROELECTRONICS and an accompanying succession of dazzling scientific and technological breakthroughs have revolutionized telecommunications and information technology in the 20th century. It would be difficult to identify or even conceive of any other contemporary technologies that have had a more striking, thorough and profound impact on everyday life. The extent and sophistication of the dramatic services and applications available to modern society as a result of advances in microelectronics are astonishing. These "high-tech" gadgets control nearly everything - from a galactic space shuttle to a domestic washing machine - and are no less important from the perspective of a soldier in combat, an airline pilot landing in zero-visibility conditions, a young video enthusiast, hikers navigating with hand-held or wearable locators, a banking executive, an entertainer, or a homemaker. The breathtaking growth of the Internet, with traffic continuing to double annually as witnessed in the last decade of the last century makes an epitome of this revolutionary trend [71]. Microelectronics has tremendous ramifications on industry, employment, the strategic position of a country, its military security, the quality of life and even on the evolution of society [96]. A case in point is the impetus the cell phone has given to both *modus vivendi* and *modus operandi* of business. The well-being of socio-economic entities like nations is contingent on the development and sustenance of intelligent products, tools and processes. Communication is one of the few fields of human endeavour in which it is natural that everyone, specialist and layman alike wonders which new applications of microelectronics are most likely to appear in the near future and what difference these applications might make for business and leisure in the 21st century. The story of cellular telephony which continues to encroach the remotest of enclaves in parts of the world that have yet to have a backbone network is perhaps an indication of things to come. It has been argued that a lack of infrastructure in certain countries can be turned into an advantage if properly managed. The crux of the argument being that these countries are not encumbered by extensive networks built

on obsolete technology, which require an evolutionary process of replacement [59]. In all this, electromagnetic field theory or specifically antenna theory plays a key role. The narration of the history of electromagnetic field theory and its interplay with antenna development is admittedly a task best left to historians. Its thrill and pivotal role in the emergence of various communications schemes, however are such that for introductory and quasi-completeness purposes, a cursory glance at some landmarks of a story as rich and fascinating as life itself appears irresistible.

At the beginning of the nineteenth century, electricity and magnetism were perceived to be unrelated phenomena. This could be attributed to the independent evolution of both areas. Coulomb had established the inverse-square law as the basic experimental postulate for electrostatics. Electrostatics received additional sound mathematical grounding by way of Gauss' divergence theorem in 1813. The Biot-Savart law can be invoked in its own right as the basic experimental postulate of magnetostatics. The discovery that a movement of charge, an electric current influences a magnet – *effectively creating a magnetic field* in 1820 by Oersted gave fresh impetus to further investigations. The era that followed was marked by a frenzy of intense and fruitful activity. Almost immediately other investigators notably Ampère elucidated the effects of current elements. *An electric current is surrounded by a magnetic field of force; the induced magnetomotive force in a closed curve is equal to the electric current passing through any surface bounded by the curve.*

It took a little more than a decade for a man with a keen sense of physical visualization in the person of Faraday to discover the reverse effect to that observed by Oersted i.e. the relative motion of a wire in a magnetic field induces a voltage in the wire – *effectively creating an electric field. A magnetic current is surrounded by an electric field of force; the induced electromotive force in a closed curve is equal to the negative of the magnetic current passing through any surface bounded by the curve.*

This discovery was important in cementing Faraday's basic scientific tenet that to every effect there was a reverse effect and that cause and effect were interchangeable. The stage was set and the world ready for a new conception for the nature of things. In 1864 James Clerk Maxwell deftly condensed the existing body of knowledge into an elegant mathematical formalism.

By invoking Stoke's Theorem on the transformation of surface integrals into contour integrals, Maxwell gave a mathematical framework to Ampère's current law [63]. To this he added his own radical and imaginative concept of *Displacement Current* thereby extending the validity of Ampère's circuital current law to time-varying fields, a masterly stroke of genius that made today's understanding of wave propagation possible.

The principal tenet of his Dynamical Theory of the Electromagnetic Field was the proposition that electromagnetic disturbance travels in free space at the speed of light, c. Maxwell's Theory established the possibility of

electromagnetic waves propagating at a speed whose value could be calculated from the results of purely electrical measurements. Conspicuous was its silence on the possibility of generating such waves. Almost a quarter of a century later Heinrich Rudolf Hertz verified Maxwell's prediction obtaining remarkable numerical accuracy between postulated and measured values of c in his brilliant epoch-making spark-gap oscillator experiments in Karlsruhe [10]. This was seminal to a general acceptance of Maxwell's Theory of Electromagnetism among the scientists of that day as fundamental laws governing the behaviour of electromagnetic waves. Hertz and Heaviside independently modified Maxwell's original equations discarding the requirement for the existence of an ether through which the displacement current and hence waves travel.

A logical consequence of this activity was the birth of wireless, a worthy fore-runner of present-day mobile communications as demonstrated by Guglielmo Marconi in 1896. Marconi's lasting merit is an unequalled capacity to put into practice all that was known at the time and finding the link between various inventions, solving a sort of jigsaw puzzle the pieces of which were the mathematical proofs of James Clerk Maxwell, the essence of experiments with electromagnetism by Heinrich Rudolf Hertz, the inventions of Oliver Lodge in England, of Adolphus Slaby in Germany, and of Edouard Branly in France.

By putting together elements of other men's inventions and making improvements on them such as Faraday's induction coils, Hertz's wave emitter, Righi's spark gap, Branly's coherer and the telegraph key of Morse, Marconi was able to herald a new day in human communications. The high-power pulses of the Hertzian oscillator were formed into dots and dashes of Morse Code for wireless telegraphy initially over a distance of two miles at about 1.2 GHz. Against all odds in the intervening years this culminated on a blustery December 12, 1901 in the successful transatlantic transmission of the Morse Code "dot dot dot" for the letter S. On a historical note, there is evidence Marconi alone may not be credited with inventing radio through which man is no longer restricted to crude and highly unreliable schemes such as the use of signs whose range does not exceed the horizon on the brightest of days or the Red Indian warrior keeping an ear to the ground to discern movement of troops. Substantial and credible evidence suggests that Alexander Popov had carried out wireless transmissions as early as 1895 [41]. Unlike practically-minded Marconi who also exhibited remarkable entrepreneurial acumen, Popov was too engrossed with science and teaching to concern himself with practical and commercial aspects of radio. Ever since wireless communication has gone from strength to strength as concerns type, size, purpose, capacity and frequency of communication systems. The charm of symmetry in modelling and the power of mathematical analysis have been brought to bear on field theory like no other sphere of human endeavour. For instance working on the premise that "*free space can be re-*

garded as a circular waveguide of infinite cross section with transmission along the z-axis" in the middle of the last century, Marcuvitz [62] obtained reasonably accurate results. Such was the success of modelling that Schelkunoff declared

> "Abstract model building in microwaves is not over. It takes a mathematician to make bold use of analogies and pictures without being ashamed of it" [84].

Wireless communication continues to be in ascendancy. Today in view of the rapid proliferation of Personal Communication Systems (PCS) and in a view to fulfill the first of the seven IEEE New Technology Directions Committee Grand Challenges in Electrotechnology for the 21st century [45] namely ***to make any person anywhere in the world reachable at his or her discretion, at anytime by communication methods independent of connecting wires and cables,*** it is apparent that innovative antennas are called for. Major technical challenges were encountered in achieving today's small feature sizes, and the number and difficulty of the technical challenges will increase with continued decrease in feature size. Over the past half century, the storage costs have plummeted astronomically as the processing speed of computers has doubled every 18 months, a phenomenon that has been dubbed Moore's law[1]. A variety of technologies – most recently, integrated circuits – have enabled this exponential increase in information processing power. But there is no particular reason why Moore's law should continue to hold: it is a law of human ingenuity, not of nature. So the question is when will Moore's law cease to hold? Indications are that the progress in microelectronics will slow down by 2015 – 2020. This is because there is a size limit below which transistors, the building blocks of computer chips, fail. Tunnelling occurs when the oxide separation goes below $\sim$1.5 nm (four atoms) inducing leakage currents and dielectric breakdown. This leads to transistors that are permanently *on* and can no longer be of use in switching. By 2025 the market may demand the exploitation of quantum behaviour in nano-scale systems and the development of a pico-technology in order to put all the power of the computer in a single molecule [19]. A shift of paradigm seems imperative. Existing materials and technologies are approaching their physical limits, and technology breakthroughs, in terms of materials and processes, will be required as device sizes decrease significantly below 100 nm [72]. It takes a "prophet" to predict the future of "high-tech" but if the current trends indeed are anything to go by (excluding the absolutely unexpected happening, that is), it would be safe on the grounds of existing tremendous momentum to say that the march will continue in the foreseeable future. Such a momentum is supported by the existing knowledge,

[1] Intel co-founder Gordon Moore made this prediction in a 1965 article barely four years after the first planar integrated circuit and an odd sixteen after the invention of the Field Effect Transistor.

powerful unwavering customer demand, and the enormous investments of capital and human resources *e.g.* the Universal Mobile Telecommunications System (UMTS).

In the near future the limits of physics and materials may spell the end of the road for conventional scaling and shrinkage. The fundamental limits on the size of an antenna with respect to wavelength at the frequency of operation mean antennas in a far greater measure than electronics cannot be indefinitely miniaturized and replaced by a chip without performance tradeoffs. The challenge is doubtless the optimization of the spatial, temporal as well as the spectral efficiency of communication systems. For instance, frequency crowding has traditionally been dealt with by a progressive drive to higher frequencies motivated by the prospect of a higher data throughput and bandwidth. The near exponential proliferation of communication services in multitudes of flavour is accompanied by a trend to higher frequencies. This has far-reaching consequences on antenna development more so as the size of systems becomes comparable to wavelength. The challenge for future systems design lies in processing and packaging of all transmit/receive modules and contending with the fundamental limits of electrically small antennas (ESAs). The development of high performance, low-profile and conformal antennas of adequate bandwidth which can be inconspicuously flush-mounted is the subject of this work. An important prospect is the microstrip antenna. Heralded in a seminal paper in 1952 by Grieg and Engelmann [27], it was left for Deschamps to come up with the earliest known realization of a microstrip-like antenna integrated with a microstrip transmission line in 1953 [18]. In 1955 Gutton and Baissinot patented a microstrip antenna design in France [29]. For lack of printed circuit boards with controlled dielectric constants, the microstrip antenna was overshadowed by the stripline which received more interest as a planar transmission line at the time because it supports a transverse electromagnetic (TEM) wave and allowed for straightforward analysis, design and development of planar microwave structures. Microstrip transmission line analysis and design methods were rigorously treated in the 1960s by Wheeler [103] and Pucel *et al* [77]. Investigation of the microstrip antenna in earnest only began after 1970 on the heels of improvements in materials preparation and processing technology in connection with the advances in printed-circuit technology. The conventional microstrip patch antenna (MPA) comprises of a metallic radiating element affixed on a grounded dielectric substrate. The radiating element may be of any shape. For ease of analysis and manufacture, rectangular, triangular, circular and annular geometries have received much attention. Today microstrip antennas permeate a wide range of products and technologies from missiles and aircraft to portable gadgets such as cell phones and tags on various commercial items owing to their small size, light weight, and low-profile geometry. Because they are easy to manufacture, they are relatively inexpensive. Microstrip antennas lend themselves well

to integration with micro- and millimetre-wave integrated circuits through MMIC processes. With miniaturization taking centre stage, it is expected that the molecular beam epitaxy and electron-beam lithography processes with a finer resolution will be of material importance. Important for future developments is another outstanding feature of the microstrip antenna: conformability and hence the prospect of aesthetic solutions through flush-mounting on various surfaces even those showing some curvature. This spells out the recession or perhaps the disappearance of cumbersome and obtrusive antennas such as parabolic reflectors and protruding wire antennas.

These notwithstanding microstrip antennas are resonant structures and as such inherently narrow-banded. As miniaturization marches on spawning one wireless wonder after another with inexorable feature size shrinkage, it becomes increasingly difficult to fit a full wavelength into a side of the antenna. Conventional small antennas have basically an omnidirectional radiation pattern. They are as a result inadequate for use in situations where energy is a critical factor. The prospect of directed radiation and economical beam forming and steering in any direction of interest is conditional on antenna size in wavelengths. Mention is made in the literature of supergain antennas of surface current distributions of arbitrary nonlinear phase with interference leading to beamwidths that are narrower than those expected from apertures of comparable size in the direction of main radiation [34; 111]. Supergain antennas are characterized by an extremely high level of stored electromagnetic energy in the vicinity of the antenna elements. As the radiation resistance is only a fraction of the input impedance such antennas have low radiation efficiencies. Their behaviour is extremely sensitive to both the phase and amplitude distributions of the sources. Besides utmost precision of fabrication, they require an exact control of phase and amplitude. They are hence technically difficult to build. It is reported that Schelkunoff, Fränz and Eckart have shown theoretically that an infinite gain can be attained using an arbitrarily short antenna [111]. However since the reactive power is by and large greater than the radiated power for such antennas, *superdirective* appears to be a more appropriate description.

In spite of substantial advances in material science, use of high dielectric constant material to electrically enlarge the component or antenna must be carefully weighed against the fact that introduction of a dielectric material not only strengthens the resonance aspect and introduces losses, it also reduces the bandwidth of planar patch antennas. This leads to a degradation of the radiating capacity of the antenna while enhancing the transmission line character of the structure. Oftentimes than not space constrains do not allow for such a dielectric. This work seeks to alleviate limits of ESAs by marrying the theory of transmission lines, antennas and resonators for more efficient and aesthetic miniaturized systems. Besides treading the path of "proven" technologies may offer few new windows of opportunity.

1.2 The Scenario

A confluence of high performance computing, communication, information and human-machine interface technologies presents the potential to solve real world problems with the result that societies are rapidly becoming reliant on various distributed collaborative communication systems. A distributed system consists of a collection of distinct entities which are spatially separated and exchanging messages with one another. A single computer can also be viewed as a distributed system in which the central control processing unit, memory units, input and output peripheral devices represent separate agents. In a distributed system as used here, the time between events within an *e-Grain* entity is negligible compared to the message transmission delays between distinct *e-Grains*. Emphasis is increasingly being placed on exchanging information itself without necessarily expending energy to move mass (persons and objects such as paper) around *just so* to transmit information. This is intrinsically linked with the drive to expand man's understanding and experience of space — the expanse in which objects interact and events occur — and in so-doing fulfill the IEEE vision [45]: ***"To allow a person to be present, by his or her choice, in any place at any time through the technologies of virtual presence and virtual reality."***

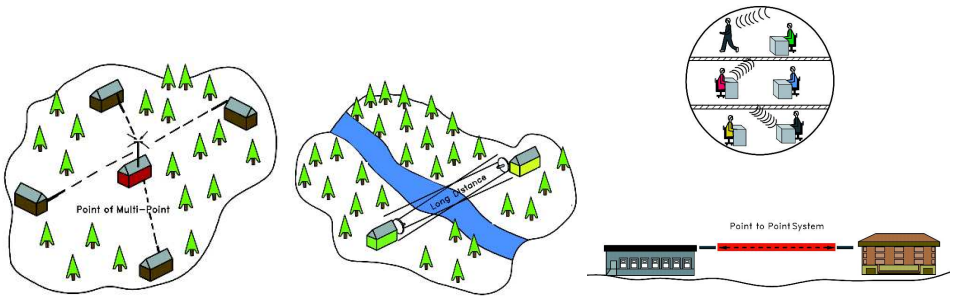

Figure 1.1: *Status quo: The Network Revolution of the 1990s.*

Not surprisingly, a recent timescale broadly shows a pre-1990 era marked by client-server systems, the 1990s characterized by the worldwide onslaught of the network revolution; see Fig. 1.1 while the drive towards the small facilitated by integration and wireless connectivity appears to be both irrepressible and irresistible in the 2000s.

The appetite for mobile data connectivity is not expected to soon wane and those parts of the globe where the fixed backbone networks are nearly non-existent are thought to have a greater potential for the development

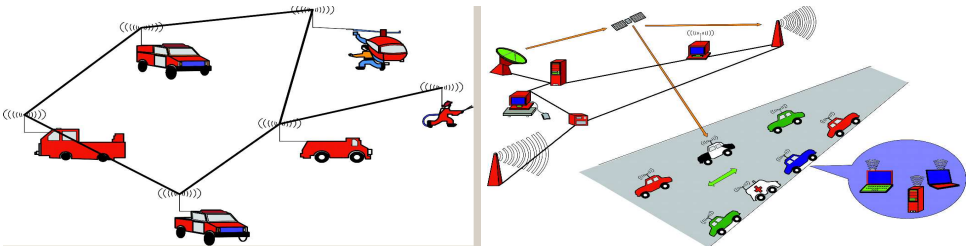

Figure 1.2: *Ubiquitous communication: tomorrow today.*

and use of wireless compared to traditional wired links. The history of technology reveals a profound interaction between the incentives and opportunities of technological innovation on the one hand and the sociocultural conditions on the other. e.g. the apparent positive feedback loop between industrial and academic activity on one the hand and the mass appeal of recent wireless technologies such as IEEE 802.11 (MAC layer protocol "Bluetooth"[2]) and UMTS on the other. In keeping with this development, the model for the future revolves around a vast network of ultra-fast fibre connecting homes, offices, mobile vehicles and neighbourhoods but for many applications and sparsely populated areas, the central theme will be cheaper but slower wireless decentralized units. New information systems as exemplified by grid computing, web services etc, are often distributed, large-scale, open, heterogeneous, and characterized by a constantly changing environment. A case in point, the Global Positioning System (GPS) is used to calculate the vehicle's position providing both voice and visual guidance to the driver's final destination. The road map for Dashboard Telematics encompasses a broader Intelligent Transportation Systems (ITS) vision for cellular and Internet services to provide drivers and passengers with hands-free communication, access to personalized information on the Internet, the ability to summon emergency services and roadside assistance, and an array of safety, convenience and entertainment applications.

The challenge lies in developing increasingly small and reliable antennas which can cope with less energy. In view of the state of advances in technology, the prospect, for the first time in history, of global connectivity for voice, video and data shifts into the realm of the feasible. The development and deployment of omnipresent wireless networks consisting of Autarchic Microsystems having a volume in the order of 1 cm^3 falls squarely in this scheme of things a hallmark of which is the collecting, retrieving and circulating of a gamut of data in diverse scenarios.

[2]The Bluetooth standard for WPAN uses Frequency-Hopping Spread Spectrum at 2.4 GHz to connect small devices in close proximity ($\leq$ 10m). Maximum data throughput is about 800 Kbps, with full-duplex voice communication at 64 Kbps. A prototype PDA with Bluetooth and optional GPS receiver integrated was demonstrated by Ericsson at the Mobile Internet 2000 Conference.

1.3 Autarke Verteilte Mikrosysteme

The project **Autarke Verteilte Mikrosysteme (AVM)** is an interdisciplinary consortium[3] entrusted with the mission to carry out research on the feasibility and development of self-sufficient fully integrated microsystems about 1 cm^3 in volume that unaided can bridge distances in the range of a meter. The AVM module shall be a cube, an elegant and symmetrical yet rarely used shape in the gadget world, with the notable exception of alarm clocks. It is envisioned to merge computation and communication with sensing and actuation. Space being at a premium, it becomes inevitable to sacrifice some performance so as to put less strain on the battery. This would mean supporting relatively low data rates ($<$ 100 kBit/sec) and as such dense deployment as in sensor or monitor networks. Apart from high module density such networks are projected to have a dynamic topology. The energy supply itself is limited to built-in batteries, as untethered operation is desired for mobility. The limited on-board power supply more than any other factor imposes an upper bound on capacity and functionality. These properties together with the low cost of production would distinguish them from more established networks such as cellular or ad hoc networks.

AVM-modules must be aware of their own capabilities and position in the environment. An important attribute in this scenario of increased complexity is adaptability. This is understood as the ability to update information while they execute particular tasks; mechanical reconfiguration being impracticable for such small modules.

Barely a few generations ago the concept of wireless services appeared utopian. Today daily life is being increasingly permeated by *wireless wonders* at the risk of being taken for granted. Many a gadget that appeared outlandish a few decades back has left its initial niche and penetrated mainstream electronics. The wide range of services currently in wide use notwithstanding, it is reasonable to assume that over the next few decades numerous other wireless technologies and services will be developed as there is still a plethora of scenarios showing need and/or potential for improvement. Presently there is need for sensor or monitor modules arbitrarily distributed in space capable of collecting processing and transmitting information in inventory management, localization of objects and persons, sensors and actuators, identification and personalization, smart textiles, environmental hazard detection, remote terrain monitoring, target tracking, enemy detection, military commanding, management of traffic, smart buildings, infrastructure maintenance and disaster mitigation. Clearly this list of applications is not exhaustive and there exist solutions in some of these areas. Hitherto and for the most part, the idea has been that of separately optimizing individual

[3]Various departments of Fraunhofer Institut für Zuverlässigkeit und Mikrointegration, Berlin, several institutes of the Technische Universität Berlin and FBH Berlin

components whereby integration represents the last step.

AVM pursues a holistic design philosophy to avert the creation of an agglomeration of discrete mosaics which function standing alone yet lack inter-operability. Primordial is a systems approach at the onset seeking to combine at least the chip, the package and board, leading to new 3-D integrated structures for continued improvement in performance. The design of various components is done in a concomitant manner aiming at a seamless integration of components. This weaving of components into one another departs from conventional multi-layer technology by aiming at true 3-D integration. The freedom to roam aside, an untethered network is energetically more viable since it is not subject to exponential attenuation inherent in cables. Envisioned is distributed computing with small, lightweight self-sufficient modules. Energy-awareness and ultra-low power consumption are thus essential for a meaningful *e-Grain* lifetime [43]. Being highly miniaturized, recharging becomes an expensive proposition.

1.3.1 On the Question of Range

Besides the use of low power CMOS-FETs, the restriction of *unaided* module range to one meter is concessionary to the energy question. The prospect of achieving any measure of directed radiation gets better the larger the module is in terms of wavelength. This, besides the avoidance of crowding at lower frequencies, speaks for a high frequency of operation. It is obvious that a trade-off must be made as atmospheric attenuation increases with frequency. This range restriction is not necessarily a limitation. A higher transmit power causes higher interference with surrounding devices, thus decreasing network throughput [78]. Contingent upon energy-efficient routing between *e-Grains*, a link between out-of-range modules can be established through intermediate modules by multi-hopping. Multi-hopping also offers an alternate communication route between two modules within range but having an obstructed line of sight. For less interference, more parsimony with energy and more security, a transmit power just sufficient for the receiver to correctly decode data signal is therefore ideal. Each module in the network may serve as an access as well as a relay point for traffic originating elsewhere in the mesh. Sending information between two points A and B separated by a free space distance r requires an amount of energy directly proportional to $\kappa \cdot r^{\gamma}$ whereby for the path loss exponent typically $2 \leq \gamma \leq 4$ holds and κ is a function of receiver sensitivity. Using just one intermediate node midway between two modules and n arbitrary but equidistant nodes, the energy to cover the distance r falls from $\kappa \cdot r^{\gamma}$ to $2\kappa \cdot \left(\frac{r}{2}\right)^{\gamma}$ and $\approx (n+1)\kappa \cdot \left(\frac{r}{(n+1)}\right)^{\gamma}$, respectively. As shown sending information through a series of intermediate hops is more economical than using one long haul. Premising on reliable and energy-smart handover, the required

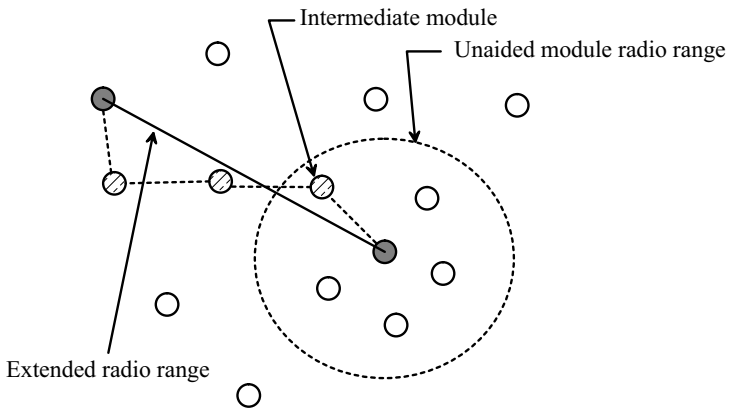

Figure 1.3: *Multi-hop: obtaining information indirectly from primary module via intermediary modules. This reduces transmission energy by tenths of order of magnitude besides enhancing reliability and robustness*

transmission energy is reduced by orders of magnitude. The similarity between the intermediate *e-Grains* and conventional repeaters is immediately obvious. Although several recent research results indicate that ideal multihop routing significantly increases the capacity of ad hoc wireless networks, achieving these gains through a non-hierarchical decentralized routing strategy remains elusive [28; 97].

1.3.2 Computation or Communication?

To reduce power consumption without overly sacrificing performance, a concept embodying "energy or power awareness" in system design is essential. The key idea is that the system only delivers the performance that is strictly required, thereby avoiding superfluous power consumption. The oldest and most straightforward technique would be to shut down unused parts of the system.

It is not improbable that an *e-Grain* spend a significant amount of time in standby.[4] Even though standby power is customarily lower than receive or transmit power, it can easily constitute the lion's share of power given the excessively low throughput and low duty factor of the *e-Grain* module. A highly modular approach where nonessential components or actions are eliminated as the situation dictates becomes inevitable. It therefore becomes necessary to switch the complete module into a state of near-zero power consumption. This would mean the modules are virtually in dormancy and sparingly come alive if and only if certain events occur that warrant action. Hence the vision of a *wattless wake up* [67].

[4] A rule of thumb for long-lived applications is ensuring that each device sleep 99 % of the time and does its energy-consuming work in the remaining 1 percent.

The onboard processor also offers other ways to save power. Communicating one bit of data through the radio transceiver costs as much energy as executing roughly 1,000 processor instructions. The module can conserve power by storing and aggregating sensor readings, rather than sending them out immediately. Hence the protocol stack offers a huge savings potential through a trade-off between transmission and computation. Since addressing provides a module not just "contents" but position information of neighbouring modules in the network, communication between modules is best carried out in a point-to-point manner. Apart from the ensuing energy economy, another advantage accruing from this is the reduction of interference between signals from other sources —good coexistence with colocated systems — and the enhanced security that goes with non-broadcast communications. The adoption of standard encryption techniques for protecting the transmitted data is not attractive in this environment as it is costly in terms of energy consumption.

The objective of multi-module systems is to control complex systems (divide and rule). These systems employ a set of modules that may be autonomous, proactive and/or adaptive. The setup may be homogeneous consisting of identical *e-Grains* or hierarchical whereby each *e-Grain* has its own abilities, status and knowledge, but needs to interact with other agents to solve complex problems such as avoiding conflicts, acquiring and spreading information. The benefits of unobtrusive miniature systems would be undeniable in the light of the task of managing a full and hectic life. The above distinctions notwithstanding, the dynamic nature of the network topology poses a real risk of fading due to multi-path propagation and polarisation mismatch. The reliability of any system being inextricably linked to its fault tolerance, a range of measures to incorporate redundancy prominent amongst which are circular polarisation and antenna diversity is called for.

In view of the necessity for such systems to be energetically autonomous, energy parsimony takes centre stage. For antenna development this translates to the development of devices capable of launching radiation preferably only in the direction in which communication is desired i.e. low or vanishing sidelobe levels. Integration and miniaturization in the design of technology are possible only to the detriment of additional product features amongst which is the capacity to generate directed radiation. While the inherent energy consumption of digital circuits is rapidly decreasing due to progress in materials preparation and ingenious design techniques, the power that is radiated does not necessarily follow this trend being strongly dependent on electrical size, materials and geometry. The field lines and thus radiation characteristics are subservient only to Maxwell's equations. Another desirable property of the antenna system is the ability to change the direction of radiation without the need to physically reconfigure the module in any manner whatsoever. Hence the need for signal processing that allows electronic switching of the radiation from one direction to another. This

makes the task a worthwhile challenge.

1.4 Outline of Key Features

From the foregone, *AVM* is therefore about the realization of the concept of "Ambient Intelligence"

- in an environment which is sensitive, adaptive and possibly responsive to certain actions or signals. An environment that adjusts activities through smart non-explicit assistance —*Autarke, autarchic*.
- In this environment technology is embedded, permeating the whole background—*Verteilte, distributed*.
- This environment shows a frugal utilization of resources and information tailored to need as appropriate by small *e-Grains* —*Mikrosysteme, microelectromechanical systems*.

The architecture of a radio device can be divided in two major functional areas, the front end and the back end. In the first, the transmission or reception of the electromagnetic waveform as well as its down-conversion to baseband is performed. The latter is dedicated to signal processing to recover the modulated and coded signal at baseband frequencies and makes the device either a terminal or a base station.

In the following pages various possibilities of meeting these goals will be examined. A cursory glance is taken at some promising techniques destined to play a major role in alleviating the difficulties plaguing communications in a dense mesh of *e-Grains*. The perspective will principally be that of antenna design, not a complete system design or implementation.

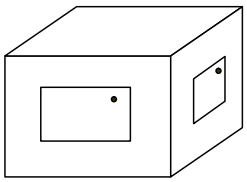

Figure 1.4: *AVM-Module: It is envisaged as a cuboid having a volume under 1 cm^3 and sides not exceeding 1 cm. System performance would be increased by employing a multi-antenna system to exploit the spatial diversity of the wireless channel on the assumption that the resulting signal strengths of individual elements are statistically uncorrelated.*

Communication is essentially stochastic in nature in accordance with the nondeterministic fashion events unfold in space-time. Shannon showed this non-determinism to be proportional to the information content [90]. In order not to miss out on information, there is need to literally stretch out one's feelers in every direction at all times — diversity.

1.4.1 Diversity

In many settings of practical interest, the transmitted signal arrives at the receiver via multiple propagation paths with different delays, thus giving rise to multipath effects. Signals from the line of sight, diffraction, specular and diffuse reflection may superpose either constructively or destructively, resulting in fading. Conventional narrow-band systems completely fail if the receiver is coincident with a multipath-related null. Minor displacements of an antenna may therefore impact significantly on the received signal amplitude. To mitigate and indeed exploit[5] the fading associated with multipath, *antenna diversity* employing a physical replication of antennas and founded on the premiss that at least one of the antennas will be in a favourable location at any given time, is used. Diversity is therefore founded on the concept of redundancy whereby reliability is enhanced by making use of several uncorrelated branches. Hardware reconfigurability is out of question for an AVM module so a *switched diversity* system involving continually switching among the antennas so as to always to use the antenna with the strongest signal harbours the greatest potentials. Switching primarily offers range extension but may also by viewed to offer the possibility of suppressing interference from directions other than that of the active beam. Diversity systems are suitable for environments in which fading is the dominant mechanism for signal degradation. This explains the popularity of Code Division Multiple Access technique (CDMA) in personal communications systems [52].

In environments with significant interference, however, simply locking onto the strongest signal is not ideal since it is not given that a co-located interferer cannot have the strongest signal. This is another argument for spectrum exploitation towards higher frequencies which presently are less crowded.

Real estate permitting, phased arrays equipped with a combination of hardware and software that make it possible for the pattern to be continually changed over time according to the operational needs at hand constitute the ideal solution. By electronically adjusting the phase and amplitude of individual elements, a fast and precise steering of the communication may be implemented as in existing wireless communications systems —*spatial diversity*. Adding a single node improves broadcast reliability dramatically. Spatial diversity is the preferred way to boost performance in sensor networks. Arrays represent a spatial diversity scheme in the strict sense of the

[5]Use of multi-element antennas at both transmitter and receiver permits transmission rates far in excess of those possible using conventional approaches. The paradigm is the exploitation, rather than the mitigation, of multipath effects in order to achieve high spectral efficiencies (bits/s/Hz) [23]. The implementation of low power multipoint RF networks using Wideband Orthogonal Frequency Division Multiplexing (W-OFDM) minimizes interference with adjacent networks. This minimisation of interference enables independent channels to operate within the same band, allowing multipoint networks and point-to-point backbone systems to be overlaid in the same frequency band.

word. For such arrays however there is a minimum separation necessary between individual elements to guarantee resolution as the mutual coupling between elements increases with proximity. Also the real estate for feed network including phase shifters and power splitter is not available with today's materials and technology. Also, a conventional variable phase shifter consisting of a movable dielectric block on the meander strip line where the phase of each element changes is not suitable for AVM because it requires mechanical movable parts. The digital phase shifter using a pin diode is out of question because it causes passive intermodulation effects [5]. In view of this conventional arrays are no option for AVM.

Polarisation Diversity

The manner in which radio frequency energy is radiated or captured from space has a profound influence upon the efficient use of spectrum, the cost of setting up new communications networks and the deliverable quality of service. In a dynamic network, change of orientation of *e-Grains* is inevitable. With this is associated the risk of link failure caused by polarisation mismatch. To mitigate this, the system antenna must be circularly polarised.

Sector Antennas

Sectorial systems have antennas constructed to cover certain fixed, preferential directions. N antennas, each covering a fixed non-overlapping arc of, say, $\frac{360}{N}^\circ$ provide full azimuth coverage. Sector antennas provide increased gain over a restricted angle as compared to an omnidirectional antenna. In other words, a sectorial antenna rejects interference from nodes beyond its pattern of coverage thereby increasing the reuse potential. Antenna switching is limited since the pattern is fixed and the ability to adaptively reject interference is not present. A four-antenna arrangement decreases the effect of loading by a factor of approximately 4. This factor is called *sectorization gain*[107, pp. 80].

1.5 Perspectives

Communication is often the dominant power sink in the complete system [88]. The requirements for the antenna system in dynamic topology plagued by a restricted power supply can thus be formulated as moderate to high gain, high directivity noticeable in a high front-back ratio, low sidelobe levels and circular polarisation.

On the road to low-energy, low-cost, small-size solutions simplicity rules! Advanced techniques used in traditional wireless links are not necessarily relevant. Standby power for monitoring connectivity and updating memory turns out to be the greatest enemy. It may easily dominate overall power.

Redundancy as a means to create robustness is imperative since *inter-e-Grain* links *can and will* fail. Intelligence such as learning about the environment may not be worthwhile if it changes too rapidly. Power saving under these circumstances appears achievable by use of simple On-Off-Keying (OOK) since only the high bits are transmitted through the channel. There is need for synchronization and verification to establish memory consistency. Non hierarchical Networks or networks showing no differentiation into master and slave *e-Grains* have little practical significance.[6] A multi-*e-Grain* program executing on a modern multiprocessor must issue explicit commands to synchronize memory access. How this is done might undermine the energy saving measures as simple as OOK and ***wake up***. A combination of advances in low-cost computing capacity and the development of new post-processing algorithms for signals from arrays of simple antennas make "intelligent antennas" possible. Very high gain antennas at very high frequencies require very precise antenna shapes and their very narrow beamwidth necessitates accurately maintained pointing (coincidence). Hence the simplest class of CP-Antennas seems to be the most expedient and useful for AVM purposes — the quest is for moderate-gain antennas, sensitive receivers, and amplifiers, if necessary. This is neither a new problem nor a new solution.

The conundrum of achieving a broadcast type of radiation for wake up and directed radiation for communication in the same *e-Grain* seems at the moment resolvable only by use of two distinct antennas. Given that the lifeblood of directivity is antenna size, a worthwhile challenge this becomes.

[6] 1st Evaluation Meeting (Statustreffen) Oct. 2003 - Prof. Wolisz

No challenge should be faced without a little charm and a lot of style.
Bluetones

2

From Maxwell's Equations to FIT

JAMES CLERK MAXWELL in his ***Treatise on Electromagnetism*** [64] essentially summarized the work of Hans C. Oersted, André Marie Ampère, Michael Faraday and others in a crisp and succinct mathematical formalism as briefly reviewed in Chapter 1. Long before Descartes and Einstein gave them a formal mathematical framework, the concepts of space and time had always fashioned human thought. The classic way to model dynamic systems is by describing their state as a continuous function of space and time. An *exact or faithful* description would entail an infinite number of intermediary instantaneous *meta*-states between any pair of initial and final states. The obvious impracticality of such an approach dictates viewing the system as discrete and exhibiting by definition discrete state changes. Discretizing or sampling opens up the possibility to reason about the radiation mechanism in a mathematical abstraction of the structure. For a model to be more than an amenable mathematical gadget, a formal connection between the complete configuration and the model (a mathematical statement) is essential. Limitations of models themselves dictate the use of empirical numerical schemes. A natural starting point in treating the propagation of electromagnetic waves both in free space and other media are the celebrated Maxwell's Equations. If the discretizing steps are small enough, then the representation may be considered accurate for all practical purposes. In spite of the ingenuity that has gone into creating segmentation schemes, a trade-off between an extremely fine discretizing for accuracy on one the hand and computer memory and CPU time on the other is inevitable.

2.1 The Cornerstone

In the following $\mathbf{r}$ is the vector from a source point (x_1, x_2, x_3) to a field point (x, y, z), ρ is the volume charge density and $\mathbf{J}$ is the current distribution while dV is the differential volume element at (x_1, x_2, x_3). Further, let the proportionality between field vectors and displacement vectors be described

by

$$\begin{aligned} \mathbf{D} &= \epsilon \cdot \mathbf{E} \\ \mathbf{B} &= \mu \cdot \mathbf{H} \qquad \text{where } \epsilon \text{ and } \mu \end{aligned}$$

will be treated in detail at present.

Maxwell's equations in differential form read:

$$\nabla \times \mathbf{H} = \frac{\partial \mathbf{D}}{\partial t} + \mathbf{J} \tag{2.1a}$$

$$\nabla \times \mathbf{E} = -\frac{\partial \mathbf{B}}{\partial t} \tag{2.1b}$$

$$\nabla \cdot \mathbf{D} = \rho \tag{2.1c}$$

$$\nabla \cdot \mathbf{B} = 0 \tag{2.1d}$$

From a mathematical standpoint these equations completely describe electromagnetism since divergence and curl of both the electric and magnetic fields have been defined in keeping with Helmholtz's Theorem [6]. Importantly Eqn.(2.1c) shows that lines of $\mathbf{D}$ in any medium start and end on charge alone while Eqn.(2.1d) underscores the source-free character of $\mathbf{B}$. The consistency of these equations is readily demonstrated by taking for instance the divergence of the first two equations (2.1a) and (2.1b) to obtain the following forms of the last two Maxwell's Equations:

$$\text{the continuity condition} \quad \nabla \cdot \mathbf{J} = \frac{\partial \rho}{\partial t}$$

$$\text{and the divergence free nature of B} \quad \nabla \cdot \mathbf{B} = 0.$$

Though Eqn.(2.1d) expresses the physical fact that a magnetic monopole has neither been isolated nor identified, magnetic charges and currents shall be introduced in section 2.4.1 to obtain a symmetric form of MaxwellŠs equations and thereby facilitate analysis. Each of these equations has an integral counterpart which can be obtained using where appropriate either Stoke's or Gauss's Theorem. In contrast to this differential formulation, the integral formulation is more convenient in treating macroscopic continua. Assuming the field sources namely current density $\mathbf{J}$ and charge density ρ, the above set of vector equations is apparently under-determined there being more unknowns than the number of equations. Maxwell's equations written out in full contain a total of 12 scalar unknowns, three components each for $\mathbf{E}$, $\mathbf{H}$, $\mathbf{B}$ and $\mathbf{D}$. Maxwell's equations are not independent as taking the divergence of the curl equations above showed. Accordingly less than 12 equations are needed to specify the field completely. The constitutive relations describing the behaviour of electromagnetic fields in the presence of media supplement Maxwell's equations for this purpose. The interaction between electromagnetic fields and matter can be described generally as follows:

$$c\mathbf{D} = \mathbf{P}\cdot\mathbf{E} + \mathbf{L}\cdot c\mathbf{B} \tag{2.3}$$
$$\mathbf{H} = \mathbf{M}\cdot\mathbf{E} + \mathbf{Q}\cdot c\mathbf{B} \tag{2.4}$$

P,**Q**, **L** and **M** are 3×3 matrices whose elements are called constitutive parameters detailing the susceptibility of the material to polarisation and magnetization. In general these parameters are functions of position and orientation.[1] Unless otherwise stated the subject of the following will be homogeneous media whereby the parameters are independent of position or change so slowly in space that for practical purposes they may be regarded as constant. Hence for linear isotropic media here of interest **E** is parallel to **D** while the magnetic field vector **H** is aligned with the magnetic induction **B**. This implies

$$\mathbf{D} = \epsilon\mathbf{E} \qquad\qquad \mathbf{B} = \mu\mathbf{H} \tag{2.5}$$

whereby permittivity and permeability of the medium are given by

$$\epsilon = \epsilon_r\epsilon_o, \quad \epsilon_o \approx \frac{1}{36\cdot\pi}\times 10^{-9}\mathrm{Fm}^{-1} \text{ and}$$
$$\mu = \mu_r\mu_o, \quad \mu_o = 4\pi\times 10^{-7}\mathrm{Hm}^{-1}$$

respectively. Writing out ϵ_r and μ_r in complex form

$$\mu_r = \mu_r' - j\mu_r'' = \mu_r'(1 - j\tan\delta_m), \quad \epsilon_r = \epsilon_r' - j\epsilon_r'' = \epsilon_r'(1 - j\tan\delta) \tag{2.6}$$

shows losses to be proportional to $\tan\delta_e = \epsilon_r''/\epsilon_r'$ and $\tan\delta_m = \mu_r''/\mu_r'$, hence the appellation loss tangent.

Media for which the electric field vector **E** is no longer parallel to the vector of displacement **D** and the magnetic field vector **H** no longer parallel to the magnetic induction **B** is said to be anisotropic. Such media are described by permittivity and permeability tensors, $\overline{\overline{\epsilon}}$ and $\overline{\overline{\mu}}$:

$$\mathbf{D} = \overline{\overline{\epsilon}}\cdot\mathbf{E} \quad \mathbf{B} = \overline{\overline{\mu}}\cdot\mathbf{H}. \tag{2.7}$$

A bi-anisotropic medium is polarisable in an electric field and is equally magnetizable in a magnetic field [53]. This cross-coupling between electric and magnetic field can be written as

$$\mathbf{D} = \epsilon\mathbf{E} + \xi\mathbf{H} \qquad\qquad \mathbf{B} = \xi\mathbf{E} + \mu\mathbf{H} \tag{2.8}$$

[1] Hysteresis in ferromagnetic media means the extent of magnetization is also dependent on the history of the material. Such material is termed non-linear since the induction is not directly proportional to the applied field.

Almost any medium displays bi-anisotropic behaviour once in motion[2]. The dependence of material parameters on frequency is termed dispersion, the propagation of different numerical wavelengths at different velocities leading to signal distortion, notably broadening of pulses.

2.2 Harmonic Time Dependence

Most phenomena in radio engineering have an $\exp^{j\omega t}$ or harmonic time dependence. By virtue of linearity, the rest of phenomena can be conveniently perceived as superpositions of possibly an infinite number of harmonics. Maxwell's equations Eqns.(2.1) may then be Fourier transformed replacing in the process the time derivatives by a $j\omega$ factor and the time-varying vector field quantities $\mathbf{A}(x, y, z)$ by their phasor counterparts $\mathbf{A}(x, y, z)$. Henceforth the $\exp^{j\omega t}$ shall be suppressed and Maxwell's Eqns.(2.1) then read:

$$\nabla \times \mathbf{E} = -j\omega\mathbf{B} = -j\omega\mu\mathbf{H} \tag{2.9a}$$

$$\nabla \times \mathbf{H} = -j\omega\mathbf{D} + \mathbf{J} = (\sigma + j\omega\epsilon)\mathbf{E} \tag{2.9b}$$

$$\nabla \cdot \mathbf{D} = \rho \tag{2.9c}$$

$$\nabla \cdot \mathbf{B} = 0 \tag{2.9d}$$

If more than one frequency is of interest, the time-varying field quantities may be obtained by first solving Eqns.(2.9) for the phasors and performing the inverse transforms. This is rarely required in antenna problems since the bandwidth is small and modulation causes just a moderate spread of frequencies around the carrier.
Exact theories for antennas accurately formulated as boundary value problems of Maxwell's Equations are rarely available. With the astonishing progress in computing, a third tool Computational electromagnetics (CEM) has come to augment the two classical tools of experimental observation and mathematical analysis. The desirable attributes in a computer model are accuracy, efficiency and utility. From the problem formulation involving facilitating approximations through to the final computation, some of these attributes may be compromised. Hence available methods show some limitations, e.g. surface waves calculations are still elusive and must be handled empirically.
SS

2.3 The Tools

Modelling, simulation, analysis, and design tools are of paramount importance in cost-effective research and development of appropriate antennas

[2]For relativistic purposes MaxwellŠs equations are form-invariant. The constitutive relations are form-invariant when written in bi-anisotropic form [89].

for evolving wireless communications. An accurate computer-aided design could substantially reduce the design-fabrication-test cycle of a new antenna and its feed network. Modifications to an existing design can be electromagnetically modelled and their effect on radiation characteristics determined prior to building a prototype and initiating costly tests. The advantage is obvious especially since technological advances point towards complete monolithic integration in emerging applications with limited provisions for post-fabrication tuning and adjustments. This, coupled with the fact MPAs and ESAs have a small bandwidth of a few percent, makes the use of an accurate EM simulator an imperative in the design and optimization processes.

Since numerical techniques as a rule involve fewer assumptions, they can be more accurate than analytical results [92]. A setback is numerical techniques churn out numbers instead of equations which may give an insight into the problem and perhaps also suggest design guidelines. An analytical background remains indispensable in assessing the credibility of a computer result. There exists a plethora of powerful methods for antenna analysis and design e.g. SPFD [70]. The more established are the Bounded Element Method (BEM), Finite Element Method (FEM), Moment Method (MM) and Finite Difference Time Domain method (FDTD). The last two stand out for robustness and efficiency in handling heterogeneous material. The MM has been in use since the 1960s [36]. Only relatively recently has the potential of the FDTD method [93] for field problems begun to be appreciated. This is therefore a rapidly growing field of interest. Broadly CEM techniques can be classified into two main classes:

- numerical methods for problems where the size of the antenna is of the order of the wavelength to a few tens of wavelength and
- high-frequency or asymptotic methods for problems where the antenna or scatterer is many wavelengths in extent.

A natural classification scheme for the calibre of numerical methods which are of interest in this endeavour is dependent on whether the formulation is based on the integral or differential formulation of Maxwell's equations. Also the classification can be carried out along the lines of the domain in which calculations are performed - time domain and frequency domain techniques. The MM is based on solutions of frequency domain integral equations for the phasor electric or magnetic currents induced on the surface of antennas. The ensuing system of linear equations gives a dense complex-valued impedance matrix and can involve thousands of equations when handling problems of moderate electrical size. Its drawback is therefore the extensive time and memory required for the treatment of the common and important problems involving pulsed excitations and transient phenomena. For such problems requiring data to be evaluated over a range of frequencies, it is

expedient to work in the time domain since data for all frequencies can be generated from a single time-domain run by means of the Fourier transform.

2.4 Finite Difference Time Domain Method

The power and appeal of FDTD lies in the excitation of a structure with a broadband pulse and subsequently obtaining the antenna's complete frequency response from this single calculation by Fourier transform. As such FDTD is well-suited for steady state single-frequency as well as for transient response investigations. Maxwell's curl equations are solved directly in differential form at points on a space grid in the time domain. Sole consideration of the curl equations constitutes no restriction as the divergence equations are contained in them. It requires no matrices implying that moderate computer resources are sufficient to allow robust widespread use of partial differential equation methods. The curl equations are approximated by the method of central differencing. Initially only nearest-neighbour interactions are considered fields farther off being advanced by leapfrogging. At any given time the appropriate boundary conditions on the source, conductors, and mesh walls are enforced.

The truncated problem space is subject to reflections of numerical waves at its faces. These can be minimized by using absorbing boundary conditions (ABC) that absorb much of the scattered wave, simulating energy propagating into infinite space.

A space and time sampling scheme that adequately resolves the fine antenna structure in space and time will account for surface currents, scattering, aperture penetration or cavity excitation and mutual coupling. Hence a wide range of electromagnetic problems can be tackled.

2.4.1 The Yee Algorithm

The essence of FDTD was laid down by Yee in a 1966 paper by employing the method of finite differences as approximations to both the spatial and temporal derivatives that appear in MaxwellŠs curl equations [109].

Discretizing and Sampling

A computation domain in which Maxwell's equations are to be solved at a finite number of discrete locations is defined. Continuous field quantities **E** and **H** are replaced by a finite sequence of sampled values. Choice of a coordinate system commensurate with problem geometry leads to a minimisation of the stair-case error introduced in the process of modelling curved surfaces and edges. Additionally implementation of boundary conditions is convenient. The Yee space lattice has an interlaced mesh for electric and magnetic fields whereby the **E** components are located along the edges of

cells, while the **H** components are positioned at the centers of the cell faces as suggested in Fig. 2.2.

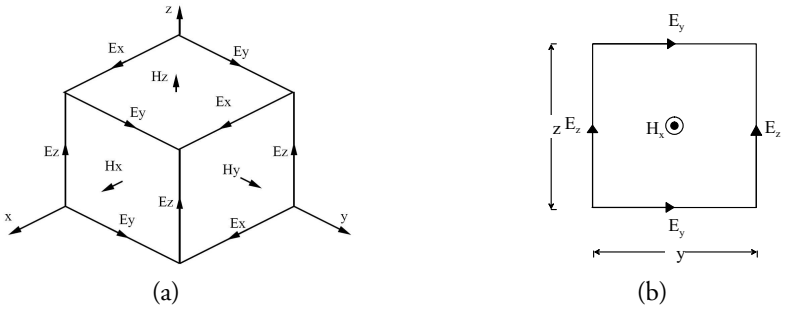

Figure 2.1: *FDTD unit cell: (a) FDTD unit cell of a Cartesian grid. Every field quantity is perpendicular to a face formed by the four field components that enter into the curl computation of the former. (b) Faraday's law for the x component*

The nodes are labeled (i, j, k) corresponding to the mesh point $(i\Delta x, j\Delta y, k\Delta z)$. The $\Delta x,\ \Delta y$ and Δz are the mesh dimensions along each coordinate dimension in a Cartesian grid. Elementary cells are thus cuboid. A recent development is the move from hexahedral to tetrahedral cells with the goal of reducing the stair-case modelling error.

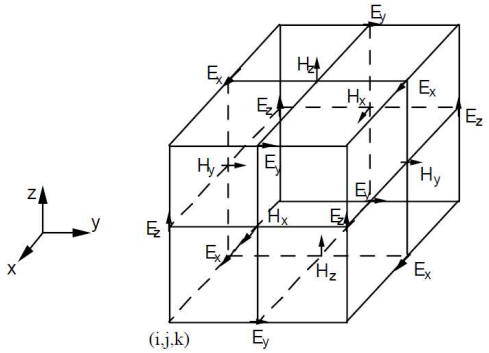

Figure 2.2: *Staggered placement of electric and magnetic field components*

The constitutive parameters for each cell edge may be set independently, thus enabling the treatment of irregular and heterogeneous geometries. The medium in each unit cell is assumed to be piecewise uniform and homogeneous, i.e. constant $\epsilon,\ \mu$ and σ. Average values are employed at a discontinuity, say, at an edge where four different materials meet, $\epsilon = \frac{1}{4}\epsilon_0(\epsilon_{r1} + \epsilon_{r2} + \epsilon_{r3} + \epsilon_{r4})$. The entire problem space is obtained by stacking the cells as shown in Fig. 2.3.

Besides the highly efficient manner in which Maxwell's Equations are discretized in space, the continuity of tangential field components on cell

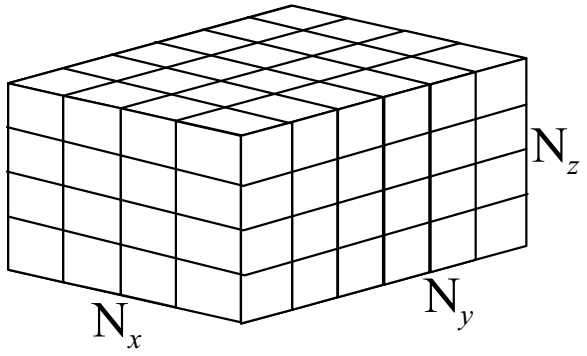

Figure 2.3: *A finite difference 3-D grid in rectilinear coordinates*

faces is automatic. Also in the charge-free case, the divergence of both the **E** and **H** fields implicitly vanishes for the Yee algorithm, as expected [93]. In like fashion, the time derivative is discretized.

Central Differencing

For purposes of exposition, the Taylor series representation of a function $f(x)$ expanded about a point x_0 with elemental offsets of $\pm\delta/2$ reads:

$$f(x_0+\delta/2)=f(x_0)+\frac{\delta}{2}f'(x_0)+\frac{1}{2!}\left(\frac{\delta}{2}\right)^2 f''(x_0)+\frac{1}{3!}\left(\frac{\delta}{2}\right)^3 f'''(x_0)+\ldots \tag{2.10a}$$

$$f(x_0-\delta/2)=f(x_0)-\frac{\delta}{2}f'(x_0)+\frac{1}{2!}\left(\frac{\delta}{2}\right)^2 f''(x_0)+\frac{1}{3!}\left(\frac{\delta}{2}\right)^3 f'''(x_0)+\ldots \tag{2.10b}$$

whereby the primes stand for differentiation. Subtracting (2.10b) from (2.10a) and dividing by δ produces

$$\frac{f(x_0+\delta/2)-f(x_0-\delta/2)}{\delta}=f'(x_0)+\frac{2}{3!}\frac{\delta^2}{2^3}f'''(x_0)+\ldots \tag{2.11a}$$

$$\Rightarrow \left.\frac{df(x)}{dx}\right|_{x=x_0} \approx \frac{f(x_0+\delta/2)-f(x_0-\delta/2)}{\delta} \tag{2.11b}$$

The central difference in Eqn.(2.11b) gives a second-order approximation of the derivative of f. This becomes exact in the limit as δ tends to zero.

Analogously for the temporal case, if the value of an arbitrary function $f(r,t)$, at coordinate $(i\Delta x, j\Delta y, k\Delta z)$ in space and $n\Delta t$ in time is denoted by $f^n(i,j,k)$ then the time derivative of $f^n(i,j,k)$ can be written as

$$\frac{\partial}{\partial t}f^n(j,j,k)=\frac{f^{n+1/2}(j,j,k)-f^{n-1/2}(j,j,k)}{\Delta t}+O(\Delta t^2), \tag{2.12}$$

where $O(\Delta t^2)$ stands for higher order terms. Retaining the first-order terms makes this a second-order approximation. A trade-off between fine sampling (prohibitively large number of cells in mesh $\Rightarrow$ heavy burden on memory) and computer time on one hand and accuracy on the other is fundamental. The method of central differences linearizes Maxwell's curl equations transforming the differential operator into a simple difference.

Leapfrog Marching in Time

The astute choice of field points as illustrated in Fig. 2.2 yields a system of finite difference equations producing a readily implementable scheme seemingly limited only by computer memory and processor speed. Assuming for simplicity that the structure is lossless the Maxwell's partial differential equations Eqns.(2.1a) and (2.1b) may then be written as

$$\nabla \times \mathbf{H} = \epsilon \frac{\partial \mathbf{E}}{\partial t} \tag{2.13a}$$

$$\nabla \times \mathbf{E} = -\mu \frac{\partial \mathbf{H}}{\partial t}. \tag{2.13b}$$

The six unique field components at a node of the unit cell in Fig. 2.2 are ascribed subscript indices i, j, and k. This assignment employs the $\pm 1/2$ space indices to simplify notation thereby rendering the formulas directly implementable on computer. The superscript n stands for time. The first-order approximations to Eqns.(2.13a) and (2.13b) by discrete centered differences means only nearest-neighbour interactions considered.

For instance, for the E_x component one obtains

$$E^{n+1}_{x\,i,j,k} = E^{n}_{x\,i,j,k} + \frac{\Delta t}{\epsilon \Delta y}[H^{n+1/2}_{z\,i,j+1,k} - H^{n+1/2}_{z\,i,j,k}] - \frac{\Delta t}{\epsilon \Delta z}[H^{n+1/2}_{y\,i,j,k+1} - H^{n+1/2}_{y\,i,j,k}] \tag{2.14}$$

The rest of the equations can be obtained in similar fashion by cyclic permutation of the ordered set (xyz) in Eqn.(2.14). They read:

$$E^{n+1}_{y\,i,j,k} = E^{n}_{y\,i,j,k} + \frac{\Delta t}{\epsilon \Delta z}[H^{n+1/2}_{x\,i,j,k+1} - H^{n+1/2}_{x\,i,j,k}] - \frac{\Delta t}{\epsilon \Delta x}[H^{n+1/2}_{z\,i+1,j,k} - H^{n+1/2}_{z\,i,j,k}] \tag{2.15a}$$

$$E^{n+1}_{z\,i,j,k} = E^{n}_{z\,i,j,k} + \frac{\Delta t}{\epsilon \Delta x}[H^{n+1/2}_{y\,i+1,j,k} - H^{n+1/2}_{y\,i,j,k}] - \frac{\Delta t}{\epsilon \Delta y}[H^{n+1/2}_{x\,i,j+1,k} - H^{n+1/2}_{x\,i,j,k}] \tag{2.15b}$$

$$H^{n+1/2}_{x\,i,j,k} = H^{n-1/2}_{x\,i,j,k} + \frac{\Delta t}{\mu \Delta z}[E^{n}_{y\,i,j,k} - E^{n}_{y\,i,j,k-1}] - \frac{\Delta t}{\mu \Delta y}[E^{n}_{z\,i,j,k} - E^{n}_{z\,i,j-1,k}] \tag{2.16a}$$

$$H^{n+1/2}_{y\,i,j,k} = H^{n-1/2}_{y\,i,j,k} + \frac{\Delta t}{\mu \Delta x}[E^{n}_{z\,i,j,k} - E^{n}_{z\,i-1,j,k}] - \frac{\Delta t}{\mu \Delta z}[E^{n}_{x\,i,j,k} - E^{n}_{z\,i,j,k-1}] \tag{2.16b}$$

$$H^{n+1/2}_{z\,i,j,k} = H^{n-1/2}_{z\,i,j,k} + \frac{\Delta t}{\mu \Delta y}[E^{n}_{x\,i,j,k} - E^{n}_{x\,i,j-1,k}] - \frac{\Delta t}{\mu \Delta x}[E^{n}_{y\,i,j,k} - E^{n}_{y\,i,j-1,k}] \tag{2.16c}$$

Hence fields at a time $(n + p/2)\Delta t$ with $p \in \{1, 2\}$ may be solved in terms of fields at an earlier time $(n - q/2)\Delta t$ with $q \in \{0, 1\}$ in keeping with the above. A leapfrog time-stepping approach for alternately updating the electric field and magnetic field is immediately apparent. Eqns.(2.14) and (2.15) spell out how to advance the electric field in time while Eqns.(2.16) apply for the magnetic field. Fields are alternately advanced till either a specified maximum number of pulses is reached or a user-prescribed termination condition is met. The ideal termination condition is the steady state when the energy in the domain has decayed beyond numerical noise. To ease the burden on memory resources, one of the fields, say **E** is stored only at time instances $n \pm 1$ with the **H** field being defined at offset time instances $n \pm 1/2$.

Inhomogeneities and Lossy Materials

In the foregone as in the original formulation of FDTD assumption was made of a lossless homogeneous medium. Practically relevant material of finite conductivity σ can be treated by adding considering a conduction-current term in Ampère's law:

$$\nabla \times \mathbf{H} = \frac{\partial \mathbf{E}}{\partial t} + \sigma \mathbf{E} \tag{2.17}$$

Proceeding as before the update equation for E_x is found to be

$$\begin{aligned} E^{n+1}_{x\,i,j,k} = \frac{1 - \frac{\sigma\Delta}{2\epsilon}}{1 + \frac{\sigma\Delta t}{2\epsilon}} E^{n}_{x\,i,j,k} + \frac{\frac{\Delta t}{\epsilon\Delta y}}{1 + \frac{\sigma\Delta t}{2\epsilon}} \left[H^{n+1/2}_{z\,i,j+1,k} - H^{n+1/2}_{z\,i,j,k} \right] \\ - \frac{\frac{\Delta t}{\epsilon\Delta z}}{1 + \frac{\sigma\Delta t}{2\epsilon}} \left[H^{n+1/2}_{y\,i,j,k+1} - H^{n+1/2}_{y\,i,j,k} \right]. \end{aligned} \tag{2.18}$$

Similarly the magnetic conduction current is assumed proportional to a magnetic conductivity σ_m and the magnetic field modifying Faraday's law to read

$$\nabla \times \mathbf{E} = -\mu \frac{\partial \mathbf{H}}{\partial t} - \sigma_m \mathbf{H}. \tag{2.19}$$

The update equation for the magnetic field reads

$$\begin{aligned} H^{n+1/2}_{x\,i,j,k} = \frac{1 - \frac{\sigma_m\Delta t}{2\mu}}{1 + \frac{\sigma_m\Delta}{2\mu}} H^{n-1/2}_{x\,i,j,k} + \frac{\frac{\Delta t}{\mu\Delta z}}{1 + \frac{\sigma_m\Delta}{2\mu}} \left[E^{n}_{y\,i,j,k} - E^{n}_{y\,i,j,k-1} \right] \\ - \frac{\frac{\Delta t}{\mu\Delta y}}{1 + \frac{\sigma_m\Delta}{2\mu}} \left[E^{n}_{z\,i,j,k} - E^{n}_{z\,i,j-1,k} \right] \end{aligned} \tag{2.20}$$

Analogously expressions for E_y, E_z, H_y and H_z fall out by cyclic permutation from Eqns.(2.18) and (2.20), respectively. For brevity they are not stated. When σ and σ_m tend to zero Eqns.(2.18) and (2.20) reduce to the previous update equations Eqns.(2.15) and (2.16), as expected.

2.4.2 Excitation

An infinite variety of waveforms for the feed such as the sine wave, a plane wave and user-defined forms is possible, but the Gaussian pulse is preferred except when strongly frequency-dependent materials are included, in which case a smoothed cosine pulse is more advantageous [57].

A Gaussian pulse is Fourier invariant and can therefore provide on a single run frequency-domain information from dc to the desired cut-off frequency. The pulse width depends on the frequency range and results are most accurate for the centre frequency. The absence of zeroes in the signal spectrum allows the calculation of scattering parameters over the entire frequency band of the Gaussian pulse.

The Gaussian pulse and its derivative are given by

$$f(t) = \frac{1}{\sqrt{2\pi}\zeta} \exp^{-\frac{(t-\nu)^2}{2\zeta^2}} \tag{2.21a}$$

$$f'(t) = -\frac{(t-\nu)}{2\pi\zeta^3} \exp^{-\frac{(t-\nu)^2}{2\zeta^2}} \tag{2.21b}$$

where ν is the mean and ζ^2 the variance.

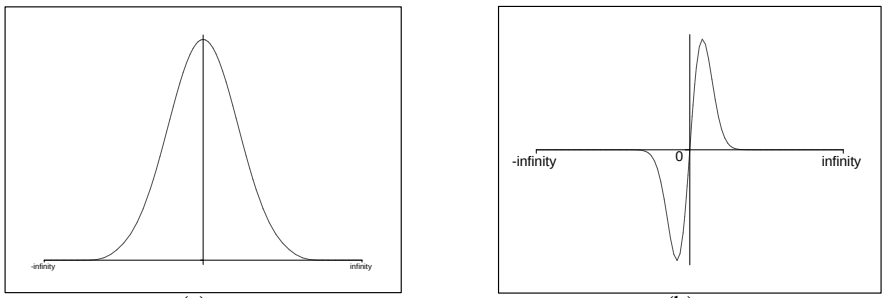

(a) (b)

Figure 2.4: *Two sample Gaussian excitation signals: (a)A Gaussian excitation ensures that a mesh with proper sampling can be created at all stimulated frequencies. (b) The Gaussian monopulse, negative first derivative of Gaussian. The absence of dc leads to a shorter computer time.*

2.4.3 Stability

To be meaningful, the leapfrog scheme must yield predictions that approximate the exact solutions of the hyperbolic partial differential equations arising from Maxwell's equations. The predictions must converge to the exact solution as the spatial grid, Δx,Δy, Δz and temporal grid, Δt, tend to zero.

However as leapfrogging proceeds, numerical dispersion may trigger results that rapidly increase without bound in the time domain and have phase errors in the frequency domain. Finiteness of energy requires that bounded input yield bounded output in physical systems. The maximum distance energy can travel in one time step is limited to $c\Delta t$, where c is the speed of light in free space. To eliminate the non physical event of energy propagating faster than light, an upper bound for Δt is given by the Courant Stability condition [93]:

$$c\Delta t \leq \frac{1}{\sqrt{\frac{1}{(\Delta x^2)} + \frac{1}{(\Delta y^2)} + \frac{1}{(\Delta z^2)}}}$$

This ensures that in one time step any wavefront does not go beyond its immediate neighbours. Hyperbolic partial differential equations modelled with an explicit differencing scheme possess conditional stability [54; 57].

2.4.4 Accuracy and Computer Time

The easily implemented leapfrog method described in the preceding sections is accurate to second order. Fineness of gridding is telling on accuracy. A guideline for good accuracy is that the side of each cell should not exceed $\frac{\lambda}{10}$ at the highest frequency of interest. The combination of high conductivity and nonlinearity favours the occurrence of the numerical dispersion effects, oscillations and noise in the FDTD results. To minimize these, the mesh points per minimum wavelength may be increased. Clearly object size in wavelengths is proportional to the number of cells and the amount of computer memory required. The number of cells in turn determines the number of time steps needed for the transient fields to die away or equivalently, attain steady state. The largest time step is theoretically only limited by the desired accuracy of the solution, time and computing power available. This implies FDTD is limited for extremely low frequencies at which resolving the fine structure of objects would require millions of time steps. For such situations other methods, such as finite elements, are preferable.

2.4.5 Variable mesh

Large heterogeneous structures pose a severe strain on resources. There might be a region of the object in which smaller unit cells are needed, for example, a region of high permittivity, or of tiny features such as the feed and thin sheets. A sub-gridding only on and possibly in the vicinity of the "thin"

element is needed while maintaining a coarser grid otherwise is economical. Non-uniform and non-orthogonal grids are expedient in these cases [86; 105]. Achievable ratios of coarse-to-fine grid sizes exceeding ten have been reported. In [105] a technique is presented that uses a weighted current value from the coarse region at the boundary with the fine-grid regions to update the fine-region tangential fields. The weighting function depends on the material properties and the relative position of the fine-region within the current contour at the boundary. Highly obtuse or highly acute angles in non-orthogonal schemes lead to asymmetric and ill-conditioned projection matrices which cause numerical instability [25].

2.4.6 Grid Termination

The leapfrogging scheme fails at the outermost walls of the grid for lack of neighbours. The formulation of ABCs beginning with Mur's in 1981 [69] may be considered to have rekindled interest in Yee's FDTD algorithm. ABCs minimize reflections from the grid truncation and so simulate an outgoing travelling wave propagating in an unbounded medium. Use of the Mur boundary condition has waned in favour of Berenger's Perfectly Matched Layer (PML), proposed in 1994 to absorb without reflection the electromagnetic waves at the extremities of the domain[7]. Its split-field formulation causes an increase in computational complexity and memory requirements for the FDTD simulation. Intense research has lead to implementations without recourse to field splitting. The details of such numerical implementation of the proposed perfectly matched absorbers are addressed elsewhere, e.g.[110].

2.5 Finite Integration Technique

A flavour of FDTD using Maxwell's equations in integral form instead is the Finite Integration Technique (FIT). These equations are transformed onto a dual grid in which the FIT state variables, electric and magnetic grid voltages and fluxes are defined as the integrals of the electric and magnetic field vectors over faces and edges of the computational grid [100][101]. The integration scheme relies on space and time stability resulting in energy and charge conservation as well as stability in long term calculations [87]. This is the foundation of the here employed EM simulator CST MICROWAVE STUDIO®.

2.5.1 Maximum number of pulses

The maximum simulation time is calculated from the product of a given maximum number of pulses and the pulse width of the excitation; see section 2.4.2. The simulation should ideally be completed before this time if

a user-defined steady state condition is met. This test considers the energy decay and also the decay of the port mode amplitudes.

2.5.2 Perfectly Matched Layers

Wavefronts increasingly approximate plane waves the farther afield they travel. Consequently better absorption of the outward travelling waves can be expected the greater distance between the antenna structure and the outer boundary. However, a large distance places extra strain on resources. The default setting for the minimum distance to the structure is five meshlines or an eighth of the smallest wavelength and can be increased especially if high accuracy is required. The distance depends on the geometry and materials used. Too short a distance may cause instabilities and inaccuracies since some field modes required for an accurate solution may be absorbed [110].

2.5.3 Boundary Conditions

Radiation and scattering cross-section results are very sensitive to unwanted reflections from the outer absorbing boundaries of the FDTD space. An adequate distance in the order of ($\geq \lambda/4$) must be maintained between the scatterer and the outer boundary. Depending on the geometry the following sort of boundaries can be implemented: perfectly electrically and perfectly magnetically conducting. For radiation problems the *open* and *open add space* boundaries are imperative.

The best way to predict the future is to invent it.

Anon

3

Candidates for Directed Radiation at 24 GHz for Ubiquitous Systems

The Stakes

IT IS LEGITIMATE to assume modules to be found at the same height in realistic communication scenarios so that it makes sense to direct radiation primarily towards the horizon, but not upward into the sky nor particularly downward. In this chapter a look will be taken at means of generating directed radiation for ranges up to one meter. The *e-Grains* offer very limited space for antennas, thereby demanding very short-wavelength (i.e. very high-frequency) transmission which incurs high attenuation losses. At 24 GHz there exist significantly fewer *co-located* technologies that will compete for channel access and generate throughput-reducing interference. Going up to 24 GHz sacrifices a measure of range in return for coexistence. More importantly the fundamental fact that directivity is proportional to antenna electrical size makes the journey to high frequencies for the realization of small 1 cm^2 system or feature size a worthwhile endeavour.

3.1 An Argument for higher Frequencies

Expensive licenses are an indication that the radio spectrum is a scarce resource that must be allocated to several applications and systems e.g. UMTS license auction in the late nineties of the last century. This places a limit on the number and bandwidth of radio channels and calls for a judicious use of bandwidth. As the intensity of radio frequency signals in the air grows, raising the strength of radio signals for a sufficiently high SNR over the electromagnetic background noise alone is not tenable on grounds of an increased burden on power supply, elevated heat dissipation and the additional interference. Bandwidth increases with frequency thus providing a measure of tolerance in design and manufacture. Furthermore, a plaidoyer for upper spectrum bands as candidates for future wireless applications is buttressed by the prospect of:

- a short wavelength (a few mm) means that directional beams can be generated with antennas only a few centimetres in width and components have convenient sizes;
- resulting narrow point-to-point radio beams increase the potential of more frequent spectrum reuse (increased spectral efficiency);

In the face of extreme spectrum shortage in the lower L and S band, clearance was given for telecommunications of a *local nature* in the 24 GHz ISM bands [52]. The stipulation that the RF-radiation be local in nature is easily met because the limited radiated power and increased path loss at these higher frequencies restricts range. Indeed it may be argued that the shorter range means both smaller frequency-reuse distances and less interference; range not being a major concern in the clustered multi-hop AVM topography. Higher frequencies are synonymous with higher bit rates. An increase in bit rate results in shorter packet transmission times. The module therefore accesses the airwaves less often and for shorter time slots for a given amount of information. Additionally, shorter packets are statistically less susceptible to interference from other systems meaning fewer collisions thus fewer requests for repeat transmission. The paucity of energy in the AVM scenario is a clarion call for every energy-saving measure and the move to a higher frequency is doubtless such a measure. However, a trade-off seems unavoidable because firstly the power that can be generated falls off with increasing frequency and secondly the power received is proportional to λ^2 or $\frac{1}{f^2}$.

3.2 The Evolution of Antennas

The antenna as a specialized transducer converting energy in free-space electromagnetic waves to alternating electric currents in circuits or viceversa is a key component in any wireless communications system. The optimum antenna for a given situation depends among others notably on the communications frequency, the desired range and available power and space. The antennas in the pioneering works of Hertz and Marconi at the turn of the 19^{th} century were resonant in nature and therefore highly frequency dependent. Ever since frequency-independent antennas whose geometry is described by angular relationships rather than lengths and widths as well as broadband antennas, the defining feature of which is a smooth transition from feed to arms have emerged. Abrupt changes in the geometry are painstakingly avoided through diligent tapering, flaring, rounding, etc. as pictorially hinted in Fig. 3.1. An historical overview illustrating some key design paradigms and exotic shapes of broadband antennas such the volcano smoke, the infinite biconical and spherical dipole antennas *inter alia* is presented in [82].

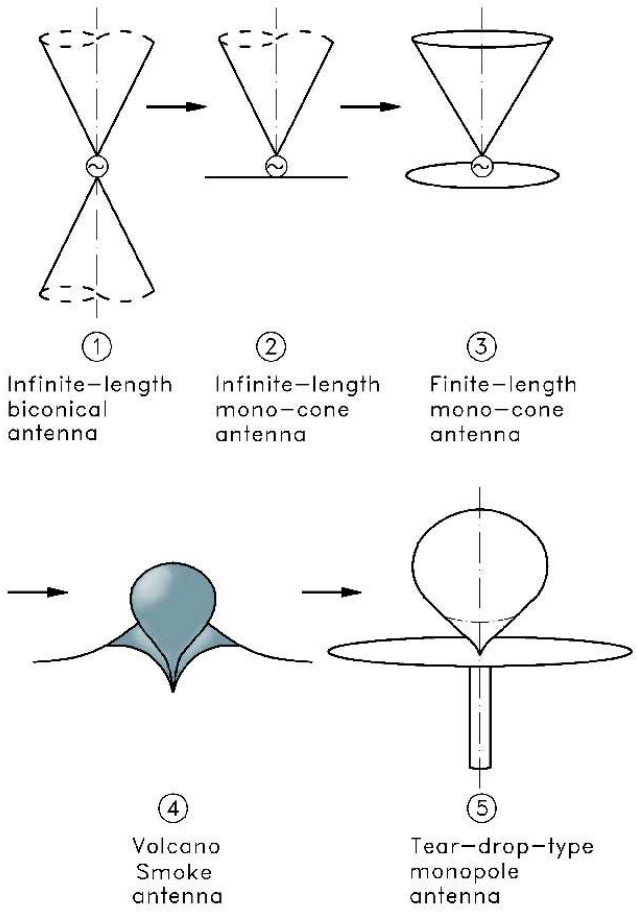

Figure 3.1: *An example of the evolution of antennas: the UWB tear-drop antenna.*

Driven by a myriad of concerns amongst which are frequency crowding, bandwidth shortage, the craving for higher throughput and last but not the least, certain aesthetic motives, there is an ever increasing drive to miniaturisation. The overriding question is how far can this go without overly compromising capacity and performance. The capacity of wireless systems today ranges from about ca. 50 kbps to 1.5 Mbps and stands a tall order from the pioneering Morse Code transmission of letter 's' in December 1901. It is estimated that half of all business and personal communications will be wireless by the year 2010 [1]. Phenomenal growth is taking place with other wireless systems such as Direct Broadcast Satellite Television, Wireless Local Area Networks, paging systems, Global Positioning System, Radio Frequency Identification systems etc. With the ubiquity of wireless systems on the rise, there is urgent need for antenna designs that are small, unobtrusive, light, cheap and conformal yet radiate efficiently. The talk is about antennas that do not quite look like antennas.

3.2.1 One eGrain, Two Antennas

The necessity for an isotropic broadcast-type radiation pattern for the case of wake-up where no *a priori* knowledge of position and orientation of other *eGrains* is available has been examined elsewhere [4; 44; 67]. An altogether different situation obtains once an AVM-Module is *awake* and communication with others is to be initiated. In case of antenna coincidence, frugality dictates the preferential use of the line-of-sight path over those of reflection or diffraction. Hence for wake-up and communication two diametrically opposed radiation philosophies are called for. It is well known that the directivity of an antenna is directly proportional to its electrical size. The suitability of dielectric materials to electrically increase the size of the antenna based on the smaller velocity of propagation, $c = \frac{c_0}{\sqrt{\epsilon_r \mu_r}}$ has been used to great effect. The losses associated with dielectrics make their use critical in low energy applications.

3.2.2 Do Arrays Stand a Chance?

Arrays can be used to produce highly directional radiation patterns which give the level of performance of a large antenna at a fraction of the space. Thus the question arises as to how suitable arrays are under the prevailing conditions of space and power allocated for AVM. Array action is founded on the interaction of two or more waves passing the same locus in spacetime. The waves may add in phase, producing a larger peak than any single wave. Conversely they may add out of phase, resulting in a smaller effect than an individual wave alone. The reinforcement and cancellation so described are termed constructive and destructive interference, respectively. For purposes of exposition, the interference of two monochromatic waves described by the following wave functions

$$\mathbf{E}_1 = \mathbf{A_1} \exp^{-j(\mathbf{k}.\mathbf{r_1}+\phi_1)}$$

and

$$\mathbf{E}_2 = \mathbf{A_2} \exp^{-j(\mathbf{k}.\mathbf{r_2}+\phi_2)}$$

is considered. The complex vector phasor for the amplitude is

$$\mathbf{A}_\nu = A_{\nu,x} \exp^{j\phi_x} \hat{x} + A_{\nu,y} \exp^{j\phi_y} \hat{y} + A_{\nu,z} \exp^{j\phi_z} \hat{z}$$

where $\nu \in \{1, 2\}$ and

$$\mathbf{k} = k_x\hat{x} + k_y\hat{y} + k_z\hat{z}$$

is the wave vector. The superposition of both waves gives

$$\mathbf{E} \quad = \quad \mathbf{E}_1 + \mathbf{E}_2 = \mathbf{A_1} \exp^{j(\mathbf{k}.\mathbf{r_1}+\phi_1)} + \mathbf{A_2} \exp^{j(\mathbf{k}.\mathbf{r_2}+\phi_2)} \qquad (3.1)$$

$\mathbf{E}^*$ being the complex conjugate of $\mathbf{E}$, the magnitude of the resultant wave is given by

$$\begin{aligned} |\mathbf{E}|^2 &= \mathbf{E}\cdot\mathbf{E}^* = A_1^2 + A_2^2 + A_1A_2\exp^{j[k(r_1-r_2)+(\phi_1+\phi_2)]} + A_1A_2\exp^{-j[k(r_1-r_2)+(\phi_1-\phi_2)]} \\ |\mathbf{E}|^2 &= A_1^2 + A_2^2 + 2A_1A_2\cos[k(r_1-r_2)+(\phi_1-\phi_2)] \end{aligned} \tag{3.2}$$

Space and Feed

As shown in the term in square brackets in Eqn. (3.2), the phase of the resultant is seen to be determined by the spatial separation between sources and the initial phases of the sources. Letting $\delta = k(r_1-r_2)+(\phi_1-\phi_2) = k\Delta r + \Delta\phi$ and assuming both waves to have the same amplitude A_0, Eqn.(3.2) can be simplified to

$$|\mathbf{E}|^2 = 2A_0^2 + 2A_0^2\cos\delta = 4A_0^2\cos^2\frac{\delta}{2}. \tag{3.3}$$

Thus two identical sources separated by some distance d can superimpose in phase to yield double amplitude and quadruple power, and superimpose 180° out of phase to yield zero amplitude and zero power. Intermediate values are obtained as the value of δ sweeps between 0 and 180°. Constructive interference with maximum reinforcement occurs when

$$\cos\frac{\delta}{2} = 1 \quad i.e. \quad \delta = m\pi \quad \forall \ \ m\in\mathbf{Z} \tag{3.4}$$

$$\Delta r = \frac{2\pi m - \Delta\phi}{k}. \tag{3.5}$$

Likewise total cancelation obtains for the following conditions

$$\cos\frac{\delta}{2} = 0 \quad i.e. \quad \delta = (2m+1)\pi \quad \forall \ \ m\in\mathbf{Z} \tag{3.6}$$

$$\Delta r = \frac{(2m+1)\pi - \Delta\phi}{k}. \tag{3.7}$$

Besides arrays, lenses as collimators and reflectors are commonly used to achieve the desired antenna directional characteristics but their material and space requirements preclude them for the present application. The amplitudes and phases of the currents with which individual array elements are driven may in general be different. Let each element i in an $N-$element array be driven by current a_i producing the electric field $a_i\mathbf{E}_i(\theta,\phi)\exp^{-j(\mathbf{k}\cdot\mathbf{r_i})}$ at position $\mathbf{r_i}$. The total electric field in the direction (θ,ϕ) at that distance $\mathbf{r}$ is:

$$\mathbf{E}(r,\theta,\phi) = \sum_{i=1}^{N} a_i\mathbf{E}_i(\theta,\phi)\exp^{-j(\mathbf{k}\cdot\mathbf{r_i})}. \tag{3.8}$$

In most cases all elements are identical and oriented in the same way and the analysis is then fairly straightforward since the *element factor* $\mathbf{E}_i(\theta,\phi) = \mathbf{E}(\theta,\phi) \ \ \forall \ \ i$. Taking this constant out of the summation yields

$$\mathbf{E}(r,\theta,\phi) = \mathbf{E}(\theta,\phi)\cdot\sum_{i=1}^{N} a_i\exp^{-j(\mathbf{k}\cdot\mathbf{r_i})} \tag{3.9}$$

The ability to control the phase of the driving current in each element of the array admits of electronic scanning of the main beam. This is the blueprint for beam forming by pattern multiplication of the element factor $\mathbf{E}(\theta, \phi)$ by the array factor $\sum_{i=1}^{N} a_i \exp^{-j(\mathbf{k}\cdot\mathbf{r_i})}$. The array factor characterizes the spatial distribution of radiating elements, the amplitudes and phases of the currents with which they are excited.

3.2.3 Mutual Coupling

Cramming elements in a fixed length may lead to large magnitudes and too rapid an excitation phase variation such that adjacent elements have currents in antiphase. In numerical calculations superdirectivity obtains only at the cost of excessive feed currents and adherence to stringent tolerances [108]. For a realizable (non-superdirective) gain, the highest mode number should be less than or equal to the electrical size *ka* of a spherical surface enclosing the antenna [13; 35; 37]. The mutual impedance is comparable in the worst case to the input impedance of the element for free space separations of ca. $\frac{\lambda}{2\pi}$. This coupling between individual array elements is exacerbated when these share the same substrate. A too small inter-element spacing compounds this problem as the interaction of higher order modes (usually evanescent) of rapidly varying phase at edge discontinuities impacts adversely on array action.

Placing array elements out of each otherŠs near-field in order to curb mutual coupling cannot be realized since at 24 GHz the AVM-Module dimension is merely 0.8λ. Apart from dielectric losses, use of high dielectric-constant substrates in arrays leads to particularly severe scan blind spots due to surface-wave effects [75]. For space reasons the elements ought to be as close together as possible. Though isolated resonant size elements (dipoles) have coupling in the H-plane that decreases as $1/r^2$, and $1/r$ in the E-plane[104], Hannan *et al* [16; 33] have shown that in an array the coupling decay becomes asymptotic to $1/r^2$. Mutual coupling thus imposes a lower bound on how close elements can be placed. On the other hand, there is an upper bound in view of the scan-blindness problem in planar array elements separated by more than one wavelength manifested in grating lobes. Cavity-backed slots possess small mutual effects thus offer the possibility of isolating one radiating element from another. Their drawback is the need for a ca. $\frac{\lambda_H}{4}$ long feed cavity (Fig.3.3(b)), broached upon in section 3.2.4. The number of elements in an array varies inversely with the square of the beamwidth i.e. narrow beamwidths require long or many-element arrays and there must be many of these to be able to offer meaningful coverage. In light of this, the proven beam synthesis technique through pattern multiplication cannot be carried out. In the following a brief look is taken at candidate antenna structures for the AVM application.

3.2.4 Integrated Slot Concepts

A slot is attractive for being flush-mountable, small and light. A slot in a ground plane of infinite extent is complementary to a dipole in free space. In an extension and generalization of BabinetŠs principle taking into account the vector nature of the electromagnetic field, Booker showed the patterns and impedances of a slot (magnetic dipole) can be obtained from the well-known properties of their complementary structure, the electric dipole. Both have an omnidirectional doughnut radiation pattern with interchanged electric and magnetic fields. The geometric

mean of the input impedance of a slot, Z_s and that of its complementary dipole, Z_d is equal to half the intrinsic impedance of free space [8] [9], i.e.

$$Z_s = \frac{Z_0^2}{4Z_d} \tag{3.10}$$

To effectively radiate a slot must be resonant so that antenna impedance is pure real since a reactive component causes large reflections in the line. In this connection the long dimension of a resonant slot is nearly a half wavelength, and the transverse dimension a small fraction of this making the perimeter nearly a wavelength.

A realistic resonant $\frac{\lambda}{2}$-dipole of length-to-diameter ratio $\frac{L}{D}$ of 100 and shortened to 0.475λ to tune out its inductance has a terminal resistance of 67 Ω. It is electrically equivalent to a strip of the same length and a width equal to $w = 2D$ [56]. By Eqn. (3.10) the terminal impedance of the complementary slot to this dipole strip is

$$Z_s = \frac{(120\pi)^2}{4 \cdot 67} = 530 + j0\Omega$$

Irrespective of excitation the electrical field distribution in a slot is sinusoidal. The requisite boundary conditions for the first resonant mode are satisfied by an electric field vector perpendicular to the long dimension of the slot and having its maximum at the centre and zero at the ends. Such a field distribution is suggestive of a rectangular wave-guide feed in the TE10 mode where for single-mode operation, the long dimension satisfies $0.5\lambda < b < \lambda$.

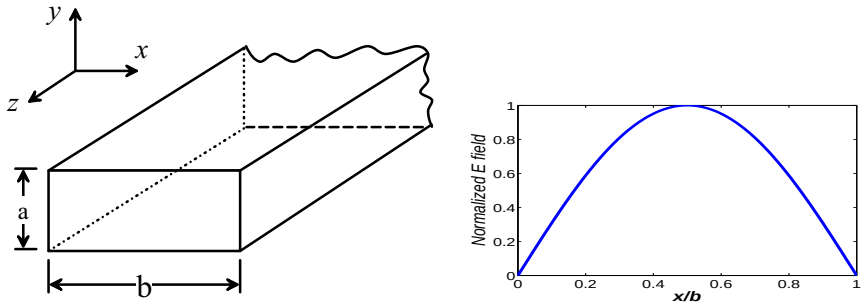

(a) Slot viewed as a rectangular waveguide opening

(b) E field across slot in TE_{10} Mode

Figure 3.2: *The slot and its aperture distribution for the fundamental resonant mode.*

For efficient coupling between the TEM mode on a coaxial cable and the TE_{10} mode in the waveguide section, a probe to strongly excite a transverse electric field in the centre of the waveguide is inserted between the broad walls (Fig. 3.3).

The distance between the probe and the short-circuited cavity rear wall is chosen to be approximately $\frac{\lambda_H}{4}$, which allows the TE_{10} mode launched backwards to reflect off the short circuit undergoing a phase reversal. With a further 180° phase change from the path difference of $\frac{\lambda_H}{2}$, it arrives in phase with the mode launched towards the right. The field may be calculated from an equivalent magnetic current given by

$$\mathbf{M} = -\hat{\mathbf{n}} \times \mathbf{E}$$

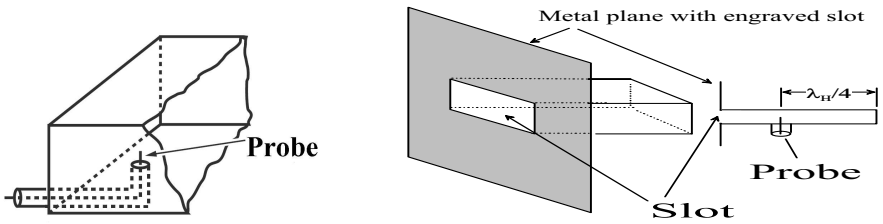

(a) Excitation cavity with coaxial cable to RWG transition.

(b) Cavity-backed slot: front and side views.

Figure 3.3: *Cavity-coupling system to launch the fundamental in a Slot radiator.*

lying along the length of the slot. This yields radiation nulls along the slot axis while maximum radiation takes place in all directions normal to the slot, hence a *doughnut* pattern; see Fig. 3.4(a). Wider beams in the principal E-plane are observed compared to the H-plane as shown in Fig. 3.4(b).

This may be explained by the fact that the electric field shows a half-sine variation along the slot length (H-plane) but drops abruptly from a constant value across slot width (E-plane) to zero on the metal edges (as the field lines terminate on surface charges). The finiteness of the metal plane and the presence of the feed at the back together mean the slot radiates preferentially in one half-space, hence the deviation from the ideal doughnut shape. In contrast to a waveguide feed, a probe feed allows easy adjustment of the resistance with minimum frequency dependence by moving along the slot. A match to 50 Ω is effected with a feed located 0.05λ from an end. Under more auspicious space conditions a balun can be used to transform the input impedance in the ratio of 10:1 and obtain symmetrical excitation at the same time. Alford and Dorne suggest an approach to treat the dependence of the radiation pattern of a slot on the shape and size of the metallic surface in which it is milled by assuming that the field arises from three sources, one at the slot proper of amplitude $1\sin(\omega t)$ and two at the edges of the plane of strength $k\sin(\omega t - \delta)$, where $k \ll 1$ and δ is the phase difference arising from the spatial separation of both edges relative to the slot source [2] in [56, pp. 310].

At a sufficiently far observation point, P in the direction ϕ (Fig. 3.5), the normalized electric field is

$$\mathbf{E} = \sin(\omega t) + k(\sin(\omega t - \delta + \Lambda) + \sin(\omega t - \delta - \Lambda)) \tag{3.11}$$

$$\mathbf{E} = (1 + 2k\cos\delta\cos\Lambda)\sin\omega t - (2k\sin\delta\cos\Lambda)\cos\omega t \tag{3.12}$$

where $\Lambda = \left(\frac{\pi}{\lambda}\right) L\cos\phi$ Hence the modulus of $\mathbf{E}$ can be determined:

$$|\mathbf{E}| = \sqrt{(1 + 2k\cos\delta\cos\Lambda)^2 + (2k\sin\delta\cos\Lambda)^2} \tag{3.13}$$

Considering that the amplitude of the edge sources is appreciably smaller that the source at the slot ($k \ll 1$), the modulus of $\mathbf{E}$ can be further simplified to

$$|\mathbf{E}| = \sqrt{(1 + 4k\cos\delta\cos\Lambda)}. \tag{3.14}$$

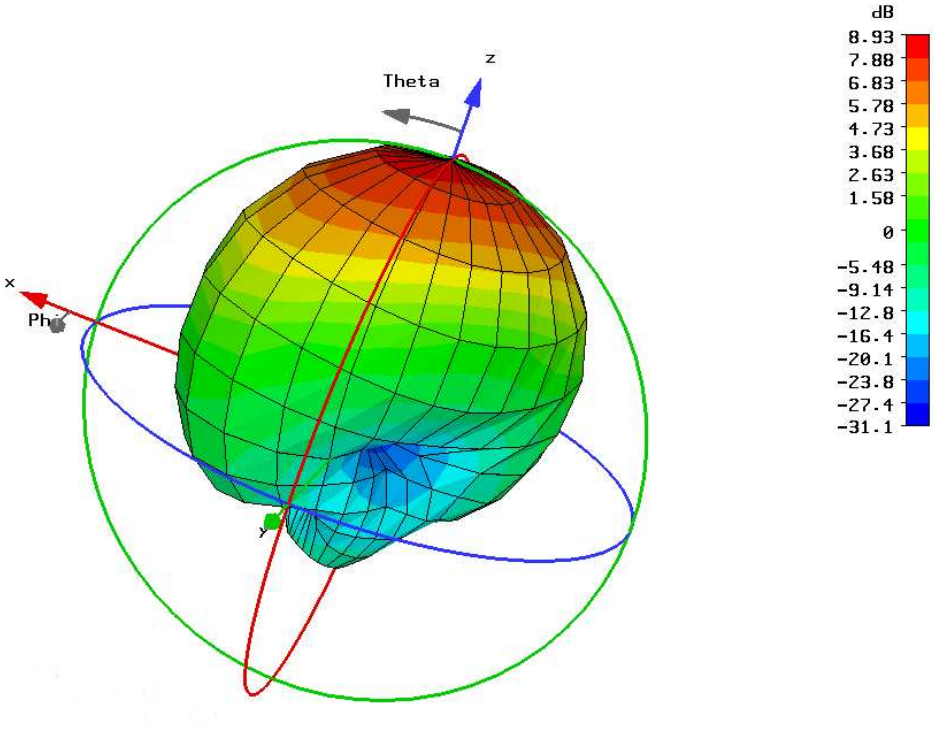

(a) Radiation pattern with nulls along slot axis.

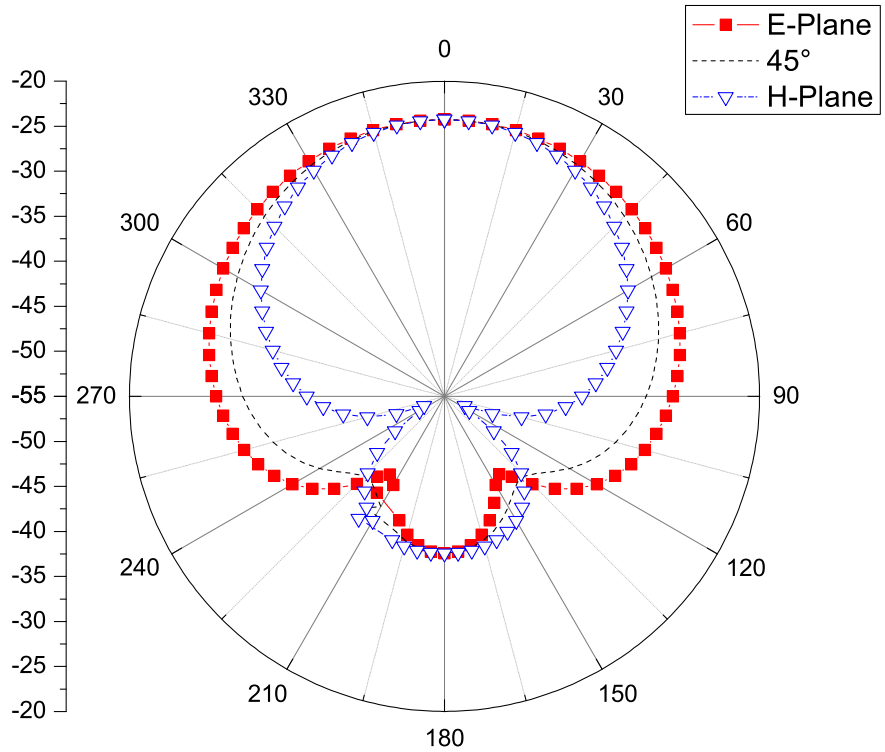

(b) Gradual electric field variation produces lower sidelobe levels in H-plane.

Figure 3.4: *3-D and polar pattern of cavity-backed slot.*

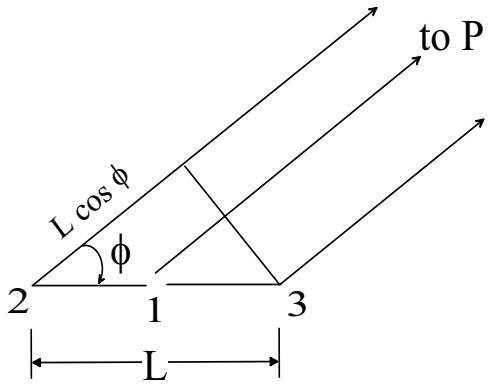

Figure 3.5: *Pattern may be explained with the aid of two additional sources placed at plane edges.*

To determine the position of relative maxima and minima, the value of path difference is set equal to a half wavelength $\Lambda = n\pi$, i.e.

$$\Lambda = \frac{\pi}{\lambda} L \cos\phi = n\pi \tag{3.15}$$

where n is an integer. Thus

$$\cos\phi = \frac{n\lambda}{L} \qquad and \tag{3.16}$$

$$\phi = \cos^{-1}\frac{n\lambda}{L} \tag{3.17}$$

It is seen from 3.16 that the locations of maxima and minima are independent of k and δ. On the assumption that $\cos\delta$ is positive, then maxima correspond to even values of n and the minima to odd ones.

Sector Slots

A thin parallel plate waveguide is partitioned into four sectors by two intersecting conducting strips running along the diagonals as shown in Fig. 3.6(a). Each of the so formed sectors is fed by a coaxial probe and its radiation mechanism is that of the well-known sector antennas. Its high aspect ratio makes it particularly attractive as a low-profile solution. Change of direction of radiation would easily be carried out by electronic switching. As evidenced in Fig. 3.6(b) the metal strip cannot adequately shield the sectors so far as the feeds share the same substrate. The given dimensions correspond to operation in the neighbourhood of cut-off where the wave is considerably attenuated over relatively short distances. This and the small aperture size explain the moderate efficiency and a front-to-back ratio of 8.0 dB.

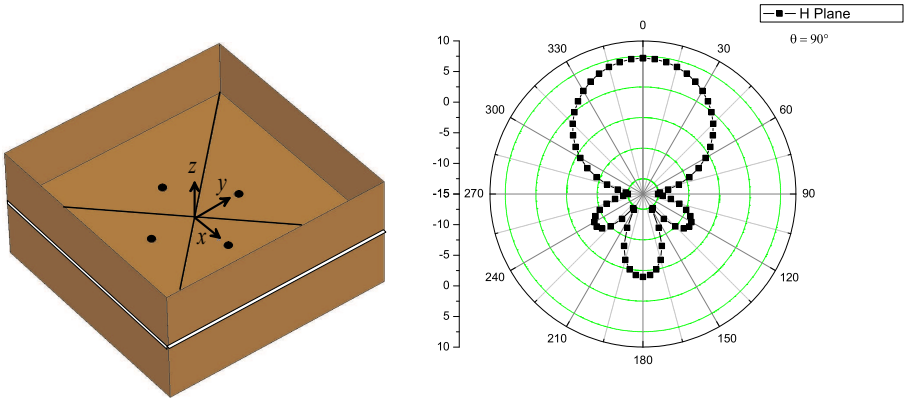

(a) Integrated slot sectorized for azimuth coverage.

(b) Radiation pattern for H-plane ($\theta = \pi/2$) for a single excited sector.

Figure 3.6: *Schematic of four-sector concept. Inefficient wave detachment and pronounced coupling into unexcited sectors leads to moderate front-to-back ratio.*

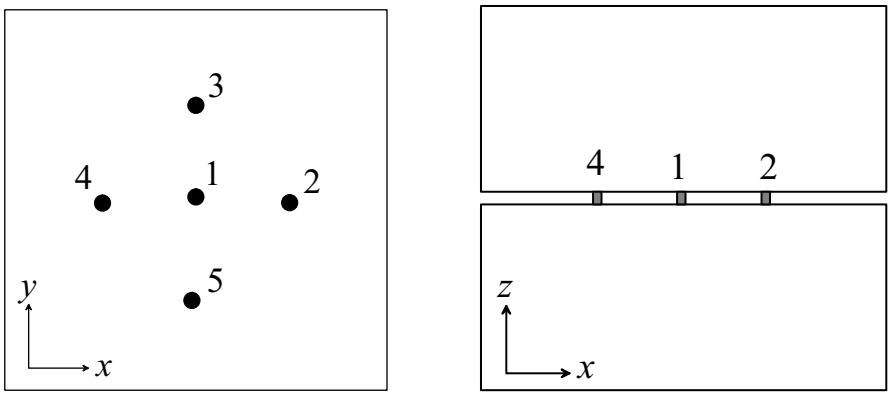

(a) (b)

Figure 3.7: *Circular array of probes in parallel plate waveguide opening into slot: (a) Top view.(b) Side view of quasi-Yagi array.*

Circular Array

A variant of the radiator in the preceding section having the prospect of offering greater flexibility in beam steering consists of a circular array of feeds centred on a middle feed, labelled '1' in Fig. 3.7. Depending on the desired direction of radiation, feeds are imparted with currents of appropriate magnitude and phase. The middle feed is always switched on. Each peripheral feed acts either as a director or reflector so that this configuration may the viewed as a *pseudo*-Yagi parallel-plate slot radiator. The analogy ends there as *reflectors* and *directors* unlike those of the Yagi-Uda antenna are of the same height. The absence of the partitioning metal plates as in the four-sector slot concept leads to a yet stronger coupling between elements. Fig. 3.8(a) shows that by exciting probe one in the middle, parasitic coupling with the other probes makes for equal radiation in all four directions. With proper phasing and amplitude weighing, it may be possible to radiate preferentially in one direction. Fig. 3.8(b) the radiation pattern when probes '4', '1' and '2' are fed with the same amplitude. Probe '4' has phase lag of -90° while Probe '2' shows a phase lead of 90° relative to the middle probe '1'.

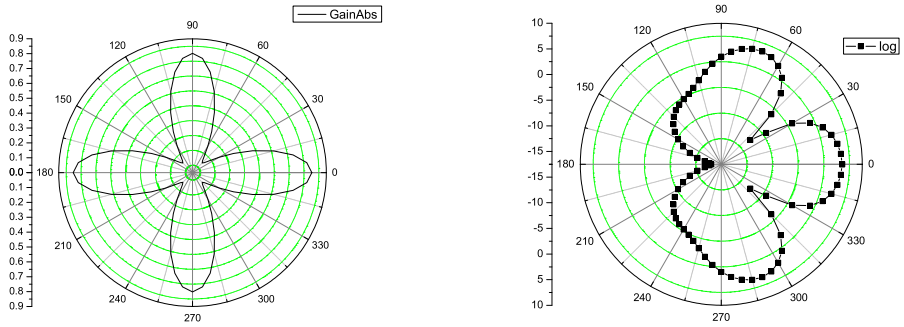

(a) (b)

Figure 3.8: *Computed radiation azimuthal pattern: (a): Probe 1 is fed, all others are parasitically coupled. (b): Probe separation of $\lambda/4$, inter-element phase difference of $\pi/4$: Strong coupling between elements such that no phase relation could be found to yield appreciable directivity.*

Though end-fire radiation along array axis may be discerned, there is appreciable radiation off axis hinting at a strong parasitic coupling between probes '3' and '5'. At high frequencies the probe feeds in the slot represent inductances which are very sensitive to position. The positioning would require utmost precision. Given this and the challenge of matching, the solution cannot be pursued at an affordable cost.

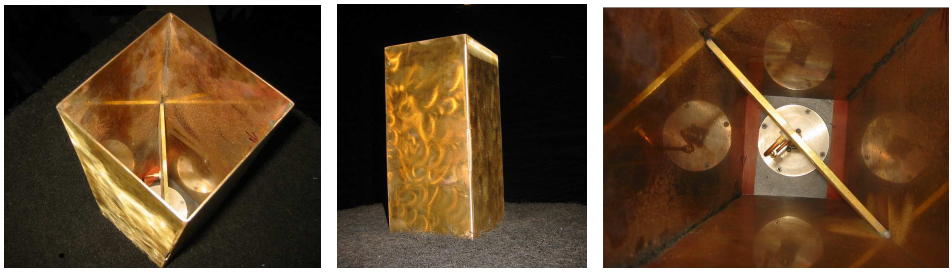

(a) (b) (c)

Figure 3.9: *Model to investigate feasibility of slot-type radiators: (a) Each slot covering nearly 180° in the azimuth. (b) Slots are concurrent with edges of internal wedge angle = $\pi/2$. (c) Slots are excited through a rectangular waveguide running across diagonal of model.*

Vertical Slots

Slots in waveguide walls radiate proportionately to current intercepted. This can be varied by tilting. Radiation from slot-like apertures in a metallic surface is therefore reciprocal to the excitation of currents by a wave incident on the surface. The reciprocity theorem points to an intimate relationship between slot radiation on the one hand and diffraction and scattering on the other. Thus diffraction and scattering theory is becoming an integral part of antenna theory. During the past six decades, remarkable effort has been directed at elucidating the mechanisms involved in scattering [48; 51; 55]. Amongst the simple geometric shapes that have been treated mathematically is the wedge, a special case of which is an edge of interior angle $\alpha = \frac{\pi}{2}$, as in the AVM cube.

To investigate the suitability of slot radiators, a scaled up model depicted in Fig. 3.9 consisting of two slots each of length 6.5 cm and breadth 2.5 mm milled along parallel diametric edges of the *e-Grain* was constructed. The scale factor was 1:12 in the *x - y* plane and 1:36 along the z axis so as to minimise the effect of the feed. The feed has a coaxial to rectangular waveguide transition for compatibility with existing instrumentation. A fan beam with a broad beamwidth in azimuth and a narrower one in elevation was experimentally verified. Full azimuthal coverage is possible using two of such slots. Its main disadvantage arises from the jump discontinuity in characteristic impedance at slot-free space interface. Wave detachment under these conditions is poor as the wave takes the path of the least resistance. The result is that the wave circulates in the parallel-plate waveguide terminating in the slot. This resonator effect leads to a low radiation efficiency.

Approximate formulas to predict the beamwidth, Θ, and gain, G, of an aperture antenna without taking into account the aperture illumination and antenna efficiency are

$$\Theta = K_\theta \frac{\lambda}{D} \tag{3.18}$$

$$G = \frac{K_g}{\theta_E \theta_H} = \frac{4\pi}{\theta_E \theta_H L_n} \tag{3.19}$$

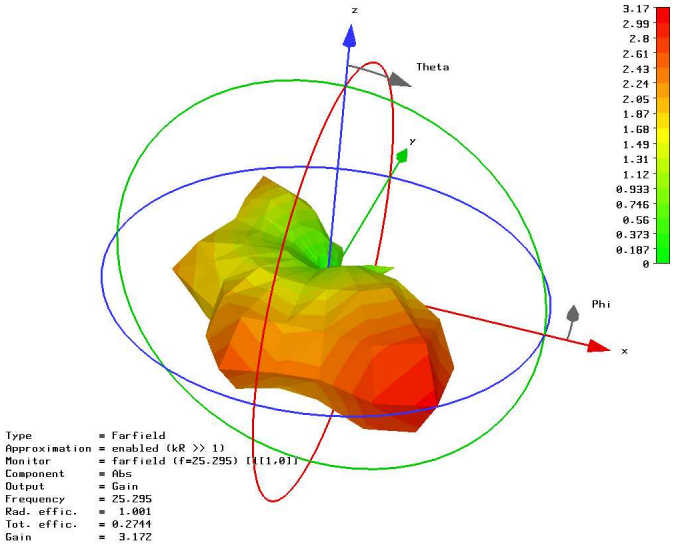

Figure 3.10: *Computed pattern in 3-D.*

where λ is the wavelength, D is the aperture dimension in the plane of the pattern, $K_\theta \approx 60^\circ$ is a dimensionless constant, θ_E and θ_H are the 3-dB beamwidths in two orthogonal principal planes, and $K_g \approx 10$, $L_n \approx 1.3$ are constants for Θ in radians ($K_g \approx 30,000$ for Θ in degrees).

Figs. 3.10 and 3.11(a) show an asymmetry because the employed simulator does not allow waveguide port placement at an angle other than 0° or 90° to any of the principal axes. The port was consequently modelled along the y-axis. The measured azimuthal pattern in Fig. 3.11(b) shows very good agreement with the computed (3.11(a)). Fig. 3.12(b) with both slots (the openings of the waveguide) open shows that total coverage is possible with two vertical slots as proposed.

Slot radiation is linearly polarised. It therefore cannot provide that degree of fault tolerance required in an interference-prone dynamic topology. Furthermore, the aspect ratio of the slot $\kappa = b/a = 125$ implies a stark disparity in wave impedance the consequence of which is a substantial mismatch between the slot and free space

$$r = \frac{Z_0 - Z_s}{Z_0 + Z_s} = \frac{Z_0 - \frac{Z_0}{\kappa}}{Z_0 + \frac{Z_0}{\kappa}} \approx 1.$$

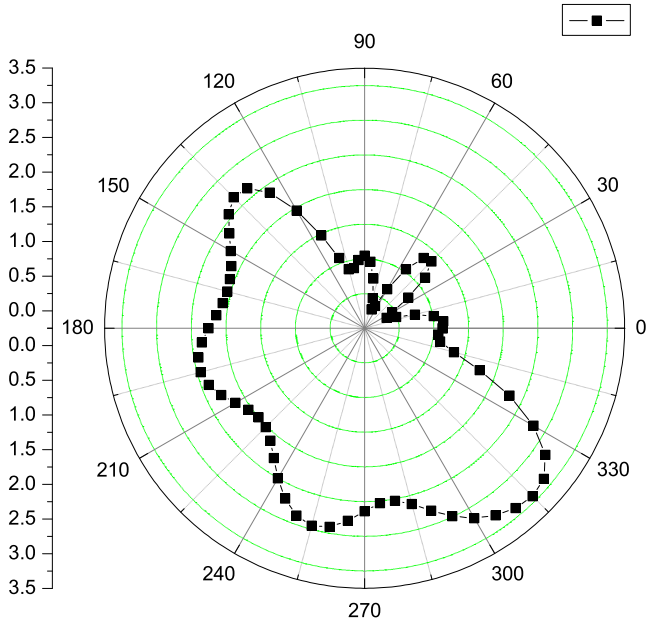

(a)

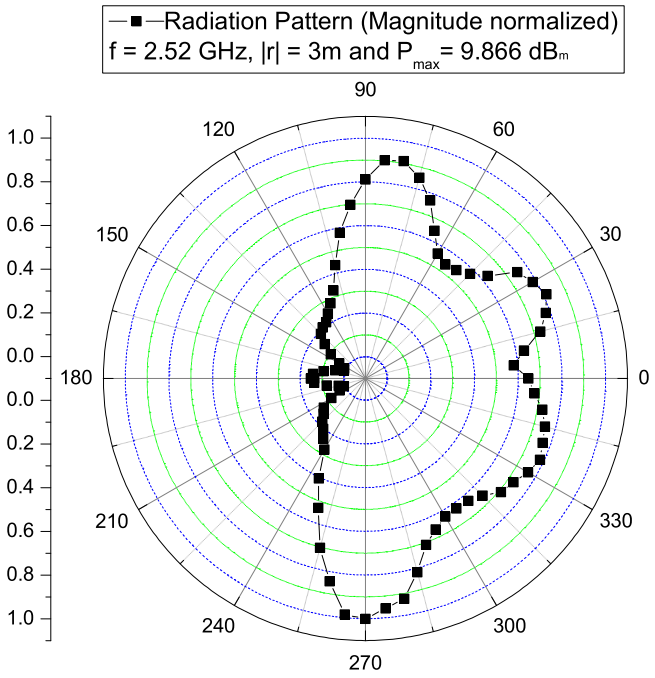

(b)

Figure 3.11: *(a) Computed azimuthal pattern, (b) Measured pattern in azimuth at 2.52 GHz. Save for a 45° offset due to mechanical constraints good agreement between computations and measurements is observable.*

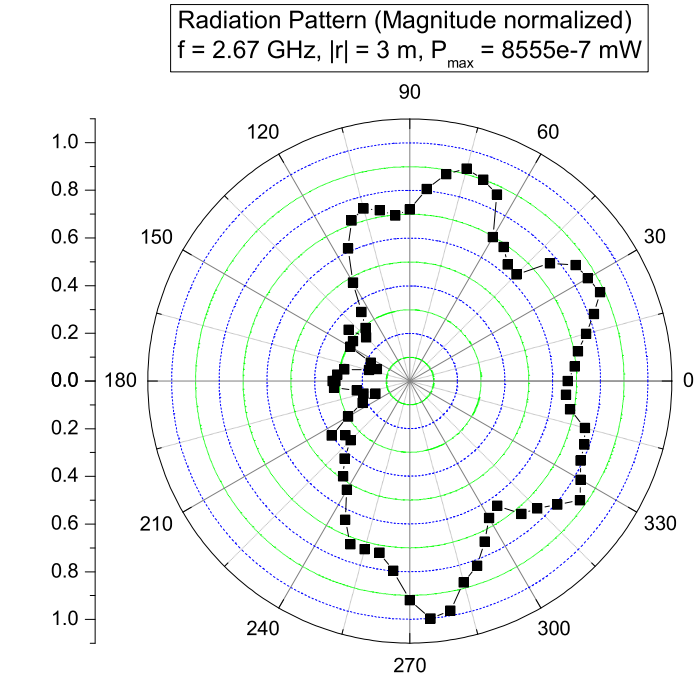

(a)

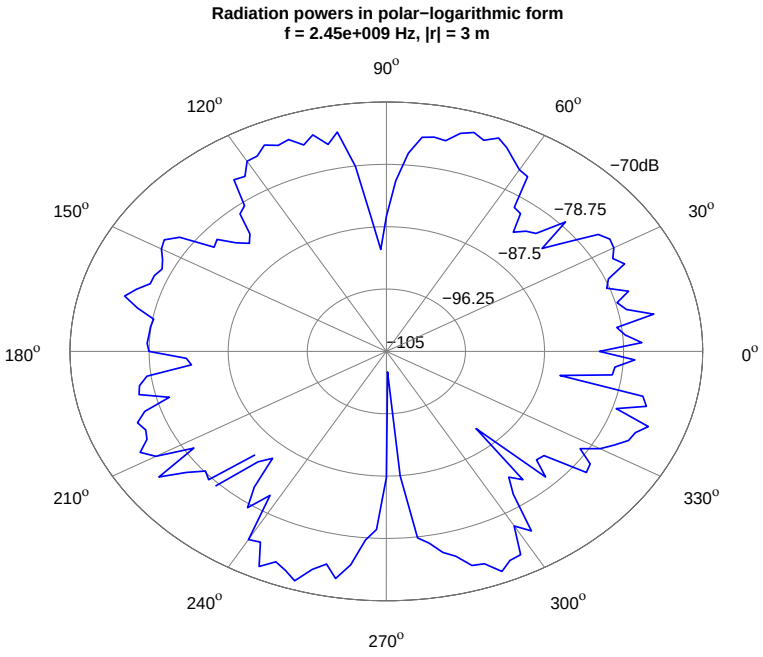

(b)

Figure 3.12: *Measured pattern is not significantly different at 2.67 GHz: (a) A single slot radiating, the other is short-circuited. (b) Both slots open quasi-azimuthal coverage is possible.*

3.3 The Microstrip Antenna

The merits of the microstrip patch antenna (MPA) are established beyond doubt. The aesthetic quality of an antenna structure is highly subjective but there is no doubt the rectangular or square MPA fits rather snugly with the cubic nature of the AVM-Module. MPAs however do come with certain inherent disadvantages. The most crucial of these are low gain, narrow impedance bandwidth, limited polarisation diversity, lack of versatility in frequency and poor scanning performance in an array environment. Microstrip antennas have bandwidths of a few percents (3 to 5). In the last decade, many researchers have studied bandwidth widening techniques for microstrip antennas [32]. A popular method uses electromagnetically coupled patches, either overlaid in multiple layers or spread out in coplanar fashion. Both methods require greater constructional effort, one increasing the thickness of the antenna and the other realizable only at the cost of increased area. While the latter is not a good prospect for AVM purposes, the former could indeed hold some promise as extremely thin-substrate technology matures. Traditionally stacked patches have been used to increase the bandwidth of the single patch. The fundamental idea in both cases is the use of patches of slightly differing but closely spaced resonant frequencies. Ideally the lower 3-dB frequency of element n, f_{nu} coincides with the upper 3-dB frequency of element m, f_{mo}. Lastly loading with resistive elements widens bandwidth at the cost of efficiency. Since the bandwidth of microstrip antennas is quite small, tuning requires the observance of tight tolerances. An often overlooked positive side effect of the narrow bandedness of the microstrip antenna is the small system noise power

$$P_N = k_B T_N \Delta f$$

where k_B is BoltzmannŠs constant, T_N the system noise temperature and Δf the bandwidth. In the following, design and material considerations will be studied to overcome some of these disadvantages as applicable to AVM communication at 24 GHz.

3.3.1 Broadside Radiator

Broadside radiation is readily obtained in a microstrip antenna. In the ubiquitous computing scenario of AVM, there is need for sideways radiation emanating from the module. This could be achieved by pasting broadside elements on the faces of the cube. Working on the premise that no communication takes place in the vertical direction the number of broadside antennas can be kept to a minimum of four. Nonetheless endfire radiation would leave the surface of the module free for other components or applications. The dominant fundamental mode has the electric field along the radiating edges in anti phase. However because the surface normals on these are antiparallel, the magnetic current sources enhance each other broadside.

3.3.2 End-fire by mode suppression

An infinite number of higher order modes which are important for satisfying boundary conditions is excited at discontinuities. The highest order modes cannot propagate energy over any meaningful distances. They are principally important in

tuning or cancelling out reactances. A judicious mode selection could enable end-fire radiation from a microstrip. For the TM_{20} mode, the radiating edges have electric fields in phase while the surface normals are still antiparallel so that a 180° phase difference in magnetic surface current $\mathbf{M} = -\hat{\mathbf{n}} \times \mathbf{E}$ results. This would lead to end-fire radiation. The efficiency of such a radiator is then lower than that of one operating in the fundamental mode. This remains however a challenge because the fundamental mode with a higher energy density cannot be suppressed — the physics of matching requires that a waveguide propagate only one mode at frequency f.

3.3.3 Feeding Methods

Optimum power transfer from generator to antenna is achieved by complex conjugate matching between the feed line and antenna input impedances. Compactness, efficiency and constructional simplicity are clearly desirable. Here follows a cursory glance at the possibilities.

Stripline Feed

The coplanar strip feed lends itself well to MMICs but incurs more gain loss and sidelobe and polarisation characteristics degradation due to radiation from a de rigeur unshielded feed. Mutual coupling represents a condiderable obstacle in stripline-fed arrays. These efficiency and cross polarisation effects are more limiting in comparison to substrate surface wave and tolerance problems. For a 5%bandwidth, an efficiency less than 55% with a sidelobe level of barely -10 dB has been reported [21]. These adverse effects may be minimised by smoothening feed discontinuities and using thin substrates of relatively high dielectric constant. Such a substrate doubtless reduces bandwidth and the above-mentioned requirements for good conduction run starkly contrary to those for good radiation. Noteworthy is the use of sequential rotation in circularly-polarised arrays yielding increased input impedance bandwidth and axial ratio bandwidth compared with a corporate feed. Further the peak sidelobes are reduced by up to 10 dB [21]. Vis-à-vis other feeding mechanisms, the stripline feed requires fairly extensive space for power splitters and phase shifters. It is therefore not a viable alternative given the AVM limitations. Matching is effected using quarter-wave transformer or an inset into the patch. The use of coplanar stripline feeds will thus give poorer performance than fully-shielded more compact feeds. A look is next taken at low-loss shielded feeds.

Probe Feed

The widely-used probe feed is shown in Fig. 3.13(a). The probe feed allows an appreciable isolation of the feeding structure from the radiating element. This is important from the viewpoint of electromagnetic interference with electronic components underneath the antenna. It also permits a relatively good alignment of layers.

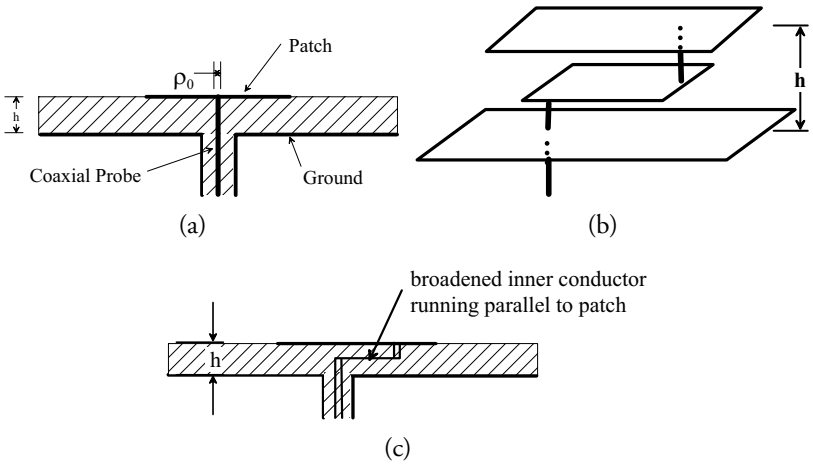

Figure 3.13: *Flattened probe (feed) within the substrate and running parallel to patch provides capacitance to tune out the inductance introduced by the vertical cylindrical probe.*

Estimating Probe Inductance

The feed has been modelled as a shorting post of length h buried in a medium of dielectric constant er so having an inductive reactance [11]

$$X_L = \frac{Z_0}{\epsilon_r} \tan \frac{\pi h}{\lambda_0} \tag{3.20}$$

Accuracy may be improved if the probe radius and patch size can be taken into account. The probe feed is regarded as the extended inner conductor of a short coaxial transmission line of inner radius ρ_0. For a circular patch, a starting point for outer radius may be taken to be the radius itself. So for a rectangular patch of length L and width W this outer radius, R_0 may be chosen to make patch area and cross section of equivalent coaxial line equal, i.e.

$$LW = \pi R_0^2.$$

A transformation of a short-circuit through a distance h in the substrate yields a reactance

$$\begin{aligned} X_L = \omega L &= Z_{coax} \tan \beta h = \frac{1}{2\pi}\sqrt{\frac{\mu}{\epsilon}} \ln \frac{R_0}{r_0} \tan \beta h \\ \omega L &= \frac{1}{2\pi}\sqrt{\frac{\mu}{\epsilon}} \ln \frac{R_0}{r_0} \quad \text{for} \quad \beta h \ll 1 \\ \text{Using} \quad \beta = \omega\sqrt{\mu\epsilon}; \quad L &= \frac{\mu h}{2\pi} \ln \frac{R_0}{\rho_0} = \frac{h\mu}{2\pi} \ln \sqrt{\frac{LW}{\pi\rho_0^2}} \end{aligned} \tag{3.21}$$

This inductance therefore introduces a frequency dependency and so restricts the impedance bandwidth of the patch antenna. Also the direct dependence on the length of the inner conductor means the effect can be managed by using extremely

thin substrates which are plagued with low radiation efficiency. In the light of this, the following narrow-band solution is proposed. The compensation capacitance could be realized by running the inner conductor in a meandering-like fashion in the dielectric so that both inductive and capacitive coupling take place. A horizontal part of a broadened inner conductor within the patch substrate provides the capacitance to tune out the inductance introduced by the vertical part as shown in Fig. 3.13. Matching the antenna impedance to the transmission-line impedance is accomplished simply by putting the feed at the proper location.

Aperture Coupled Feed

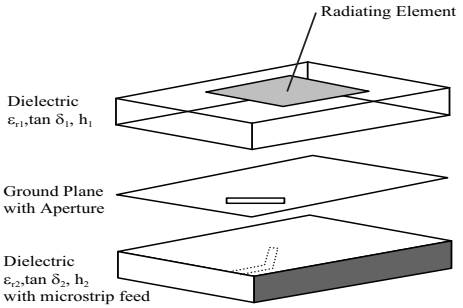

Figure 3.14: *Various layers in aperture-coupling in perspective.*

As frequency increases feed vias become increasingly inductive. The resulting narrow feed bandwidth makes matching of such an antenna an enormous challenge. Furthermore milling probes in the substrate to the requisite precision at high frequencies is beset with difficulties. This can be alleviated through aperture coupling: a slot is cut in the ground plane under the radiating element and excited with a microstrip line traversing the slot on the opposite side of the ground plane. This is shown in Fig. 3.14.

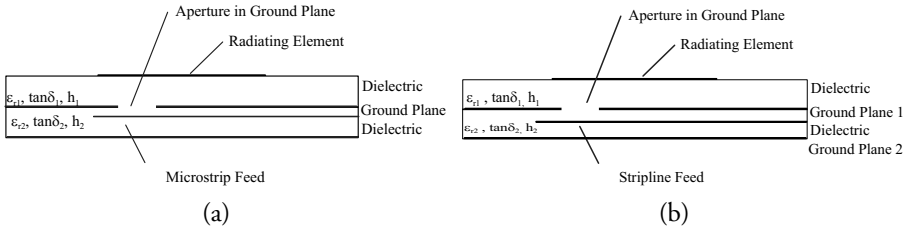

Figure 3.15: *Side view of aperture-coupled patch.*

Electromagnetic coupling using two distinct substrates for the feed network and the radiating element opens up the possibility of independently designing and optimizing the feed and radiating structures [76]. Furthermore, by placing the ground plane between the radiating element and feed, radiation arising from the feed is shielded. Further degrees of freedom in impedance matching are that the reactive part of the input impedance of APC antennas is determined by the length of the

stripline extending beyond the aperture whereas the resistive part is dependent on aperture size. The printed slot has a wider impedance bandwidth than an MPA [12; 91]. In the light of the bandwidth problem of the microstrip antenna, it is tempting to ask if an aperture slot/patch hybrid offers any bandwidth gain. Simulation results show this question can be answered in the affirmative. On the basis of the original aperture coupled microstrip antenna configuration [74], the following structure is put forward for its simplicity and efficiency to obtain circular polarisation and a good measure of isolation as evidenced by the simulated front-to-back ration of 16 dB. A probe for otherwise the same structure gave a front-to-back ratio of 23 dB. The configuration schematized in Fig. 3.15(a) consisting of a stripline fully immersed in a substrate which is sandwiched by two ground plates yields a better isolation of the radiating element from the circuitry. Due to the excitation of higher order modes in the cavity however, its efficiency is smaller.

Irrationally held truths may be more harmful than reasoned errors.
T.H. Huxley

4

Theoretical Aspects of Microstrip Antennas

THE MICROSTRIP ANTENNA comprises of a dielectric slab of permittivity ϵ and thickness h sandwiched between a radiating patch and a ground plane as shown in Fig. 4.1. Its defining attribute is low-profile surface conformability. In addition to being light and easily fabricated, it holds great promise to strike the much desired yet elusive compromise between aesthetics and functionality (design and function).

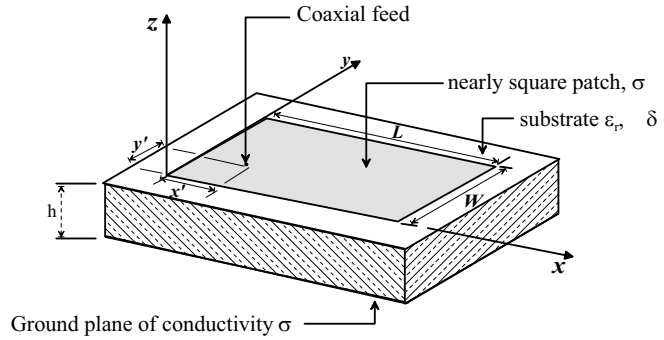

Figure 4.1: *Schematic of a rectangular microstrip patch antenna*

The choice of microstrip technology for antennas in various applications with stringent requirements such as satellite communication as far back as the early eighties to its widespread present day use in tiny gadgets in emerging pervasive personal communications is testimony to its ascendancy. In the wake of its significance, four separate methods for the analysis of varying ease, accuracy and flexibility have evolved. For the sake of brevity, herein unless otherwise stated, the antenna will be treated in the transmitting case and corresponding results being valid for reception by virtue of reciprocity. Seminal to radiation is the mismatch at the air-dielectric interface with a reflection coefficient

$$r = \frac{Z_0 - \frac{Z_0}{\sqrt{\epsilon_r}}}{Z_0 + \frac{Z_0}{\sqrt{\epsilon_r}}}.$$

Besides the low reflection coefficient, a low ϵ leads to loosely bound fields in the substrate. This explains the preferential use of high ϵ substrate material in circuits and low ϵ material for antenna design. Among the various analytical approaches to elucidate the properties and radiation mechanism are the transmission line model, the cavity models and full modal expansion techniques. The most telling performance indicators of an antenna are indubitably its radiation pattern and input impedance. In this effort emphasis will be placed on the latter, the determination of the former having been reliably established.

4.1 Transmission Line Theory

If both the thickness and relative permittivity of the substrate are sufficiently small so that surface wave excitation is negligible, radiation can be analysed using the transmission line theory (TLT). The simplest approach offering physical insight consists in viewing the microstrip antenna as two radiating edges parallel to the y-axis of length W separated by $L \approx \frac{\lambda_\epsilon}{2}$ along the x-axis behaving effectively

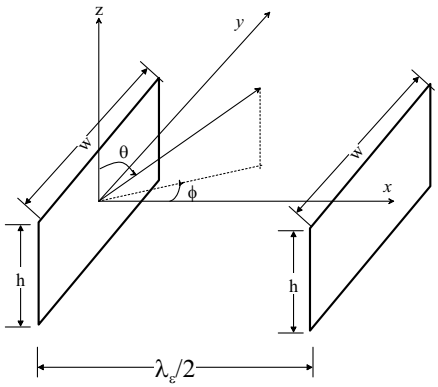

Figure 4.2: *Schematic representation of microstrip antenna as two-element array of radiating edges of length w and height h whereby h is exaggerated for illustration.*

as a two-element broadside array as shown in Fig. 4.2. λ_ϵ denotes the dielectric wavelength. This model, the transmission line model [68], pictures radiating edges interconnected by a transmission line of low impedance Y_C determined by the aspect ratio W/h and the relative permittivity of the dielectric slab ϵ_r and a loss tangent δ_s as suggested in Fig. 4.3(b). The patch is characterized by its length L, width W, thickness t, conductivity σ and surface roughness $\Delta\rho_s$. For purposes of analysis, both the substrate and ground plane are assumed to be infinite in extent. The unknown tangential magnetic field over the screen is taken as the field which would exist if the screen were infinite rather than finite. In other words, waves reflected inward from the edges are neglected. The substrate material is assumed to be homogeneous and hence isotropic. Provided the statements $h \ll \lambda$ and $h \ll W$ hold true, a quasi-TEM field can be assumed.

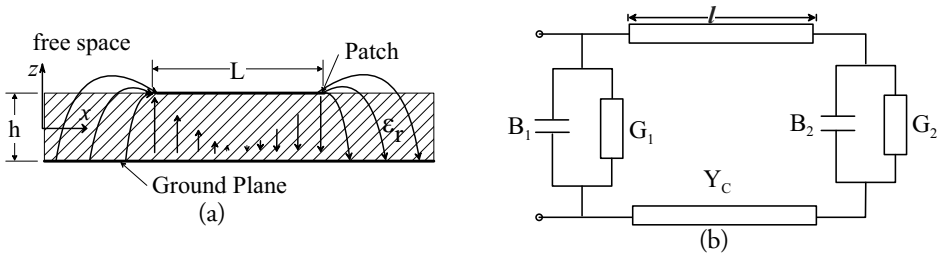

Figure 4.3: *The fundamental TM_{10} mode: (a) Fringing E-field lines. (b) Transmission line theory Equivalent circuit Model of a rectangular microstrip patch antenna.*

There obtains thereupon a uniform electric field distribution over the plane of each radiating edge described in the co-ordinate system in Figs. 4.2 and 4.3(b) by

$$\mathbf{E} = \begin{cases} E \cdot \mathbf{z}, & |z| \leq \frac{h}{2}, \\ 0 & \text{elsewhere.} \end{cases} \tag{4.1}$$

The field distribution corresponding to the boundary conditions for the fundamental is shown in Fig. 4.3(a). The electric field is constant along the width and there exists a phase difference of π between the slots. The two slots separated by $L \approx \frac{\lambda_\epsilon}{2}$ are the radiating edges. The other two slots of length $\frac{\lambda_\epsilon}{2}$ separated by a distance W are non-radiating in the main planes as the magnetic currents cancel out. The TLT equivalent circuit of the patch antenna consisting of two slots as depicted in Fig. 4.3(b) has been found to be useful. The radiation from an edge is similar to that from a slot antenna. Each such slot is equivalent to a magnetic dipole with the magnetic current

$$\mathbf{M} = -2\hat{\mathbf{n}} \times \mathbf{E}, \qquad |y| \leq \frac{w}{2} \tag{4.2}$$

where $\hat{\mathbf{n}}$ represents the outward normal to the slot and the factor two expresses the reinforcing effect of the image produced by reflection on the ground plane. Both open-end terminations may then be viewed as capacitively loaded slots with a conductance G and susceptance B. Under the premise that the slot conductance equals that presented to a TEM wave normally incident on a small parallel-plate waveguide slot radiating into a half-space, the conductance G and susceptance B of the slots are given by [37]

$$G = \frac{\pi}{\lambda Z_0}\left[1 - \frac{(kh)^2}{24}\right] \tag{4.3}$$

$$B = \frac{1}{\lambda Z_0}\left[3.135 - 2\log(kh)\right] \tag{4.4}$$

where $Z_0 = \sqrt{\mu_0/\epsilon_0}$ is the free-space wave impedance, k is the wave number. The conductance G represents dissipation including radiation and surface waves if these are excited while the susceptance B models the stored energy in the vicinity of the edges. For all modes, the field distribution is such that the same magnitude of the voltage occurs at the radiating edges. The sinusoidal voltage distribution translates to a phase difference between the radiating edges always equal to an integral multiple of 180°.

The fundamental mode is excited with the greatest amplitude and is responsible for the most radiation. A $\frac{\lambda}{2}$-transformation through the low-impedance line of from Slot 2 to Slot 1 yields the input admittance

$$\begin{aligned}\tilde{Y_2} &= Y_C \frac{1 + j\frac{Y_C}{G_2+jB_2}\tan\beta l}{\frac{Y_C}{G_2+jB_2} + j\frac{G_2-B_2}{G_2+jB_2}\tan\beta l} \\ &= Y_C \frac{G_2 + j(B_2 + jY_C\tan\beta l)}{Y_C - B_2\tan\beta l + jG_2\tan\beta l} \end{aligned} \tag{4.5}$$

At resonance the admittance is pure real. Setting the imaginary part in Eqn. (4.5) to zero, a relation between the electrical length of the line and the edge parameters reads

$$\tan\beta l = \frac{2Y_C B_2}{G_2^2 + B_2^2 - Y_C^2}.$$

For an arbitrary feed point at a distance χ from one edge (and $\approx (\frac{\lambda_e}{2} - \chi)$ from the other), transforming the slot admittances as in Eqn. (4.5) to the feed point and adding gives

$$Z_{in}(\chi) = \frac{1}{2G}\left(\cos^2(\beta\chi) + \frac{B^2+G^2}{Y_C^2}\sin^2(\beta\chi) - \frac{B}{Y_C}\sin(2\beta\chi)\right). \tag{4.6}$$

For all intents and purposes $B \ll Y_C$ and $G \ll Y_C$ so that the above simplifies to

$$Z_{in}(\chi) = \frac{1}{2G}\cos^2(\beta\chi) \tag{4.7}$$

For an edge-fed patch ($\chi = 0$), a plausibility check by appreciating that a $\frac{\lambda}{2}$ admittance transformation along a lossless line affects only the phase and not the magnitude of the admittance and so the transformation from Slot2 to Slot1 may be written as

$$\tilde{Y_2} = \tilde{G_2} + j\tilde{B_2} = G_1 - jB_1 \tag{4.8}$$

hence

$$Y_{in} = Y_1 + \tilde{Y_2} = 2G_1 \tag{4.9}$$

which is in keeping with Eqn. (4.7) with $\chi = 0$. To account for the coupling or reaction between the radiating edges, a mutual conductance G_{12} augments the expression for the input impedance thus

$$Z_{in}(\chi) = \frac{1}{2(G_1 \pm G_{12})}\cos^2\chi$$

The plus sign (+) describes modes with edge voltages in anti-phase while the minus (−) applies for modes with in-phase edge voltages. It has been shown that the mutual conductance is negligible compared to the self-conductance of the single slot [17]. Contrary to assumption, the substrate is finite resulting in field lines running both in the substrate and in air. Fringing makes the patch appear electrically larger than its physical dimensions. Accordingly the resonant frequency is slightly less than that predicted using TLT. In other words the relative effective permittivity is smaller. The extent of fringing depends mainly on dimensions and only weakly on the dielectric constant of the substrate. For a substrate of height h, a crude estimate

of the virtual patch extension into air can be taken empirically as $\Delta L = h/2$ [61]. The difficulty at arriving at an exact and simple closed-form expression has lead to the introduction of approximate formulas for the effective dielectric constant ϵ_{reff} *e.g.* Schneider's relation [85]

$$\epsilon_{reff} = \frac{\epsilon_r + 1}{2} + \frac{\epsilon_r - 1}{2}\left(1 + 10\frac{h}{W}\right)^{-1/2}. \tag{4.10}$$

There has been a substantial improvement on the above model [31]. An approximation to the normalized apparent extension of the length of the patch which takes into account the dielectric properties and height of substrate according to Hammerstad is [30]

$$\frac{\Delta L}{h} = 0.412\frac{(\epsilon_{reff} + 0.3)\left(\frac{W}{h} + 0.264\right)}{(\epsilon_{reff} - 0.258)\left(\frac{W}{h} + 0.8\right)}. \tag{4.11}$$

Therefore for the fundamental mode there is an apparent increase in length of $2\Delta L$. This means the microstrip antenna must be made a fraction shorter than half-wavelength if it is to operate at the desired frequency. Thus the transmission line model gives an accurate value for the resonant frequency for the fundamental mode as

$$f_{\text{res}} = \frac{1}{2(L + 2\Delta L)\sqrt{\epsilon_{reff}}\sqrt{\mu_0\epsilon_0}}. \tag{4.12}$$

In general, the substrate height is barely a fraction of the wavelength and fringing is not pronounced for thin substrates. For a rectangular patch (the obvious choice for AVM purposes) having the feed point near one of the radiating edges, good agreement between theory and CST computations obtains. TLT takes into account only a single (the fundamental) mode whereas higher order and evanescent modes characterized by rapidly varying fields exist in the immediate neighbourhood of the feed and at the edges. These play an important role in matching boundary conditions. For greater accuracy in the determination of feed impedance and radiation characteristics, the cavity model is more appropriate.

4.2 Cavity Models

If the feed is moved towards the centre of the patch, TLT predicts an impedance locus symmetric about the real axis of the Smith chart. What obtains instead is a shift into the inductive region. A precise prediction of the input impedance is therefore not possible. TLT is directly valid only for rectangular or square patches. This is compounded by the following shortcomings: the length extension ΔL must be painstakingly empirically determined, the assumption of a constant field along the radiating edges seldom obtains in practice, etc. These drawbacks necessitate the development of more accurate models.

4.2.1 Baseline Cavity Model

The field underneath the patch cavity is assumed to be approximated by the dominant mode of the cavity derived from the antenna by giving its non-metallic periphery a magnetic wall. From this field, radiative and ohmic losses associated with the antenna are approximated together with stored energies. The conductance G and

quality factor Q at resonance are computed. From these the impedance is found from

$$1/Z = [1 + jQ(f_o/f - f/f_o)]$$

where f_o is the resonant frequency. The impedance locus is also symmetric about the real axis of the Smith Chart and thus not very inaccurate [79].

Simulations showed that TLT predictions for the input impedance while exciting away from the radiating edges are inaccurate. Same holds true for the single mode cavity theory especially the higher order modes. At the $m = M$ and $n = N$ mode resonance, the contribution of the MN^{th} modal term to the total field is preponderant. Thus if the fundamental mode is not strongly excited – a situation tantamount to appreciable energy being distributed over higher order modes, both analysis methods fail. The higher order modes obviously have different wave impedances and their contribution to the total radiation can no longer be neglected when the fundamental mode is only poorly excited. A detailed exposition of the multi-mode cavity model is found in Appendix A.

4.2.2 Radiation

A concise treatment of radiation employs a hybrid of image theory and Huygen's principle which may be viewed as the field theory expression of the observation that an effect may become a cause, reinforcing the original cause and producing the same effect in an intensified form, and so on indefinitely. Huygen's augmented principle allows for a determination of the radiated fields without knowledge of the innermost field constitution of the cavity if appropriate equivalent surface electric and magnetic currents as shown in Fig. 4.4(b) on the cavity exterior can be found [83]. The tangential electric fields on the patch and ground plane vanish since by hypothesis they are perfectly conducting. So too does the tangential magnetic field on the perfectly magnetically conducting sidewalls. The only effective equivalent sources are due to the tangential electric field E_z on the magnetic walls as shown in Fig. 4.4(b).

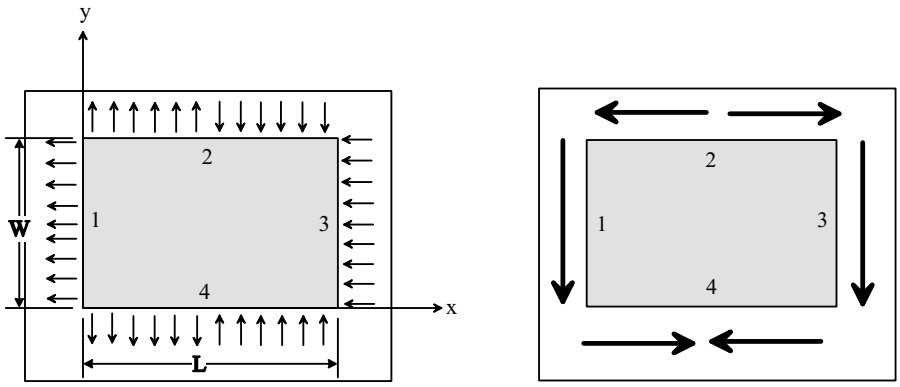

Figure 4.4: *(a) Field distribution along the edges of the radiating patch from which the radiating and non-radiating edges can be discerned. (b) To the right is shown the magnetic surface current along the four sidewalls.*

These images are subject to reflection on the perfectly conducting infinitely large ground plane. The enforcement of the above boundary and initial conditions produces a total equivalent magnetic current equal to

$$\mathbf{M} = -2\hat{\mathbf{n}} \times \mathbf{E} \tag{4.13}$$

where $\hat{\mathbf{n}}$ is the unit outwardly directed normal on the sidewall.

The magnetic vector potential due to a magnetic surface current source at any arbitrary observation point r may consequently be computed according to [38]

$$\mathbf{F}(\mathbf{r}) = \frac{\epsilon_0 h}{4\pi} \int \frac{\mathbf{M}(\mathbf{r'}) e^{-jk_0|\mathbf{r}\text{-}\mathbf{r'}|}}{|\mathbf{r}\text{-}\mathbf{r'}|} dc' \tag{4.14}$$

where the integration is carried out over source points on the perimeter of the patch. The far fields in free space are evaluated through the relations:

$$\mathbf{H}(\mathbf{r}) = -j\omega\mathbf{F}(\mathbf{r}) \tag{4.15}$$

$$E_\theta(\mathbf{r}) = Z_0 H_\phi(\mathbf{r}) = jk_0(-F_x \sin\phi + F_y \cos\phi) \tag{4.16}$$

$$E_\phi(\mathbf{r}) = -Z_0 H_\theta(\mathbf{r}) = -jk_0(F_x \cos\theta\cos\phi + F_y \cos\theta \sin\phi). \tag{4.17}$$

The field pattern of each surface current element is dual to a magnetic dipole, thus omnidirectional. From Fig. 4.4 on the preceding page, the radiation from sides 2 and 4 cancels out in the main planes. The pattern of a patch over a large ground plane may thus be calculated by modelling the radiator as two parallel (sides 1 and 3) uniform magnetic line sources of length W as in Eqn. (4.13), separated by the distance L. It is noteworthy that this solution produces finite fields in the cavity region and outside of it, vanishes at infinity thus fulfilling the radiation condition.

4.3 Gain

The Friis transmission formula for a communication link of distance d with spelt out dependence on impedance and polarisation mismatch reads

$$P_R = p(1 - |r_R|^2)(1 - |r_T|^2) P_T G_T G_R \left(\frac{\lambda}{4\pi d}\right)^2 \tag{4.18}$$

where p is the polarisation mismatch (defined in section 4.4 on the following page), r_i, P_i and G_i, $i = R \vee T$ stand respectively for the reflection coefficient between antenna and line, the power and gain in transmit or receive case. Transmit power is limited either by regulation or by capacity. Beyond a certain distance in accordance with Eqn. (4.18) and depending on receiver sensitivity, a signal below a pre-specified threshold is undetectable. Given transmitted power and frequency and assuming matching, the gain is of cardinal importance for an adequate signal to noise ratio (SNR).

The size of the AVM module imposes a limit on the size and therefore capacity of batteries to drive the *e-Grain* module. It becomes a matter of utmost importance to achieve an appreciable gain. To this end a design concept embodying a maximum use of available space appears reasonable since the effective capture area is directly proportional to the physical area. Conventionally phased areas are the answer for directivity. Since the dimension of the AVM is hardly a wavelength at 24 GHz,

it might at first seem tempting to use arrays of thin high-permittivity substrates elements. Such attempts lead to all-round degradation in performance since the element spacing is such that the highest engineering and fabrication standards are required to cope with mutual coupling effects which get out of hand for elements mounted on the same substrate. Under these circumstances the individual patterns change radically when a new element is placed in the array. To avoid the energy being trapped in the cavity, the use of low-dielectric constant low-loss substrates is imperative.

A perfect ground plane restricts radiation in one half-space equivalent to a 3 dB gain. The radiating edges can be viewed as two dipoles and thus represent another increase of 3 dB. With increasing substrate thickness, just before the onset of surface waves, an optimum thickness will get another 2 to 3 dB of extra gain yielding a total of 8 to 9 dB for a single element. The structure of greatest promise is a nearly-square patch as will be seen in section 4.4

4.4 Circular Polarisation

Reliability would be best served by a radiation pattern independent of the operational environment. The presence of conducting structures does not only lead to specular reflection, there is also the risk of detuning. Circularly polarised radiation is desirable in scenarios where the risk of fading due to multi-path propagation and loss of signal due to polarisation mismatch is high. The power received is proportional the polarisation mismatch loss, which is defined by

$$p = |\rho_t \cdot \rho_r^*|^2 = \cos^2\psi = \frac{|\mathbf{h} \cdot \mathbf{E}^i|^2}{|\mathbf{h}|^2 |\mathbf{E}^i|^2} \tag{4.19}$$

where ρ_t, ρ_r and ψ are the transmit polarisation unit vector, the receive polarisation unit vector and is the angle between the two unit vectors, respectively.

For a dynamic and adaptive system such as AVM, circular polarisation takes on the quintessential in view of the ***different locations as well as arbitrary orientations*** of modules. That the *e-Grains* are identically constructed implies that the sense of polarisation of the antennas is the same and the movement of the E vectors between any two *e-Grains* in communication is akin to that of either left or right screws rotating into each other around their common axis. In the light of the stringent conditions on the magnitude and phase difference between sources for circular polarisation and this only for a narrow frequency band, CP is often obtained at the expense of considerable effort. The space requirements for the attendant circuitry to lodge power dividers, phase shifters and impedance matching networks has made the realization of compact CP somewhat of an art.

Microstrip antennas may be designed for circular polarisation by tweaking physical dimensions so as to produce two degenerate orthogonal modes within the cavity region under the patch. Degenerate modes have the same resonance frequency but different field distributions. This leads to radiation of two orthogonally polarised waves near the broadside direction. Circularly polarised radiation is obtained if and only if two orthogonal modes are excited with equal amplitude and in-phase quadrature. The direct approach to obtain circular polarisation is to superpose radiation from two separate and spatially orthogonal feeds excited with a relative phase shift of 90°. This configuration thus provides two orthogonal linearly polarised

waves which are in time phase quadrature. Straightforward splitting of the signal in half can be done with a Wilkinson or similar splitter. Creating a patch that simultaneously radiates vertically and horizontally can be done using two feed points. A $\lambda/4$ line section introduces a 90° delay can be in one of the signal lines. Recognizing the patch as a parallel RLC resonant circuit at the high frequencies and the narrow bandwidths needed, a solution constitutes in designing a patch with two close resonant frequencies, introducing the phased difference and using the antenna right in between these two resonances.

Though this works well, the splitter and delay line take up valuable board space let alone their radiation corrupting the intended radiation pattern. A range of feed structures such as the rampart line, chain antenna, square loop line, crank line, herringbone, slot-dipole array for circular polarisation are known [46]. These however, come in contention only when relatively adequate space is available.

The trick is creating the required 90° shift to obtain "two" useful antennas with a single feed. These and other techniques [81, pp. 24 - 28] are well established for conventional antennas, and the point here is that they are more difficult to translate to printed elements in view of the constrained planar geometry (one degree of freedom less) and feeder space requirements that the envisioned *e-Grain* cannot fulfill. It is nonetheless inspiring to note the innovative enhancement of circular polarisation characteristics by sequential rotation of elements [95], incorporation of finite substrate effects [50], novel feeder arrangements [39] and many more.

Several methods have been proposed to provide circular polarisation without the complexities inherent in the multi-feed devices. One such approach is to attach a single feed at a location so as to excite two equal-amplitude degenerate orthogonal modes and then to introduce some asymmetry in the cavity so that the degeneracy of the modes is removed. If the asymmetry is properly applied, one mode will decrease in frequency by a specified amount while the orthogonal mode will increase by that amount. The equivalent circuit for such a configuration is two uncoupled parallel resonant circuits excited by a common current source.

Corner-fed rectangular patches are the simplest class of circularly polarised antennas and seem to be the most useful. For a nearly square patch with dimension $L \approx W$, the spatially orthogonal degenerate TM_{10} and TM_{01} modes will have closely spaced resonant frequencies so that only these two modes need be considered. Richards *et al* [79] have found the magnetic surface currents of the modes to be given by

$$\mathbf{M}_{sx} = \mathbf{x}\frac{j\omega I_{in}}{\epsilon LW}\left\{\frac{1}{\omega^2-\omega_{10}^2\left(1+\frac{j}{Q_{10}}\right)}+\frac{\cos\frac{\pi x}{L}}{\omega^2-\omega_{01}^2\left(1+\frac{j}{Q_{01}}\right)}\right\} \quad (4.20)$$

$$\mathbf{M}_{sy} = \mathbf{y}\frac{j\omega I_{in}}{\epsilon LW}\left\{\frac{\cos\frac{\pi y}{W}}{\omega^2-\omega_{10}^2\left(1+\frac{j}{Q_{10}}\right)}+\frac{1}{\omega^2-\omega_{01}^2\left(1+\frac{j}{Q_{01}}\right)}\right\} \quad (4.21)$$

For circular polarisation, $|\mathbf{M}_{sx}| = |\mathbf{M}_{sy}|$ and $\angle(\mathbf{M}_{sx}, \mathbf{M}_{sy}) = +90°$. An optimum choice for L and W results when $L = W(1+1/Q)$. This is the defining feature that sets this design apart from the conventional patch antenna. It separates the two resonant frequencies by f_o/Q and results in the largest band of frequencies of good axial ratio. If L is slightly greater than W, simulations show the TM_{01} mode having a higher Q and hence a smaller bandwidth than the TM_{10}, as expected.

4.4.1 Feed Methods for Circular Polarisation

As seen above, substantial effort is needed to create the stringent conditions on amplitude and phase propitious for CP. Due to space reasons, a solution involving external polarizers, multiple-feed networks of power splitters and phase shifters is ill-suited to AVM. In keeping with the basic idea that CP is the superposition of two orthogonal radiating linearly polarised modes of equal amplitude, the simplest means would be the superposition of such elements. The complexity can be greatly reduced by using a single feed to excite both modes. This idea and some other feeding methods are shown in Fig. 4.5 on page 64.

4.5 Efficiency and Quality factor

There are four mechanisms that cause losses in the antenna structure: dielectric, metal, radiation, and surface wave losses represented by P_d, P_σ, P_{SW}, respectively. In the first two cases, these losses cause the amplitudes of the propagating modes to decay as $\exp^{-\alpha z}$, where $\alpha = \Re\{\gamma\}$ is the attenuation constant.

Viewed as a dielectric sandwiched between two perfect conductor plates, the MPA behaves like a lossy resonator with the predominant loss occurring by radiation leaking at the air-dielectric interface. Radiation according to the cavity model is possible when a slight field perturbation [37, pp. 432] results in complex eigenvalues less than the real static wavenumbers given in Eqn. (A.8). From this, Poynting's vector is computed to obtain the total radiated power

$$P_{rad} = \Re \int_0^{2\pi} \int_0^{\pi/2} (E_\theta H_\phi^* - E_\phi H_\theta^*) r^2 \sin\theta d\theta d\phi \tag{4.22}$$

Assuming that the wall conductivity is high enough to have only a negligible effect on the transverse properties of the modal field patterns, the current per unit width on the cavity walls $\mathbf{M} = \hat{\mathbf{n}} \times \mathbf{H}$ and the surface resistance $R_\square$ are determined. Together with the stated loss tangent $\tan\delta$ of the substrate, the losses are evaluated. The total quality factor of the patch antenna is defined as

$$Q = \frac{\omega(\text{ stored energy})}{\text{power loss per cycle}} = \frac{\omega(\text{ stored energy})}{P_{rad} + P_d + P_\sigma + P_{SW}}$$

whence the following relation

$$\frac{1}{Q} = \frac{1}{Q_{rad}} + \frac{1}{Q_d} + \frac{1}{Q_\sigma} + \frac{1}{Q_{SW}} \tag{4.23}$$

results. The stored electrical energy is equal to

$$\bar{W}_e = \frac{\epsilon'}{4} \iiint_V |E|^2 dV = \frac{\epsilon' h}{4} \int_{y=0}^{W} \int_{x=0}^{L} |C_{mn}|^2 \cos^2 \frac{m\pi x}{L} \cos^2 \frac{n\pi y}{W} dx dy \tag{4.24}$$

Observing that at resonance the average stored energy in the electric field equals that stored in the magnetic field ($\bar{W}_m + \bar{W}_e = 2\bar{W}_m = 2\bar{W}_e$), total stored energy is

$$W_{tot} = 2\bar{W}_e = \frac{\epsilon' h}{2} \frac{|C_{mn}|^2 LW}{\delta_{nn'}\delta_{mm'}}$$

For all intents and purposes the term, Q_{SW} for surface waves is negligible for the electrically thin microstrip antenna here of interest [73]. For dielectric and Ohmic losses the following relationships hold

$$Q_d = \frac{1}{\tan\delta} \tag{4.25}$$

$$Q_\sigma = \frac{h}{\chi_0} \qquad \text{where} \qquad \chi_0 = \sqrt{\frac{\omega\mu\sigma}{2}} \tag{4.26}$$

is the skin depth. The radiation quality factor is given by [11]

$$Q_{rad} = \frac{2\omega\epsilon_r W}{hG}K \qquad \text{where} \tag{4.27}$$

$$K = \frac{\iint |E|^2 dS}{\oint |E| dl} \tag{4.28}$$

The microstrip antenna is a strongly resonant device. A quality factor dominated by the radiation term is indicative of how efficiently energy escapes from the cavity by radiation. The high Q-factor explains the small impedance bandwidth [47]:

$$BW = \frac{100(S-1)}{Q\sqrt{S}} \qquad \text{where S the VSWR is}$$

$$S = \frac{1+|r|}{1-|r|}$$

In general Q is dominated by the radiation term.

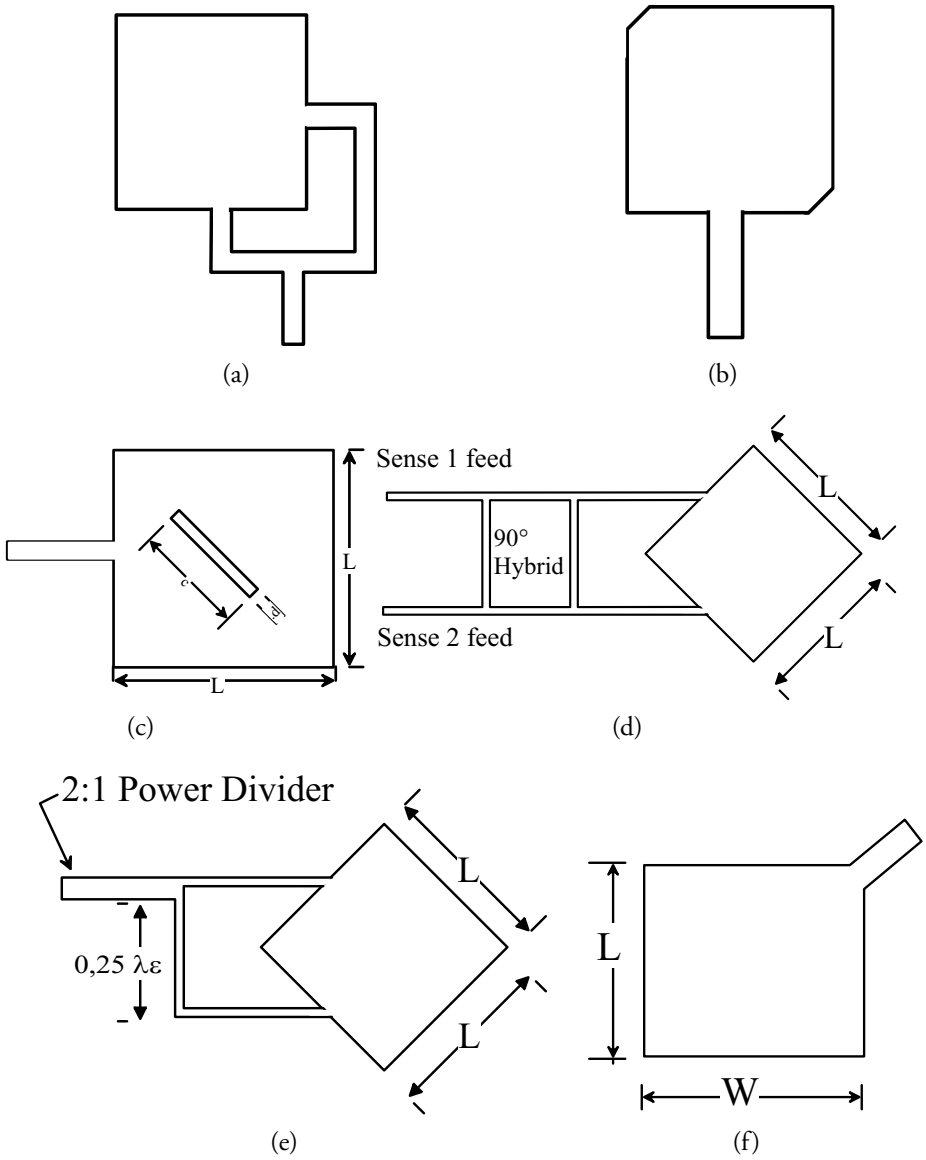

Figure 4.5: *Some compact feed methods for Circular Polarisation using neither multiple feeds nor external polarizers: (a) Orthogonal feeds with a path difference of $\frac{\lambda_\epsilon}{4}$ to reactively split modes, (b) Perturbation segments by means of corner truncation – GPS antennas (c) Diagonal slot cut out in patch (d)90° hybrid (e) 2: 1 power (Wilkinson) divider (f) Corner feed along diagonal.*

4.6 Finite Ground Plane Effect

The ground plane, a large, perfectly conducting screen placed behind a radiating element serves as a screen shielding against backward radiation and also affects, depending on its spacing, the forward pattern. Improved directivity in the normal direction is possible only to a limited degree because different path lengths lead to a less than optimum illumination of the reflecting screen and the rays reflected from more distant zones produce, in part, out-of-phase contributions. The finiteness of substrate and ground plane poses a tough challenge to the development of comprehensive and reasonably accurate approximate methods; as evidenced at times by inaccurate predictions notably in the transition regions. Edge effects from the primary aperture, secondary, and/or support structures are important for miniatures and sensitive radar. The concept of edge diffraction has been used in many fields notably in acoustics where reflections from wedge-shaped discontinuities between layers of different media have been invoked to quantify the sound field which must be added to the geometrical acoustics sound field to reach a correct total sound field. The basic problem in edge diffraction is that of diffraction from an infinite wedge irradiated by a point source. Diffraction is most pronounced when the wavelength of the radiation is comparable to the linear dimensions of the obstacle. The *e-Grain* edges are ca 80% of the wavelength. The patch induces currents on the whole surface of the *e-Grain* which acts as a gain-enhancing ground. The whole surface may thus be considered as an integral part of the antenna. Diffracted rays are produced when a ray strikes an obstacle such as a surface, an edge or a vertex. Physical optics would predict a sharp shadow boundary. Diffraction therefore offers a better description of matters by allowing a smooth transition, physical phenomena hardly being discontinuous in nature. The amplitude of the diffracted field is proportional to the incident field and a diffraction coefficient which is dependent solely on local field properties in the immediate vicinity of the point(s) of diffraction. The finite edge effect associated with the MPA can be viewed broadly as a superposition of two canonical problems, that of wedge diffraction and two tip diffractions. Each point along the wedge is considered a source of secondary waves. The envelope is a quasi-cylindrical wave centred at the edge and propagating a scattered field of the form

$$dE = \frac{C}{\sqrt{r}} e^{-j\beta r} dr. \tag{4.29}$$

Likewise for the metal tip where two edges meet, a quasi-spherical radially propagating scattered field may be postulated. From the tips of the edge emanate spherical waves

$$dE = \frac{C}{r} e^{-j\beta r} dr \tag{4.30}$$

There is a propagation delay due to the reduction of the speed of light inside the dielectric substrate. In the immediate neighbourhood of the edges, the field is much more complicated being better approximated by Hankel functions of the second kind. This is the subject of numerical investigations in section 5.1.2.

In theory, there is no difference between theory and practice.
But, in practice, there is.

Jan L. A. van de Snepscheut

5 Numerical Modelling

THE EXISTENCE NOWADAYS of programs that make use of realistic equivalent models for components and processes makes their use for an efficient and cost-effective design of antennas or antenna arrays including where necessary feed and matching networks indispensable. The results of the numerical modelling presented in this chapter are based upon a 3D electromagnetic field simulator implementation of Maxwell's governing equations using FDTD. The approximations and assumptions made in the application of these equations, how they are solved and the representation of physical processes are treated in Chapter 2.

5.1 Investigations

It is well-known that MPAs have certain characteristics which make them attractive for some applications. It is also true that exact solutions for antennas rigorously formulated as initial and boundary value problems of Maxwell's Equations are rarely available. In view of the daunting mathematical intractability even where exact and explicit solutions are known, the potentialities of CAD and numerical modelling warrant investigation. An important goal remains the acquisition of knowledge of the influence of diverse parameters that come together in a single system. Seldom is a property of interest such as the input impedance dependent on a single parameter in any simple way. This represents a particularly difficult problem because various parameters often cannot be independently optimised. For illustration, smallness of design providing large coverage is incompatible with high gain.

Not surprisingly, a drawback has been a dearth of quantitative experimental data on the effects of the various parameters such as patch length, patch width, height and dielectric constant of the substrate on the performance of the MPA. For miniatures, the relative size of patch to the ground plane is clearly an important parameter. The subject of this section is the numerical investigation of these parameters using a commercial tool, CST Microwave Studio®.

Microstrip structures in the microwave frequency range are subject to potentially performance-limiting losses arising from the finite conductivities of the metal plate and the dielectric substrate. The dependence of conductor losses on the frequency of operation, width, thickness, and surface roughness of the conductor as well as, the height of the substrate is reasonably well documented [14]. These particular factors usually do not vary greatly. Dielectric losses depend on layout, dielectric constant, frequency, and loss tangent, *cf.* Eqns. (4.27) and (4.28). Dielectric constant and loss tangent also vary with operating conditions of tempera-

ture humidity. The dielectric constant values usually vary between 0 and 0.05 % over a 100°C range for most polytetrafluoroethylene (PTFE) based laminates. The loss tangent however, can change significantly, up to 200 %, with moisture absorption of barely 0.25 % of dielectric weight [80]. We here use substrates showing little moisture absorption and assume stable ideal conditions of operation. Consequently the temperature and humidity dependence will receive no further attention.

5.1.1 Substrate Height

As the substrate thickens, fringing increases the effective distance between radiating edges, so that the resonant frequency decreases roughly linearly with increasing substrate thickness. Simulations reveal the resonant resistance as a complex function of substrate thickness with thicker substrates yielding large bandwidths. This dependence is weak compared to the effect of the feed point position; see section 5.1.6. As the thickness of the substrate increases, so too does the area of interaction of the wave with the surrounding medium. In other words, a larger structure has a smaller Q-factor which translates to a larger bandwidth. Beyond a certain point when the height is an appreciable fraction of the wavelength, diminishing returns set in. Paramount is the excitation of surface waves which are not restricted to the radiating edges of patch antennas but extend to all dielectric-free space discontinuities. The excitation of propagating higher-order modes having both z dependence (because the substrate is no longer electrically thin) and variation in the plane of the patch distorts both the pattern and impedance characteristics. Because a greater proportion of energy is now present in both the propagating and evanescent higher order modes, the efficiency drops.

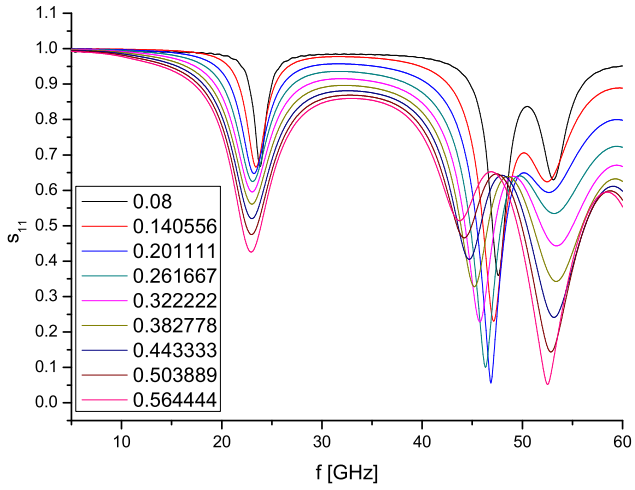

Figure 5.1: *Schematic of the dependence of resonance frequency and input reflection coefficient on the height of the substrate. Substrate height varies from 0.08 to 0.56 mm*

Use of common stripline and probe feeds becomes increasingly difficult as the substrate thickens. The probe introduces a series reactance directly proportional

to the substrate thickness as set forth in Eqn. (3.21). Hence the line inductance becomes significant with respect to the antenna radiation resistance and that way hampers proper matching.

For fixed stripline impedance, the width is proportional to the dielectric thickness neglecting edge effects. Since the patch dimensions for a fixed frequency of resonance are only weakly dependent on the dielectric thickness (through the fringing field) the width of the feed line will become considerable as the substrate reaches a certain thickness. As a result the radiation pattern of the antenna will be affected on two grounds: the covering of a radiating edge by the line and the increased radiation from the feed line in its own right. In view of the above phenomena, electromagnetic coupling is considered a viable option for electrically thick MPAs. In particular, promising results have been obtained for the stacked geometry discussed in section 3.3.3. To deal with surface waves for a given substrate height, low-permittivity or equivalently foam structures are found to be efficient. The radiation pattern is relatively insensitive to substrate height.

5.1.2 Relative size Patch to Ground Plane

Theoretical investigations of the gain and the radiation pattern almost always assume a reflecting ground plane of infinite extent. Yet any antenna has a finite size dictated by the application environment. The truncation of the antenna ground plane influences its radiation characteristics and necessitates an accurate prediction of its effects. While the radiation pattern in the forward direction may be predicted with reasonable accuracy, no method gives any indication of the intensity of radiation diffracted in the transition region. One of the first reports on the gain and pattern of finite-size MPAs was made in a missive [42] in which the edge diffracted field from the ground plane of a rectangular MPA was calculated. The analysis was limited to those cases where the distance between ground plane edge and radiating edges is greater than a quarter wavelength (ground plane size $L_{gnd} \geq \lambda$).The effective impedance is a complex function of the radial distance ρ from the feed point. At short wavelengths or equivalently when the dimension of the ground plane $L_{gnd} \approx \lambda$, the edges cause a perturbation of the current distribution on the patch that may extend back over an appreciable distance. The edge effect may be treated by assuming total reflection of the patch current at the edges (*i.e.* $|r| = 1$) such that it returns with the propagation constant of a metal plate located in the air-dielectric substrate interface. This abrupt change of geometry gives rise to the excitation of higher order modes. A more complete treatment would involve the reflected current in the radiation integral. Although this current is exponentially attenuated for lossy dielectrics, an asymptotic evaluation of the integral can be carried out only for large ground planes. It is only at points many wavelengths away from the edge discontinuities that the excited modes have been attenuated to negligible amplitudes. This endeavour seeks to numerically clarify these issues for patch antennas with a finite ground plane not exceeding one free-space wavelength in extent.

In section 4.4 the patterns in the principal E-plane and H-plane generated by the TM_{10} and TM_{01} modes in a rectangular patch were found useful for circular polarisation. In the E-plane, the field angular variation is small and for common substrate permittivities ($\epsilon_r \approx 2.2$), its magnitude does not decrease excessively from

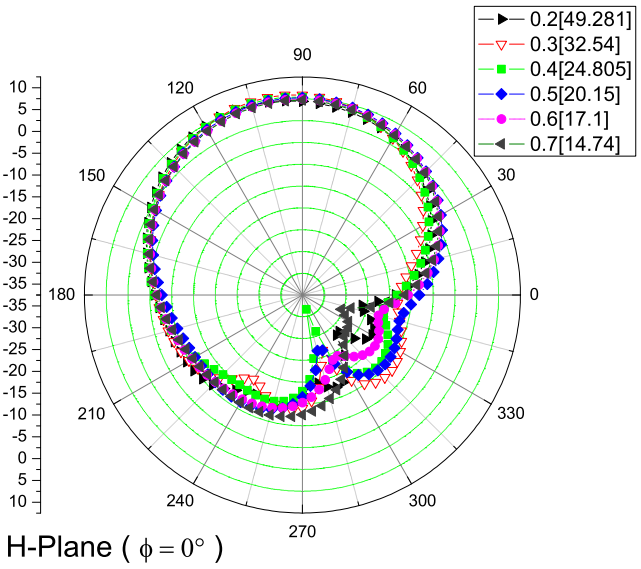

(a) H-Plane

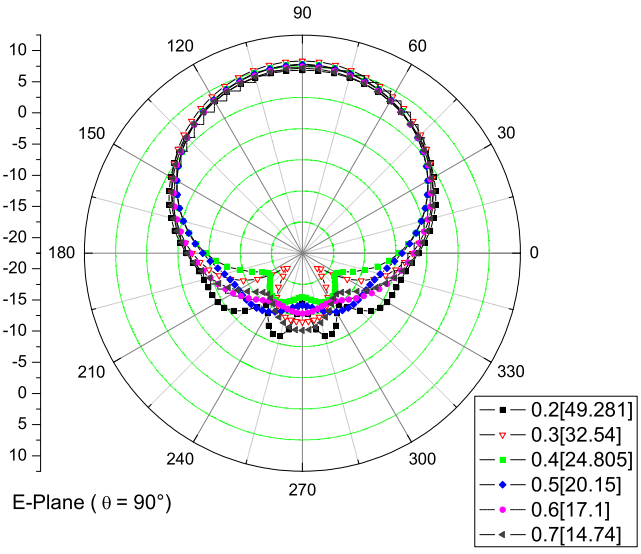

(b) E-Plane

Figure 5.2: *Radiation pattern: Both patch and ground plane are square and the patch length varies from 20 - 70 % of the ground plane. Stated in square brackets is the resonant frequency in GHz.*

its peak value at boresight. The H-plane on the other hand shows a greater sensitivity. (Fig. (5.2)).Since the peak cross-polarisation in the diagonal plane is proportional to the difference of the E- and H-plane patterns, microstrip antennas exhibit large cross-polarisations with an infinite ground plane. As the ground plane size decreases, the contribution of edge diffractions to the radiation becomes more significant resulting in remarkable changes in far field patterns. The size of the ground plane thus becomes a dominant parameter in shaping the far field pattern. Fig. 5.2 shows patterns for which the ground size was held constant at $\lambda \times \lambda$ and patch size varied as indicated. Fig. 5.3 on the other hand shows the pattern for a constant patch and varying ground plane size. In the limit when the ground plane size becomes smaller than the wavelength, spurious radiation from the ground plane tends to balance the patch radiation and the E- and H-plane patterns move closer to each other. So, by reducing the ground plane size, the pattern roll-off increases in the E-plane but decreases in the H-plane. They eventually square off for ground plane size in the order one half free space wavelength, where the cross polarisation is minimized. This is shown in Fig. 5.3(c). The ground plane shape also influences the patch radiation significantly but does not impact strongly on the patch impedance and bandwidth. Reducing the ground plane size adversely affects the impedance of the antenna, distorts the radiation pattern as the gain drops as back radiation rises. Drop in gain of about 4.5 dB for the same patch on a large ground plane was noted as the ground plane took on the value of ca. 0.5λ. Use of the surface of the *e-Grain* as enlarged ground plane does not bring about any detuning.

5.1.3 Effect of Higher Modes

Sidelobe attenuation and suppression require space and computing resources. To avoid secondary lobes, it is necessary to excite modes which do not have a zero along the radiating edge like the TM_{10} and TM_{01} modes. Since different modes may have the same frequency, the choice of the aspect ratio is very important *e.g.* if $L = 2W$, the TM_{10} and the TM_{02} modes are degenerate leading to poor polarisation properties.

5.1.4 Patch Size

Whereas there exists a direct relation between the antenna input impedance and the radiated power, there is no simple relationship between any of the above parameters and the gain. The single factor playing a most determining role on the gain is the electrical size of the antenna. In order to generate an adequate SNR, ample antenna physical dimensions are needed in view of the direct proportionality between physical size and effective capture area. The region beneath a patch is basically a high-Q cavity with more or less uniform but fringing fields along the edges. To radiate effectively a wide patch to enlarge the radiating circumference is called for. The requirement for maximum patch size is realizable only with substrates of low permittivity since patch length must be in the order of half dielectric wavelength.

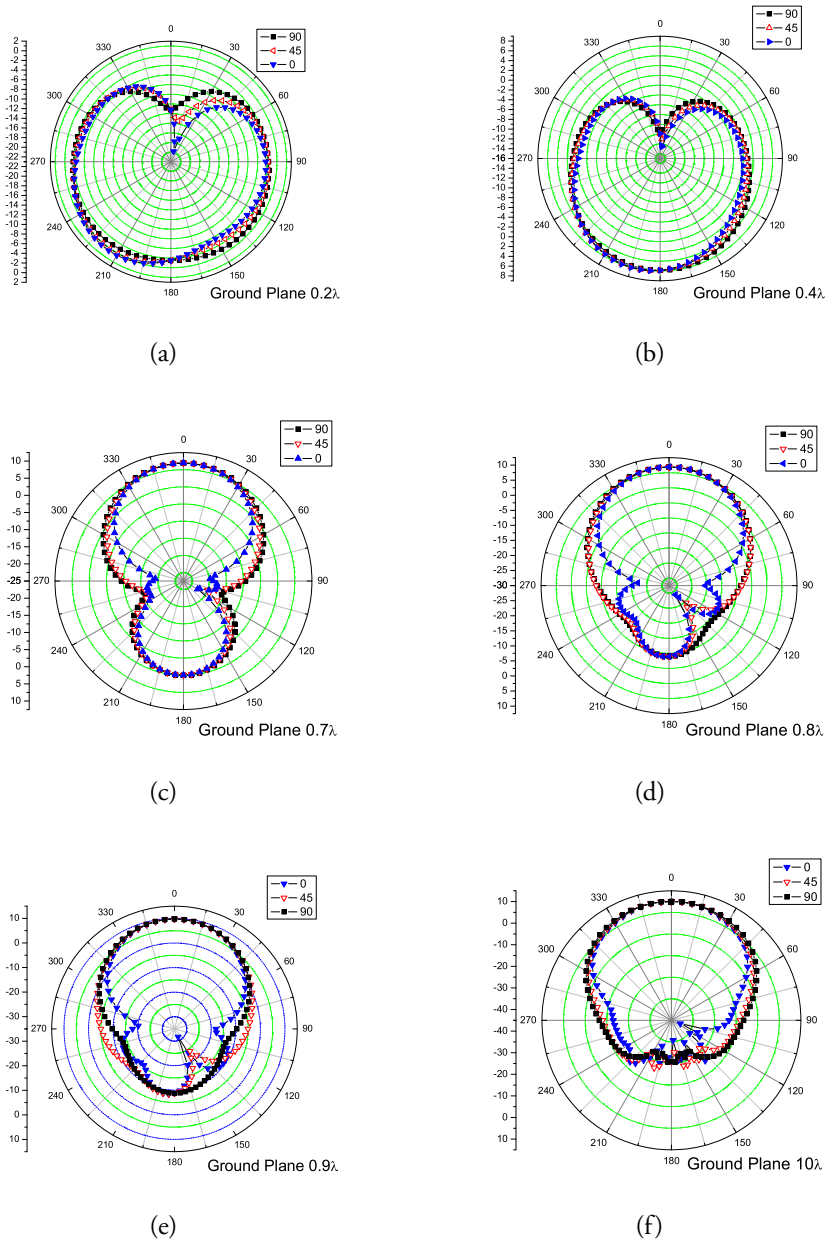

Figure 5.3: *Effect of (square) ground plane size – E-Plane (square) H-Plane (filled triangle) 45° Plane (hollow triangle) In general H-Plane is more susceptible to asymmetries due to off-centre feed position:- (a)* 0.2λ *and (b)* 0.4λ *ground plane smaller than patch → Reversal of direction of main radiation. (c) 0.7* λ*, (d) 0.8*λ*, squaring off of patch and ground plane radiation in case of equality in size: (e) 0.9*λ*, (f) 10* λ

5.1.5 Aspect Ratio L to W

For an antenna of given dimensions and material properties, the resonant frequencies and modes are completely specified. Yet an aspect ratio is critical since modes with distinct spatial configurations may have the same resonant frequency, e.g. the TM_{10} and the TM_{02} for $L = W$.

The physical aspects of the problem would lead one to expect that the variations in the lengths and feed position would be more noticeable in the H-plane patterns than in the E-plane. This is indeed the case.

5.1.6 Feed Position

The current along the patch is greatest in the centre and approaches zero at the edges. Exactly the opposite holds true for the electric field. This opens up the theoretical possibility of matching any arbitrary impedance between 0 Ω in the middle of the patch to infinite impedance at the edges. However edge effects and the presence of infinitely many modes effectively restrict the range of values realizable. In light of this a variation of feed position for minimum input reflection coefficient s_{11} or maximum transferred energy must be empirically carried out. Fig. 5.4 shows the dependence of the input reflection coefficient in the case of a linearly polarised patch antenna (a) and a circularly polarised one (b). Both make clear that the voltage-current relationship is a tad more complex than sinusoidal. There is no monotonic variation from zero Ω to the edges. Also an appropriately dimensioned patch fed along the diagonal gives CP only at a certain distance in this case 0.7 mm. This is but only approximative since the effect of fringing around the post is hardly considered.

5.2 Concluding Remarks

The basic patch is easy to build but shows a number of disadvantages; the foremost being the limited bandwidth. Increasing the bandwidth makes a design resistant against the usually small tolerances. The extremely complex design challenges cannot be solved with low cost tools.

A more spacious and possibly cumbersome conventional microwave antenna will doubtless out-perform its thin conformal planar counterpart but many systems particularly the aerospace, personal communications systems (PCS), stealth and the budding ubiquitous systems are only made feasible through the latter. The path to the future will go through integrated electronically beam-scanned arrays and switched antennas. If the trend towards higher frequencies leads to systems with wavelengths which are comparable to the size of a raindrop, diffraction, atmospheric absorption and distortion of waves by raindrops will play an even greater role. Error-correcting codes, higher than necessary input power and antenna diversity will receive more attention. With feature size on the fall and frequency on the rise, such systems may well be restricted to indoor use.

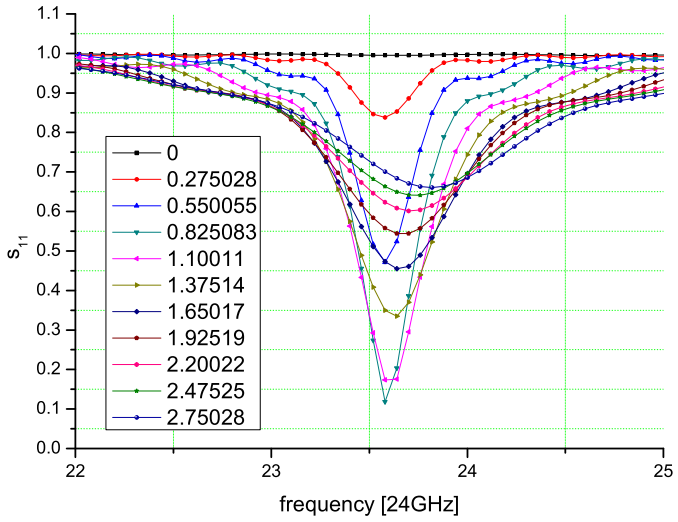

(a) Linear polarisation

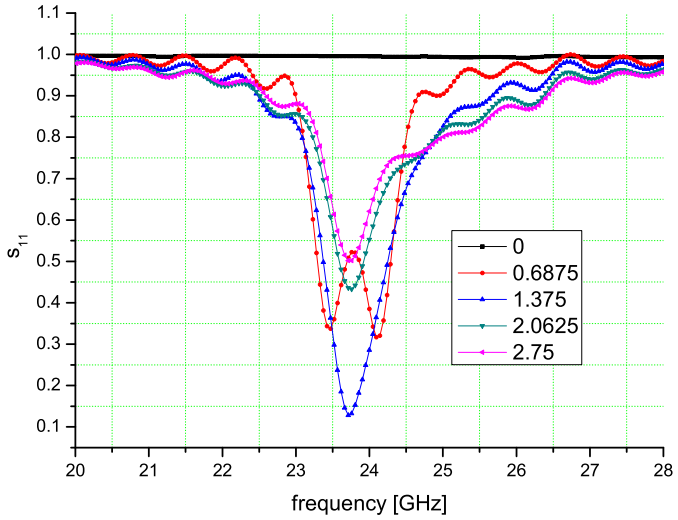

(b) Circular polarisation

Figure 5.4: *Feed Position: (a) s_{11} Variation of feed between edge and middle of patch, (b) Variation of reflection coefficient with distance from patch centre along diagonal. Red curve shows clearly the principle of circular polarisation.*

In der Beschränkung zeigt sich erst der Meister.

Goethe

6

Electrically Small Antennas

SMALL APPLICATIONS REQUIRE antennas that fit. A lofty goal of miniaturisation is to shrink devices, render them integrable into a wireless network while at the same time maintaining or improving performance expected of a much larger antenna. The aim here is to design and investigate an antenna structure of the order of 1 cm that *inter alia* shows a measure of ruggedness against proximity effects such as detuning. The frequency range of interest is 700 to 900 MHz where a full-sized quarter wave whip would be from 8.0 to 10.0 cm long. Its pattern should be omnidirectional in the horizontal plane.

6.1 The Appeal of the Electrically Small Antenna

Electrically Small Antennas (ESAs) have found use principally at long wavelengths where designs would otherwise be cumbersome and impractical on grounds of aerodynamic drag, size, weight and cost. In the wake of miniaturisation the risk is real that antennas may become prohibitively large and easily surpass the target feature size. Of increasing importance is the design of structures that radiate efficiently over a given band of frequencies yet have a maximum dimension that is only a small fraction of the free-space wavelength. Expressed mathematically such eminently appealing antennas fulfill the condition:

$$ka \ll 1,$$

a being the radius of the smallest virtual enclosing sphere. The reciprocal of the wavenumber $k^{-1} = \frac{\lambda}{2\pi}$ may be interpreted as the radius of a sphere centred on the antenna within which the reactive or stored power density exceeds the radiation power density. The capacity to efficiently couple power to free space is proportional to antenna size in wavelengths. The great strides made towards miniaturisation of next generation wireless communication systems notwithstanding, antenna size stands out as the most difficult parameter to reduce. The reason being that the free space wavelength obviously cannot be miniaturised. Chu [13] followed up Wheeler's work [102] with an analysis of ESAs using the theory of spherical harmonics since at sufficiently large distances, an antenna may be viewed as a point source emitting spherical waves. Enclosing the antenna in a virtual sphere, the minimum Q is found to be inversely proportional to the cube of sphere radius in radian wavelengths when the radius is much less than the latter. In that work he used a partial fraction expansion of the wave impedance of spherical modes that exist outside the smallest circumscribing sphere surrounding the antenna to obtain

an equivalent ladder network from which the Q could be found by conventional circuit analysis. Accordingly the lower limit of the Q-factor of any linearly polarised antenna obtains on exclusive radiation of the lowest spherical mode. Thus, in order to approach the theoretical limit of the performance index Q , the antenna structure should fill as efficiently as possible the enclosing sphere for sole excitation of either the fundamental electric dipole mode (TM) or the fundamental magnetic dipole mode (TE). In either case, the lower limit for the radiation is [35; 65]

$$Q = \frac{1}{(ka)^3} + \frac{1}{ka} \tag{6.1}$$

A noteworthy attempt to approach this limit in practice is the capacitively loaded multi-element monopole due to Goubau [26].

6.1.1 Penalties in Antenna Size Reduction

Limitations in the performance indicators efficiency, impedance matching, frequency bandwidth, radiation pattern and gain arise on reducing antenna size. Antenna engineering is as such faced with the dilemma about how to design small antennas that satisfy both performance specifications and aesthetic concerns of users. Microstrip antennas appear to have the edge over other candidates because of various attractive characteristics outlined in Chapter 4. Yet for most present-day mobile communication systems in the lower regime of the microwave spectrum (<3 GHz) even microstrip antennas in their conventional form would be unwieldy. The recent literature is awash with concepts to reduce the size of the radiating element. Typical methods of reducing the size of a microstrip antenna and the associated trade-offs are summarized thus:

- Loading with a high-dielectric constant material ϵ_r incurs bandwidth and efficiency losses owing to the high loss tangents can considerably degrade the radiation performance. The property of being narrowbanded is compounded dictating the observance of tighter manufacturing tolerances.
- A quarter-wave resonator instead of the half-wave patch is used. cf. the relation between a wire dipole and a wire monopole. Drawbacks are the reduced impedance bandwidth and the increased level of cross-polarised radiation. e.g.conformal folding along the line of zero electric field [67].
- Use of a shorting post in close proximity to the probe feed as shown in Fig. 6.1(a) [99] (for a stacked set-up [98]). It is realized with respect to size reduction that shorted patches, in the limit, are very similar to planar inverted-F antennas [94].
- Loading patch antennas using resistive terminations instead of shorting pins without reducing the associated impedance bandwidth [106]. A critical disadvantage of using resistive terminations is the inherent reduction in radiation efficiency.

6.1.2 General considerations

Similar to plane waves, the ratio of the transverse electric and magnetic field components is constant throughout a waveguide cross-section. The modal wave impedances

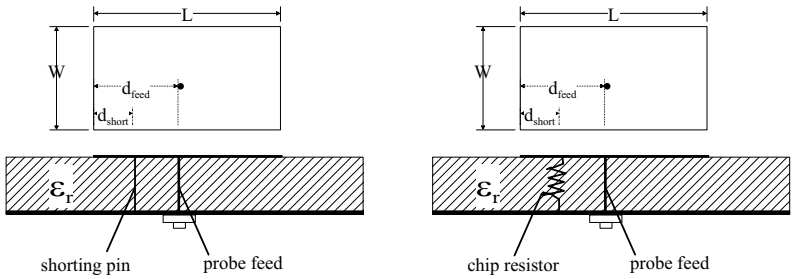

(a) Shorted post in probe vicinity. (b) Chip-resistor loading of patch.

Figure 6.1: *Two size reduction approaches*

for TE and TM modes show fundamentally different frequency dependencies

$$Z_{TE} = \frac{j\omega\mu}{\gamma} \tag{6.2}$$

$$Z_{TM} = \frac{\gamma}{j\omega\epsilon} \tag{6.3}$$

highlighting the matching problem in ESAs. The endemic proliferation of wireless communications is accompanied by an increased likelihood of susceptibility to interference. An antenna based on a magnetic dipole is preferable to small electric dipoles and ferrite antennas from the viewpoint of its reduced susceptibility to the finite (imperfect) ground plane and other environmental influences [24]. Heat losses in metal and dielectric parts of an antenna are inevitable and the current injected into the antenna goes in part to set up oscillating non-propagating electromagnetic fields. Consequently the driving point resistance of an antenna differs from its radiation resistance as calculated from electromagnetic theory

$$R_m = Z_0 \frac{2\pi}{3} \left(\frac{\beta A}{\lambda} \right)^2 \text{ for a loop antenna and} \tag{6.4}$$

$$R_e = Z_0 \frac{2\pi}{3} \left(\frac{\Delta l}{\lambda} \right)^2 \text{ for the Hertzian dipole.} \tag{6.5}$$

A is the loop area and Δl the length of the Hertzian dipole. The radiation current is substantially less than the feed current. The result is a low radiation resistance, low efficiency and large frequency-dependent reactance. These are characteristic of an ESA and explain the very small impedance bandwidths. This renders impedance matching difficult. However, the radiation resistance and with it, the efficiency of a loop tends to increase with frequency ($\propto f^2$). Responsible for the far field radiation in a tuned antenna installation is the current circulating in the radiating structure. The moment of a loop and thus its capacity for radiation stand in direct proportion to loop area and current, both of which are scarce in this scenario. Loop antennas are usually used as receiving antennas with many such single loop designs being used for pagers and other mobile communications equipment, while multi-turn loop antennas are used for AM broadcast receivers.

Recognizing the need for further miniaturisation, this endeavour seeks to investigate with a view to unit the merits of microstrip technology with the potential of the miniloop that has been considered an optimum design for a miniature.

6.2 Miniloop or An Optimum Design for a Miniature

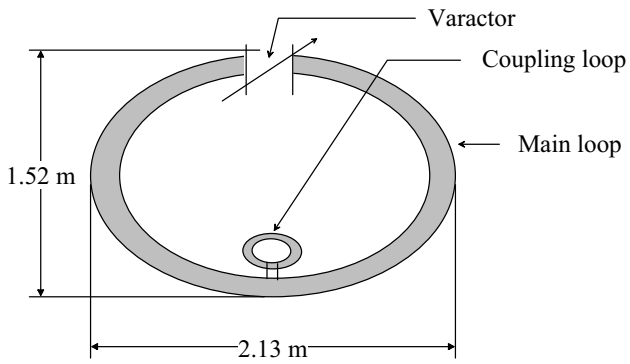

Figure 6.2: *Configuration of a typical miniloop structure with the outer loop capacitively tuned to the desired frequency by a varactor.*

A rigorous treatment of the principle of operation of the loop antenna of circular shape has been carried out *inter alia* notably in [49]. Patented in 1971, the HF miniloop antenna is an electrically small but physically large tunable one-turn loop configuration (Fig. 6.2) in which an electrically small, capacitively tuned outer loop radiates based on inductive excitation by an even smaller inner loop that is fed by a transmission line for high-power (1 kW, CW) transmission and reception in the 3 - 30 MHz frequency band [20]. By virtue of the sharp nulls in its figure-of-eight pattern, it found use initially in direction finding, radar and communications applications that require a compact antenna with a measure of azimuthal directivity as on aircraft and ships [60]. Its impedance can be easily matched to a 50-Ω transmission line at resonance over a relatively wide range while maintaining the radiation pattern and good overall performance. A single remotely controlled high-Q varactor is the sole variable RF component for tuning. The small size and surprisingly high efficiency render it, in effect, a tuned filter of high selectivity possessing enhanced signal to noise characteristics for reception and making duplex communications an affordable prospect. Hence it was considered an optimum design for a miniature antenna. Electrical balance with its support mast acting as ground at its neutral point makes it relatively immune to local interference and so may be installed at low heights above ground.

ESAs are even more enticing as antenna design grapples with the challenges brought up by miniaturisation and the progression from low frequencies to higher and higher frequencies. Such antennas are forcibly resonant in character, whereby at the natural or resonant frequency,[1] the electromagnetic energy is stored over a time interval long compared with the period of the wave. At resonance the current flowing in the radiating structure may be significantly larger than the feed current. Additionally resonance makes possible a coupling by backscatter of the transmitter to the receiver in the far field as implemented in RFID systems. This is in contrast to load modulation which couples via electromagnetic inductance, the $1/r^3$ dependence limiting the range to the near field [22].

[1] Beyond the first resonance a description by the capacitances and inductances to be derived shortly becomes less accurate.

Figure 6.3: *A pair of miniloops mounted on a lorry: US Army*

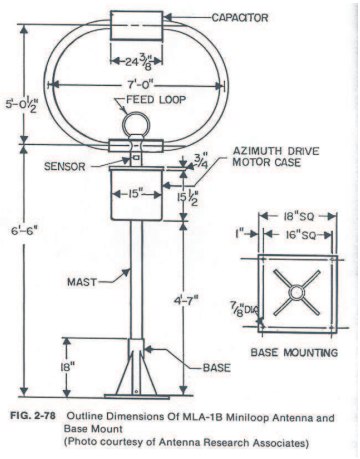

Figure 6.4: *Schematic of the miniloop after Preston E. Law[60, Shipboard Antennas]*

From the foregone an improperly designed ESA may be very inefficient. Ideally its input reactance must be zero to avoid a high insertion loss, a matching circuit being dissipative and requiring space. Though dielectric-loaded antennas will yield reasonably sized antennas, the exacerbated bandwidth problem and losses render their use less tempting hence the following proposal which is based on a magnetic dipole and so needs little counterpoise. It offers many degrees of freedom in design and more robustness in face of proximity to other materials and bodies.

6.2.1 Resonant Cavities

The theory of transmission line circuits and that of waveguide systems are formally the same. The fundamental difference between low-frequency and microwave circuit analyses is electrical length or size. Using this formal equivalence and that high-Q tuned circuits are usually built from low-loss inductors and capacitors, a miniloop antenna is derived and consistently implemented in microstrip technology. Using the concept of distributed parameters, resonant antennas may be built in the form of resonant cavities. Strictly speaking, use is made rather of *pseudo*-cavities which are only partially surrounded by conducting walls to admit coupling/feeding and so allow for radiation.

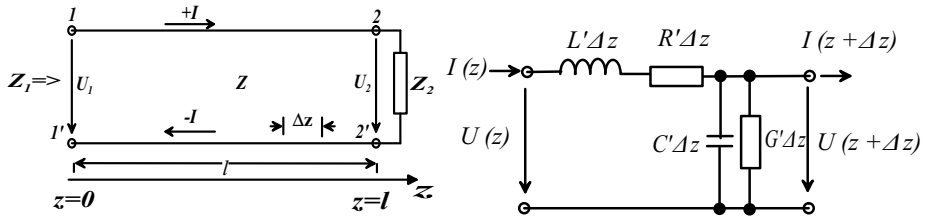

(a) Calculation of input impedance (b) Distributed parameters in a differential piece of transmission line Δz.

Figure 6.5: *Voltage and current relations in a piece of transmission line.*

Distributed Parameters

In Fig. 6.5 R', L', G' and C' denote the series resistance, the series inductance , the shunt conductance and shunt capacitance per unit length, respectively. On the basis of TLT, the voltage and current in a short section of homogeneous line are found to be [14; 83]

$$V(z) = V(l)\cosh\gamma(l-z) + ZI\sinh\gamma(l-z) \tag{6.6}$$

$$I(z) = \frac{V(l)}{Z}\sinh\gamma(l-z) + I(l)\cosh\gamma(l-z) \tag{6.7}$$

where the propagation constant

$$\gamma = \sqrt{(R'+j\omega L')(G'+j\omega C'} = \alpha + j\beta$$

and the characteristic impedance

$$Z = \sqrt{\frac{R'+j\omega L'}{G'+j\omega C'}}.$$

Hence the input impedance seen by a source at $z = 0$ is

$$Z(z) = Z\frac{1+\frac{Z_2}{Z(l)}\tanh\gamma(l-z)}{\tanh\gamma(l-z)+\frac{Z_2}{Z(l)}} \tag{6.8}$$

A straightforward enforcement of the short-circuit condition at terminal 2 transforms to an impedance at terminal 1 of

$$Z_{sc}(0) = Z\tanh\gamma l$$

while an open-circuit in the same plane shows

$$Z_{oc}(0) = Z\coth\gamma l.$$

The attenuation constant α is small if the line sections are made of good conducting copper. Additionally, the transmission lines are very short compared to the

wavelength; so incur little losses. Hence the following simplification can be carried out:

$$\begin{aligned} Z_{sc}(0) &= Z\tanh\gamma l && (6.9)\\ &= Z\frac{\alpha l + j\tan\beta l}{1 + j(\alpha l)\tan\beta l} && (6.10)\\ &\approx jZ\tan\beta l \qquad \text{since} \quad \alpha l \ll 1 && (6.11) \end{aligned}$$

This means the hyperbolic functions may be replaced by their trigonometric counterparts as was done in [3] :

$$\begin{aligned} Z_{sc}(0) &= jZ\tan\beta l = jZ\beta l\\ Z_{oc}(0) &= -jZ\cot\beta l = -\frac{jZ}{\beta l} \qquad \text{for} \quad |\beta l| \ll 1, \quad \tan\beta l \approx \beta l. \end{aligned}$$

If the strip width w and substrate thickness h satisfy $w \geq 2h$, a quasi-static approximation of the characteristic impedance of the microstrip line [56]

$$Z = \frac{Z_0}{\sqrt{\epsilon_r}(w/h + 2)}$$

gives the *lumped* circuit parameters as

$$L = \frac{\mu_0\mu_r l}{(w/h_1 + 2)} \tag{6.13a}$$

$$C = \epsilon_0\epsilon_r l(w/h_2 + 2). \tag{6.13b}$$

In view of the opposite signs of the reactances in Eqns. (6.13) and their dependence on the electrical parameters of the transmission lines, in theory at least, any arbitrary value of inductive and capacitive reactance can be obtained from an open-circuited and a short-circuited transmission line, respectively. It would therefore be possible to obtain resonance at any desired frequency. Apart from fitting the AVM

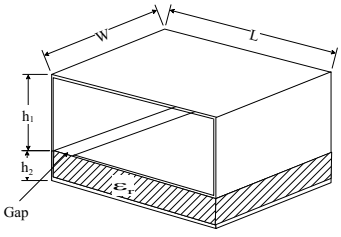

Figure 6.6: *Miniloop-Microstrip hybrid: Length, $l = 10mm$, height of short-circuited topmost section $h_1 = 3.5mm$, height of open-circuited section underneath the former $h_2 = 0.64mm$, width of strip $w = 9.8mm$, the gap is 1 mm broad.*

form, a rectangular shape also expedites construction. An innovative yet eminently practical radiating structure using short pieces of transmission lines for the purpose of realizing the reactive elements is shown in three-dimensional view in Fig. 6.6. It consists of a wide strip of width, w wrapped around to form a loop and a parallel-plate capacitor in a single piece. *It thus shows an uncanny similarity to ρ (inverted*

*σ) and it is tempting to call it a **rho antenna**.* The inductance is created from the air-filled short-circuited topmost section. Beneath the inductance, the capacitance to tune out the former is derived from a second transmission line section which this time around is open-circuited (not short-circuited as in the first case) and filled with dielectric material of $\epsilon_r = 9.8$. There exists no galvanic contact between its left end and the leads of the short-circuited topmost section hence the gap as suggested in Fig. 6.6.

Effectively the loop is resonated by an integrated capacitor made of an Al_2O_3 ceramic slab metallised on both faces. Conventionally loops with a circumference less than half a wavelength are not often used because they exhibit very large reactances. Space being at a premium, a one-turn inductive loading of the loop which is reminiscent of a potential divider will be employed to reduce this reactance. Hence this physically and electrically small set-up using microstrip lines offers radiation characteristics comparable to the more conventional case of loops having a circumference of one wavelength at the operating frequency.

6.2.2 Principle of Operation

Effective Current Path

In an antenna which is small compared with the wavelength, current is essentially uniform all around the loop perimeter. The coaxial-cavity coupling shown in Fig.

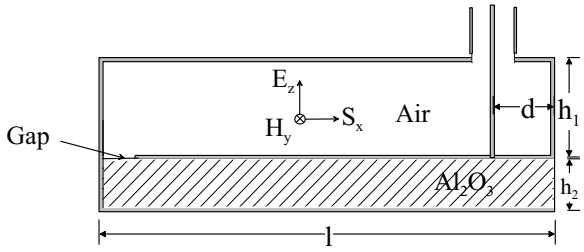

Figure 6.7: *Probe through the loop shows elements of both an inductive and capacitive coupling. Also shown is the flux linkage through loop area $A = l \cdot h_1$*

6.7 leads to current flow principally on the inner side of the strip. Thus a single feed excites both electric and equivalent magnetic currents. Due to the ratio of the heights of the air-filled and dielectric-filled regions, the effective current for radiation is confined in the loop as sketched in Fig. 6.8(a). The voltage shows a slight linear increase towards the open-circuit (gap) end of the tuning capacitor. If the height of the dielectric slab h_2 is small compared to loop height h_1, the effects of the currents in the x and $-x$ directions cancel out. Since most of the area has uniform current and the highest voltages are localized in a comparatively small space region along the gap, the magnetic component dominates. Magnetic fields are founded on the movement of charges, the acceleration of which exerts a force on other charges and thus ensues radiation. That the current flowing in the capacitor beneath the loop is small compared to that in the latter is confirmed in the computation result shown in Fig. 6.8(b).

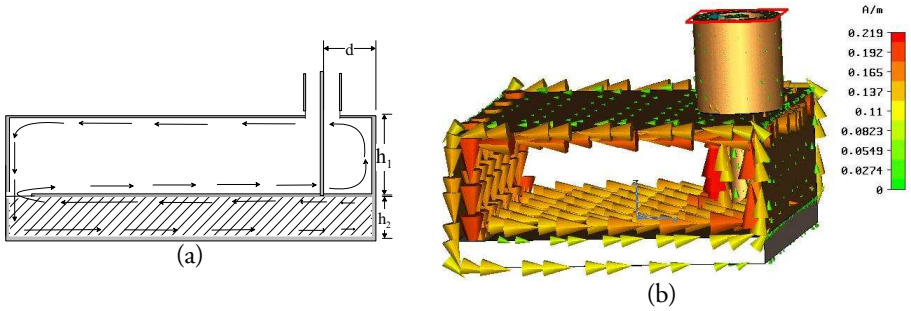

Figure 6.8: *Current distribution in the microstrip miniloop antenna: (a) Expected current distribution (b) Computed current distribution.*

The magnetic induction due to any elementary loop of area dA is identical with the electric field due to a certain electric dipole of moment Id. This moment is associated with the current in the capacitance that tunes out the loop inductance. Since the loop approximates a magnetic dipole, the far-field radiation can be obtained readily from that of the well-known electric dipole by duality [56]:

$$H_r = \frac{IA}{2\pi}\exp^{-j\beta r}\left(\frac{j\beta}{r^2}+\frac{1}{r^3}\right)\cos\theta \tag{6.14a}$$

$$H_\theta = \frac{IA}{2\pi}\exp^{-j\beta r}\left(-\frac{\beta^2}{r}+\frac{j\beta}{r^2}+\frac{1}{r^3}\right)\sin\theta \tag{6.14b}$$

$$E_\phi = \frac{Z_0 IA}{4\pi}\exp^{-j\beta r}\left(\frac{\beta^2}{r}-\frac{j\beta}{r^2}\right)\sin\theta \tag{6.14c}$$

A z polarised wave having an x-directed Poynting's vector and a magnetic field of

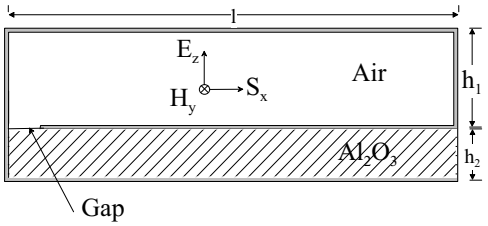

Figure 6.9: *Flux linkage through area of loop.*

magnitude H_{0y} represents optimum flux linkage because there is no polarisation mismatch. The linkage through the area enclosed by the loop is depicted in Fig. 6.9. Using Faraday's law, the amplitude of the induced voltage that appears in the loop can be expressed as

$$\int_A \nabla\times\mathbf{E}\cdot d\mathbf{A} = -\int_A \frac{\partial\mathbf{B}}{\partial t}\cdot d\mathbf{A}$$

$$U = -j\omega\mu_0 H_{0y}A = -j\beta A E_{0z}$$

6.2.3 Lumped element circuit model

In a first order approximation, the loop may be regarded as a inductance which is resonated by the above derived capacitance yielding a pure real driving point impedance, Fig. 6.10. All losses i.e. skin effect, radiation and dielectric losses are lumped in the resistance R_{tot}.

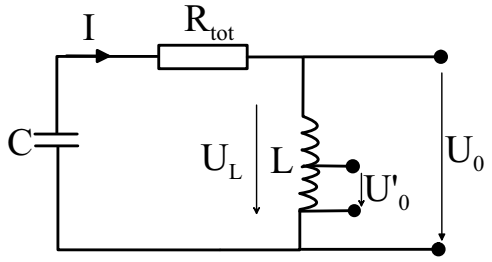

Figure 6.10: *Equivalent Circuit of unloaded Antenna with a one-coil transformer coupling schematized*

Tapped Coupling

To simplify construction and in contrast to the conventional miniloop system, the inner conductor of a coaxial cable runs through the main loop and makes contact with the upper plate of the capacitor thus creating the coupling loop. There are two closed paths around the field with the primary and secondary currents sharing a path segment. This may be viewed as a one-coil transformer. Letting the distance of the inner conductor from the wall be d (see Fig. 6.7), the coupling coefficient κ may be defined as the ratio of the coupling area to the area of the whole loop which equals $\kappa = d/L$. The short-circuit loop current may be determined to

$$I_{sc} = \frac{-j\beta_0 A E_{0z}}{R_{tot}}. \tag{6.15}$$

The maximum available open-circuit voltage which occurs near the gap is

$$U_0 = I_{sc} j\omega L = -j\beta_0 A \cdot \frac{j\omega L}{R_{tot}} \cdot E_{0z}. \tag{6.16}$$

From Eqn. (6.16) an expression for the effective height of the antenna is imminent

$$h_{\mathit{eff}} = \beta_0 A Q \tag{6.17}$$

bringing to light the importance of the enclosed area $A = l \cdot h_1$ and indirectly the magnetic dipole moment $\mathbf{P_m} = \mu I \mathbf{A}$ in this solution. This can be generalised to

$$h_{\mathit{eff}} = \beta_0 A Q \sin\theta$$

whereby θ is the angle between the polarisation vector of the antenna and that of the incident wave. Using the coupling coefficient, the open-circuit voltage in the case of reception may be written as

$$U_0' = \kappa U_0 = \frac{d}{L} \frac{\omega L \beta_0 A E_{0z}}{R_{tot}} \tag{6.18}$$

This tapped/transformer coupling of the loop antenna was confirmed experimentally and via electromagnetic simulation as shown in Fig. 6.11. In view of the

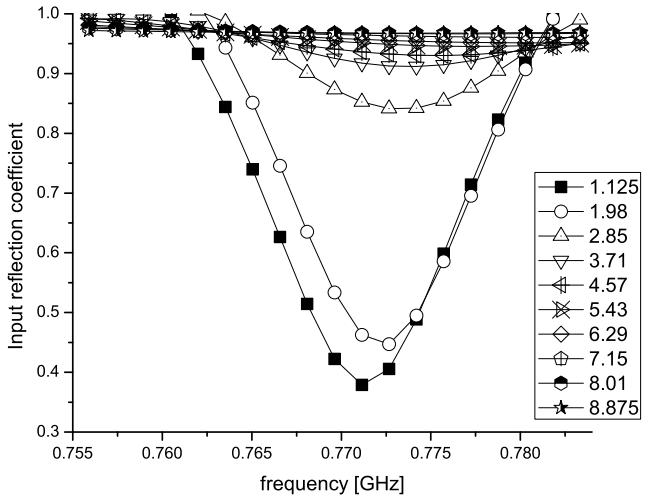

Figure 6.11: *Variation of the input reflection coefficient vs. distance, d along the line of symmetry between "short-circuit" and "open-circuit". Symmetry espcially in the feed is important for the resonant modes. Any breach of symmetry is noticeable in the radiation pattern and return loss.*

advantages of an omni-directional pattern in the horizontal plane, and that any asymmetry in the structure impacts directly on the pattern, it may at first sight seem judicious to position the feed at the geometrical centre of the capacitor. Though the amplitudes of multipole modes are negligible, their contribution leads to a high input impedance sensitivity to position. The most efficient coupling in terms of VSWR as the diagram shows takes place just in the vicinity (ca. 1.25 mm) of the "short-circuit" point. Mechanical and material constraints permitted a value for the distance d of 1.75 mm in the prototype. It resonated at 745 MHz with an input reflection coefficient, S_{11} of 0.45.

Quality Factor and Bandwidth Neglecting in a first approximation the effect of coupling through the loop, $Q = \frac{\omega L}{R_{tot}}$ is the unloaded Q-factor of the loop and the input impedance of the tuned loop evaluates to

$$Z_{in} = \frac{(R_{tot} + j\omega L)j\omega C}{R_{tot} + j\omega L - (j/\omega C)} = \frac{(R_{tot} + j\omega L)/j\omega C}{R_{tot} + j\omega L(\omega^2 - \omega_0^2)/\omega^2} \tag{6.19}$$

where $\omega_0^2 = 1/LC$. For an electrically small structure Q is large because the stored power density outweighs dissipation power density, the bandwidth small and so ω may be replaced by ω_0 near resonance to obtain the following approximation

$$(\omega^2 - \omega_0^2)/\omega^2 \approx 2\omega_0(\omega - \omega_0)/\omega_0^2 = 2\omega_0/\Delta\omega.$$

Hence the input impedance takes the form:

$$Z_{in} \approx \frac{1+jQ}{j\omega_0 C[1+j(2Q\Delta\omega/\omega_0)]}.$$

Considering the equality of the inductive and capacitive reactance at resonance, $\omega_0 C$ may be expressed as $\frac{1}{QR}$ so that the input impedance reads

$$Z_{in} \approx \frac{(1+jQ)QR_{tot}}{1+j(2Q\Delta\omega/\omega_0)} \approx Q^2 R_{tot} \quad \text{since} \quad |2Q\Delta\omega/\omega_0| \ll 1. \tag{6.20}$$

Viewed as a transformer, the quality factor in Eqn. (6.20) is analogous to the turns ratio. This impedance step-up at resonance permits a small antenna to extract from a radio wave and deliver to a load an amount of power independent of antenna size [102]. Eqn. (6.20) emphasizes that maximum available power is transferred to a load of $Q^2 R_{tot}$ not R_{tot}. This explains performance superior to that expected of the small loop radiation resistance, R_m.

The tapping distance d must be properly chosen to match the antenna impedance to the load to circumvent potential losses in a matching circuit.

A large Q brings about a high selectivity meaning only the signal matching the (natural) resonant frequency is detected and amplified, even though signals from various sources may concurrently impinge on the antenna. The current enhancement, and hence the step-up in the antenna resonant resistance over R_{tot}, is to a good degree of approximation proportional to the square of the Q factor; see Eqn. (6.20).

The radiation resistance of a small loop antenna as stated in Eqn. (6.4) is

$$\begin{aligned} R_m &= Z_0 \frac{2\pi}{3} \left(\frac{\beta A}{\lambda}\right)^2 \\ &= Z_0 \frac{\pi}{6} \left(\frac{4\pi A}{\lambda^2}\right)^2 \qquad (6.21a) \\ &= Z_0 \frac{\pi}{6} \left(\frac{A}{\lambda^2/4\pi}\right)^2 \qquad (6.21b) \end{aligned}$$

In a very small antenna, the radiation and loss power factors may be so small that their ratio is difficult to measure. Eqn (6.20) provides a simple method to match the low resistance R_m of a resonant loop antenna to the high impedances (several KΩ) required by CMOS integrated circuits if Q is suitably high. The transformer action leads to a good match at the fundamental. Away from the fundamental, mismatch is considerable and the input impedance of the primary is extremely small, so that $I^2 R_m$ radiated power is also small.

However, because of the impedance transformation discussed above, it is found in empirical computations that for a tuned small loop, the input reflection coefficient varies as the loop height divided by the wavelength, all raised to the second power. Also S_{11} measurements do indeed seem to indicate that the loop antenna works much better than expected from theory.

Frequency Pulling From the equivalent circuit of the antenna Fig. 6.10 the second-order differential equation

$$\frac{d^2\xi}{dt^2} + 2\sigma\frac{d\xi}{dt} + \omega_0^2 \xi = f(t) \tag{6.22}$$

may be readily derived where ξ stands either for current or voltage, σ for the damping constant ($\propto R_{tot}$), ω_0 for the natural frequency and f for the forcing or driving function. Laplace transforming it and solving for the transfer function yields

$$U(s) = \frac{\Xi(s)}{F(s)} = \frac{1}{s^2 + 2\sigma s + \omega_0^2} \tag{6.23}$$

Eqn. (6.23) can then be expanded into partial fractions as follows

$$U(s) = \frac{j}{2\omega_L}\left(\frac{1}{s+\sigma+j\omega_L} - \frac{1}{s+\sigma-j\omega_L}\right) \tag{6.24a}$$

$$s_{1,2} = -\sigma \pm \sqrt{\sigma^2 - \omega_0^2} \tag{6.24b}$$

$$\omega_L = \sqrt{\omega_0^2 - \sigma^2} \tag{6.24c}$$

where the singularities are at $s_{1,2}$ and ω_L is the new natural resonant frequency of the loop. Eqn. (6.24) shows a certain degree of detuning when the attenuation constant $\sigma \neq 0$. This explains the observation that the prototype of the microstrip miniloop antenna (MML) resonates at 745 MHz corresponding to an error of 3.6 % with respect to the target frequency of 771.1 MHz according to simulations. The theory here developed predicts resonance at 802 MHz. The homogeneous solution to Eqn. (6.22) is known as

$$v(t) = V \exp^{-\sigma t} \sin \omega_L t \tag{6.25}$$

whence the stored energy is proportional to the time average value of $v^2(t)$. Assuming small losses ($\sigma \ll 1$) the afore-mentioned quantity is

$$W \approx \frac{1}{2} V^2 \exp^{-2\sigma t} \tag{6.26}$$

whence the average power in the system is readily arrived at as

$$P = \frac{dW}{dt} = 2\sigma W \tag{6.27}$$

From the definition of the quality factor $Q = \frac{\omega_0 W}{P}$, the *de facto* resonant frequency is

$$\omega_L = \omega_0 \sqrt{1 - \frac{1}{4Q^2}} \tag{6.28}$$

This provides a means of determining the losses in the antenna structure.

With a loss tangent of 10^{-4} dielectric losses are negligible compared to copper losses. The radiation efficiency can therefore be expressed as

$$\eta = \frac{R_m}{R_{loss} + R_m} \tag{6.29}$$

$$R_{loss} = \frac{1}{\sigma}\frac{2(l+h_1)}{\chi_0 w} \tag{6.30}$$

An impedance-matched and therefore efficient ESA has percentage instantaneous bandwidths which are intrinsically narrow. For instance, the minimum Q for the

loop whose dimensions are given in Fig. 6.6 is 600. That the bandwidth of an ESA can be increased by loading with resistive elements, alas at the cost of efficiency and gain has been treated by several authors formulating in the process the so-called bandwidth-efficiency product [15; 35]. With the recent allocation of spectrum for commercial UWB, bandwidth considerations shift back to focus. The performance of loop antennas can be enhanced by ferrite-loading the core. This does not only increase the flux linkage for a given field strength, it also increases the radiation resistance. Adding resistive elements increases bandwidth but also increases the Noise Figure and reduces the effective isotropic radiated power. This was not taken up owing to anisotropy in ferrites. An attractive prospect entails the electronic tuning of ESAs using various frequency dependent matching networks.

6.3 Link Budgeting

The path loss may be described by the ratio of received to transmitted power $\frac{P}{P_{max}}$. It is therefore an essential parameter of a communication link

6.3.1 RCS Measurement

Apart from the impracticability of measuring the open circuit voltage and short circuit current through a miniature, there are difficulties arising from interaction with conductive objects in close proximity to the small antenna. Measurement of voltage and current in such small antennas for internal impedance determination is as such beset with enormous difficulties.

Use is made of a *wireless* measurement technique which encompasses simultaneous emission and susceptibility measurements in a GTEM cell first presented in [67]. A GTEM cell may be viewed as a pyramidal extension of a round coaxial feed line to a rectangular waveguide. It has a flattened inner conductor (septum), which is offset from the middle of the cell to enlarge the usable test volume. The cross section is designed to maintain an impedance of 50 Ω. At the rear of the cell, the flared waveguide is terminated by a combination of discrete resistors and RF absorbers. The former provides low reflection termination at low frequencies while the latter are effective at high frequencies. The measurement technique is based on the theorem of reciprocity. If a current I_1 is injected into the cell (the equivalent input voltage is $U_1^h = I_1 Z_L$) which sets up a fairly homogeneous field around the AUT:

$$E_1 = \frac{I_1 Z_L}{h_s} \tag{6.31}$$

Hence the open-circuit voltage induced across the terminals of the AUT is

$$U_2 = h_{\mathit{eff}} \frac{I_1 Z_L}{h_s} \tag{6.32}$$

R_C is the distance from the tip of the cell to position of the AUT. α is the apex angle of the cell so that the relevant septum height at the AUT $h_s = R_C \cdot \alpha$. The induced voltage generates a loop current I_2. The circulation of I_2 results in radiation or *re*radiation so that a voltage U_1 is induced across another antenna coincident with the input terminals of the cell. This induced loop current is identical to I_{sc} at resonance. It acts in turn as a source of radiation which is dual to that of an electric

dipole, as treated in section 6.2.2. The secondary magnetic far field induced by the loop at a distance r in free space can be expressed as [37]

$$H_{sy} = \frac{I_{sc}\beta_0^2 A}{4\pi r} \tag{6.33}$$

If S_p and S_s represent the magnitudes of the Poynting's vector of the primary incident wave and the *re*radiated wave emanating from the loop, respectively, then radar cross section may be written as follows

$$\sigma_{rcs} = 4\pi r^2 \frac{S_s}{S_p} = 4\pi r^2 \left(\frac{H_{sy}}{H_{py}}\right)^2 = 4\pi L_r^2 \tag{6.34}$$

where L_r denotes the *radar scattering radius*. The quotient $\left(\frac{H_{sy}}{H_{py}}\right)^2$ is the square of the reflection coefficient which can be read off the network analyzer in the experimental setup schematized in Fig. 6.12.

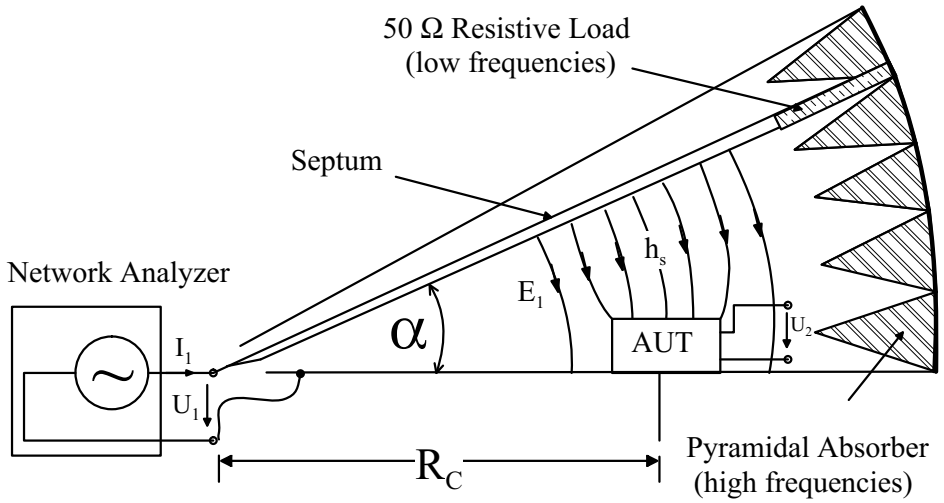

Figure 6.12: *Determination of the scattering radius of antenna by measurement of the reflection coefficient in a GTEM Cell.*

Earlier efforts in characterizing scattering include [40] in which a *scattering coefficient* was discussed. The radar scattering radius was postulated in [66] as *Radarrückstreulänge*. If viewed as a radius, it would describe a sphere of surface area equal to the radar cross section, hence the appellation radar scattering radius. The radar scattering radius is found using Eqns. (6.15) and (6.33) in equation (6.34) to be

$$L_r = \beta_0^2 A^2 \cdot \frac{Z_0}{2\lambda R_{tot}} = \left(\frac{h_{eff}}{Q}\right)^2 \cdot \frac{Z_0}{2\lambda R_{tot}} \tag{6.35}$$

6.3.2 Power Assessment

In transmission mode, a loop current I_{tr} in an equation similar to (6.15) corresponds to a maximum available power for transmission P_{max} of

$$P_{max} = \frac{1}{2} I_{tr}^2 R_{tot} \tag{6.36}$$

For a power-matched situation in the reception case, the following holds. The field impinging on a receiving antenna of the same type at a distance r is

$$E_z = \frac{I_{tr} \beta_0^2 A Z_0}{4\pi r} \tag{6.37}$$

Hence using Eqns. (6.17) and (6.37) the received power can be written as

$$P = \frac{1}{2} [E_z \cdot h_{eff}]^2 \cdot \frac{1}{4R_{tot}} \tag{6.38}$$

It is now possible on making use of Eqns. (6.36) and (6.38) together with Eqn. (6.37) to give a power assessment for a link between two similar antennas representing two *e-Grains* as

$$\frac{P}{P_{max}} = \left(\frac{\beta_0^2 A Z_0 h_{eff}}{4\pi r} \right)^2 \left(\frac{1}{2R_{tot}} \right)^2$$

On inserting Eqn. 6.35 this can be expressed in terms of L_r as

$$\frac{P}{P_{max}} = Q^2 \left(\frac{L_r}{2r} \right)^2 \tag{6.39}$$

In view of Eqn. (6.39) it is tempting to think the ratio $\frac{P}{P_{max}}$ is directly proportional only to the square of the quality factor. This is only apparently so since the radar scattering radius as given by Eqn. (6.35) is also in direction proportion to the quality factor:

$$L_r = Q \frac{\beta_0^2 A w}{4\pi} = Q \frac{w h_2}{4\pi \epsilon_r l}.$$

Consequently Eqn. (6.39) shows the following dependence on geometric and material properties

$$\frac{P}{P_{max}} = \frac{Q^4}{4} \left(\frac{\beta_0^2 A w}{4\pi r} \right)^2 = \frac{Q^4}{4} \left(\frac{w h_2}{4\pi \epsilon_r r l} \right)^2$$

This underscores the importance of a high quality factor for a favourable link budget.

6.4 Impedance and Pattern Measurements

6.4.1 Impedance Measurement

Optimizations, an excerpt of which is shown in Fig. 6.11 predict a feed position of minimum return loss about 1.75 mm from the short circuit end. This was readily verified within the bounds of the given manufacturing process; see Fig. 6.13.

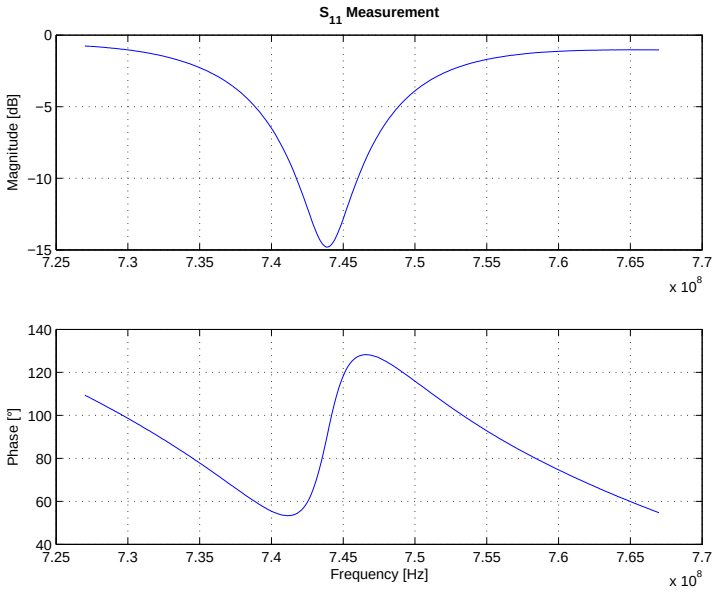

Figure 6.13: *Measured s_{11} showing a larger bandwidth than expected*

The employed first-order approximation predicts resonance at 802.5 MHz. The MML prototype operates at 743 MHz with the 3-dB bandwidth covering the band of frequencies from 739 to 746 MHz. This corresponds to a bandwidth of 1 % lending credence to the impedance step up by a factor Q^2 (very much larger than CST computation). The frequency deviation may be explained along the lines frequency pulling in section 6.2.3.

6.4.2 Pattern Measurement

The shape of the loop is irrelevant when considering the far-field radiation pattern of an electrically small loop antenna. The y-directed magnetic dipole moment $\mathbf{P}_m$ leads to an omni-directional pattern dual to that of a similarly oriented electric dipole moment $\mathbf{P}_e$. The maximum of the directional pattern is thus in the plane of the loop and the nulls perpendicular to that plane forming the well-known doughnut.

Unlike the impedance behaviour, the pattern measurements proved inconclusive in initial measurements. There was an apparent directionality thus deviating from the expected omni-directional pattern; see Fig. 6.18(a).

Pursuant of high efficiency, the coaxial cable was located at the point of minimum reflection coefficient. This point is not coincident with the physical centre of the antenna. Hence a measure of asymmetry in the radiation pattern is expected.

However, near field effects such as diffuse and specular reflections from surroundings that cannot be satisfactorily clad with absorbers were found to be significant. Because of the imbalance of the impedance to ground from the feed, common-mode currents flow on the feed line (Fig. 6.17(a)).

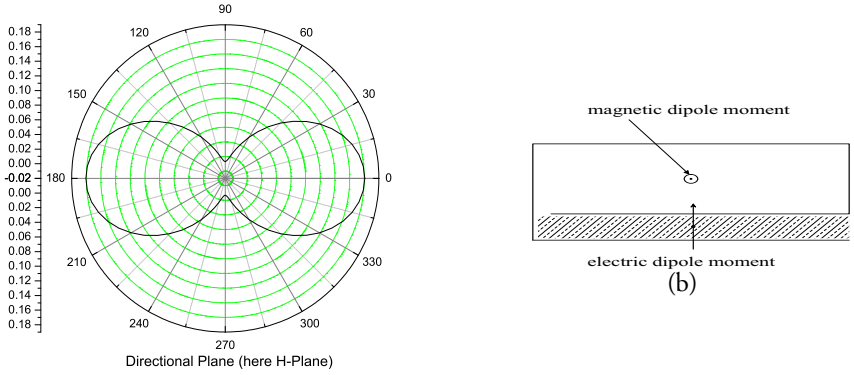

(a)

Figure 6.14: *(a)Computed H-Plane radiation characteristic of the MML. Not so sharp nulls are indicative of the filling effect of the electric dipole moment. (b) Orientation of the two dipole moments.*

(a) (b)

Figure 6.15: *(a) Microstrip Miniloop Antenna, MML. (b) Relative size of MML:* $\lambda/40$ *at operating frequency.*

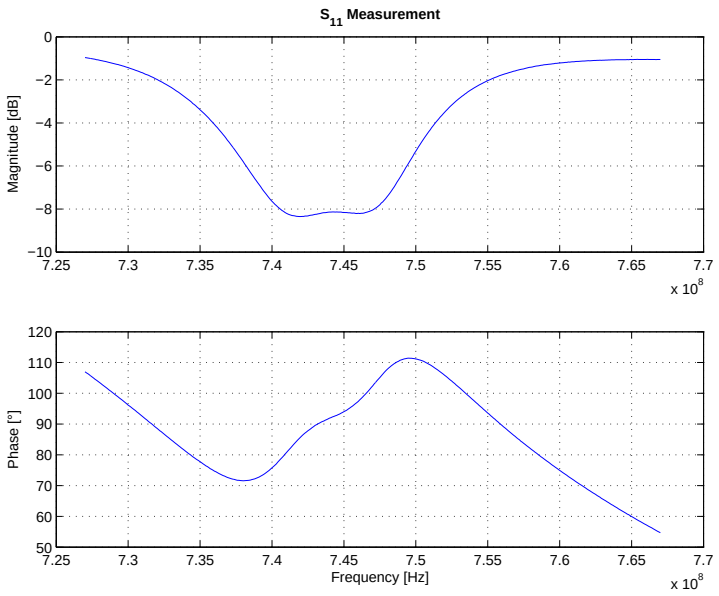

Figure 6.16: *The choke and antenna being two strongly frequency dependent structures when critically coupled yield a band filter.*

Quarter-wave Choke

An attempt to suppress these using a $\lambda/4$-choke was inconclusive. The coaxial cable RF interference choke assembly for reducing transmission, via the outside of the outer coaxial conductor, of RF signals of a given frequency while passing RF signals of the same predetermined frequency on the inside of said coaxial conductor is shown in Fig. 6.17(b). The choke offers infinite inductive impedance theoretically only at a single frequency.

To incorporate some flexibility, an annular ring of PVC ($\epsilon_r = 3.18$) was inserted between the coaxial feed and the $\lambda/4$ choke. In the latter was milled a slit so that the ring could be moved and so influence the action of the choke. The impedance measurements show that effectively two critically tuned circuits were capacitively coupled resulting in a filter; see Fig. 6.16.

This shows somewhat that antennas can be excellent filters. The $\lambda/4$-choke is narrow-band solution. If the frequency of operation of choke and antenna are not the same but lie sufficiently close to one another, a critical coupling might lead to the formation of a band filter as shown is in Fig. 6.16

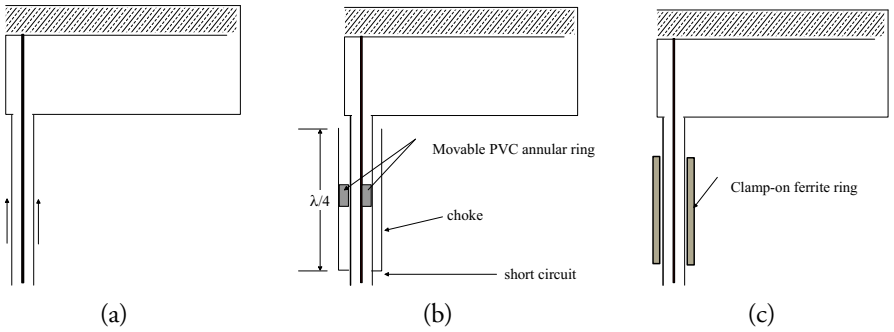

Figure 6.17: *(a)Common mode currents flow on the surface of the coaxial feed line (b) Partial suppression of spurious radiation using a $\lambda/4$-choke and a sliding PVC annulus.(c) The clamp-on ferrite proved a more efficient means of muzzling unintended radiation.*

Clamp-on Ferrites

Most often the choke is an inductor with a ferrite core used in the frequency range where the ferrite is lossy. The signal maxima lobes are a bit broader than the nulls.

The unbalanced mode radiation and the loop radiation proper give an omnidirectional pattern inevitably needed in mobile communications. The TM or electric dipole component is manifested in the not so sharp nulls of the computed diagrams and also the fact that the MML-antenna is predominantly but not purely linearly polarised.

The E-Plane is more sensitive to near field effects. Since in the final product such a feed shall not be used, the MML antenna may be considered an adequate antenna for use in such scenarios.

The presence of a null in only one position, is an indication that the loop has become unbalanced and the feedline part of the antenna. Testing for signal deterioration by touch hinted at the presence of common-mode currents. A clamp-on ferrite provided significant suppression as comparison of the subfigures in Fig. 6.18 reveals.

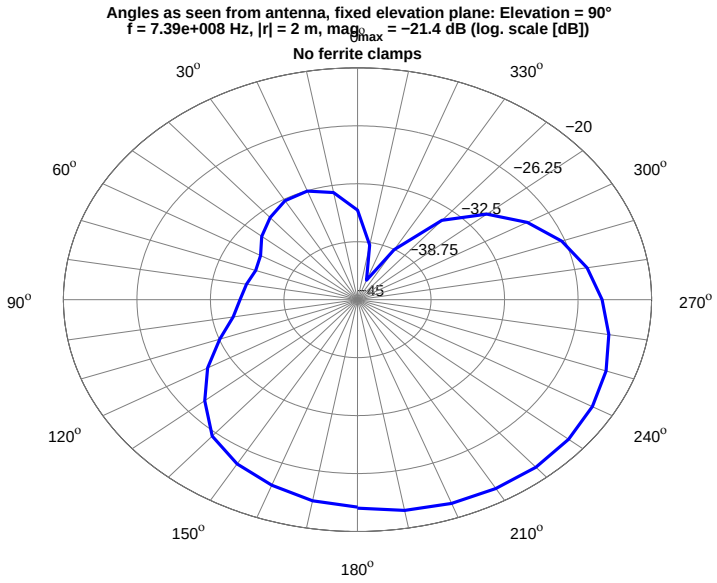

(a)

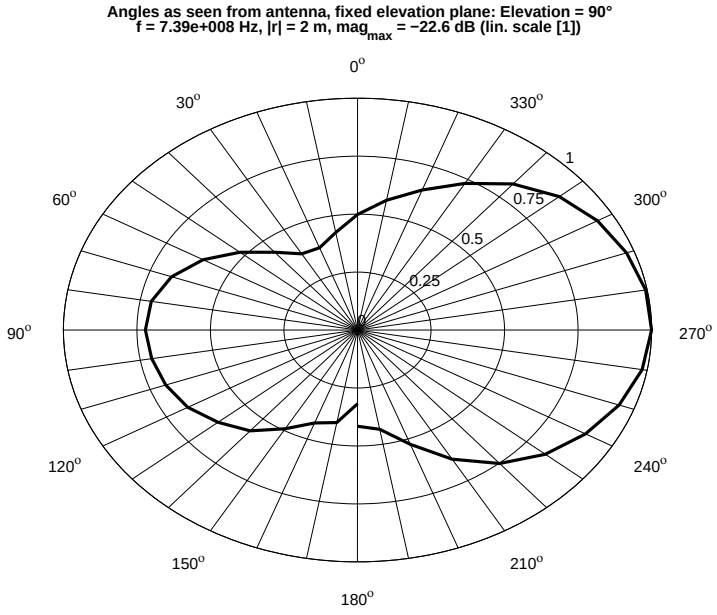

(b)

Figure 6.18: *(a) H-plane pattern without Clamp-on ferrite (b) Effect of suppression of feedline common-mode currents*

6.4.3 The Prospect of an MML-Turnstile

Theoretically an array of isotropic point sources can be conceived which will produce any arbitrary pattern. Often e.g. if the deduced reflector profile varies significantly within a wavelength, realisability as was seen in section 3.2.2 on page 34 can be a problem. It is well known that in principle a linearly polarised antenna can be converted to perfect circular polarisation by superimposing upon its radiation characteristics, those of its dual radiator having transposed E- and H-field sources. For instance, a wire dipole (electric source) would need to be combined with a wire loop (magnetic source), but in reality it is physically impossible to construct or feed such an arrangement precisely and compromises are made such as the employment of crossed-wire dipoles which yield circular polarisation in a limited region of the hemisphere and over restricted bandwidth. It is established that the smallest circularly polarised antenna is obtained for a properly weighted combination of TM and TE-modes in phase quadrature[65]. The MML with the feed structure here presented possesses both magnetic and electric dipole moments the relative magnitudes of which can be varied.

To improve product performance in an interference-prone environment, a balanced ground-independent antenna is given preference. Imbalances or asymmetry must be avoided or minimized to reduce common mode noise. Feed position should be determined with the goal of minimizing insertion loss Ţ

The purpose of models is not to fit the data but to sharpen the questions.
Samuel Karlin

A Multimode Cavity Theory

THE STRONG FREQUENCY sensitivity of the microstrip antenna requires a more accurate theory. In a full modal expansion theory seems to lie the possibility of handling several modes and feed structures [79]. Feeding either with a strip line or coaxial cable can be modelled as a uniform strip of vertically ($z-$) oriented electric current. Due to fringing in the neighbourhood of the feed, the width of the equivalent feed is larger than the centre conductor of the coaxial feed. The observation that a narrower feed introduces a greater inductance is of importance in impedance matching. On account of the thinness of the substrate, the $z-$directed feed current is also independent of z. Using the stationary property of the energy, it is readily established that the mode associated with the lowest eigenvalue contributes the most to radiation. Since there are infinitely many modes and particularly in situations where the fundamental mode is not strongly excited, it becomes necessary to expand the field under the patch in terms of a *complete orthonormal* set of functions [58].

A cavity composed of a homogeneous dielectric enclosed by perfectly conducting walls admits of an infinite set of resonant frequencies having a lower bound but no upper bound. The cavity model is founded on the premise of an electrically thin substrate. The oscillating electromagnetic modes of interest are the transverse magnetic (TM) modes because the transversal magnetic field component vanishes ($\mathrm{H}_z = 0$) and $\mathrm{E}_z \neq 0$ at the edges. For the purpose of analysis all non-metallic antenna peripheries may then be enclosed within a magnetic wall. Such a closed cavity is more susceptible to resonate having for that matter a purely reactive input impedance of either zero or infinity rather than radiate. However, a perturbational approach shows the field structure in the MPA to be approximated by essentially that in the resonant cavity [58].
Using the established method of separation of variables the following statement for z-directed orthogonal electric field mode functions for the rectangular patch ψ_{mn} can be derived

$$\psi_{mn} = C_{mn} \cos \frac{m\pi x}{L} \cos \left(\frac{n\pi}{W} y \right) \tag{A.1}$$

where C_{mn} is an amplitude constant, both $m, n \in N$ and may not be simultaneously equal to zero. The electric field has zero divergence and does not vary in z by hypothesis ($\frac{\partial}{\partial z} = 0$) implying

$$\nabla \cdot \mathbf{E} = \frac{\partial E_x}{\partial x} + \frac{\partial E_y}{\partial y} = 0.$$

Both E_x and E_y are independent of E_z. Whence the magnetic field is given by

$$-j\omega\mu\mathbf{H} = \nabla \times \mathbf{E} \tag{A.2a}$$

$$= \hat{x}\left(\frac{\partial E_z}{\partial y} - \frac{\partial E_y}{\partial z}\right) + \hat{y}\left(\frac{\partial E_x}{\partial z} - \frac{\partial E_z}{\partial x}\right) \tag{A.2b}$$

$$= \hat{x}\frac{\partial E_z}{\partial y} - \hat{y}\frac{\partial E_z}{\partial x} \tag{A.2c}$$

In the above use is made of the open-circuit condition of vanishing tangential component of $\mathbf{H}$. Since the magnetic field depends only on E_z, the tangential components of $\mathbf{E}$, E_x and E_y must be constant and an expedient choice is E_x = E_y = 0. Thus for $\mathbf{E}$:

$$\mathbf{E} = \mathrm{E}_z = \psi_{mn}\hat{z} \tag{A.3}$$

A patch driven by a current $z-$directed I_0 in a coaxial feed of radius r at $y = \frac{W}{2}$ and $x = x'$ may be assigned a current density $\mathbf{J} = J_z = \frac{I_0}{2\pi r}\delta(x - x')\delta(y - \frac{W}{2})$. This current excites a field which satisfies the wave equation

$$\nabla \times \nabla \times \mathbf{E} - k^2\mathbf{E} = -j\omega\mu\mathbf{J} \tag{A.4}$$

where $k = \omega\sqrt{\epsilon\mu}$. Making use of the identity $\nabla \times \nabla \times \mathbf{E} = \nabla\nabla \cdot \mathbf{E} - \nabla^2\mathbf{E}$ and specifying the divergence to $\nabla \cdot \mathbf{E} = 0$ the following obtains:

$$\nabla^2 E_z + k^2 E_z = j\omega\mu_0 J_z \tag{A.5}$$

The total field E_z is the sum of all discrete modes excited in the cavity by the probe current. By completeness property of the mode functions Eqn. (A.1), the total field can be written as

$$E_z = \sum_{m=0}^{\infty}\sum_{n=0}^{\infty} C_{mn}\cos\frac{m\pi x}{L}\cos\frac{n\pi y}{W} \tag{A.6}$$

where $n, m \in \mathbb{N}$. Substituting E_z in Eqn. (A.5) yields

$$\sum_{m=0}^{\infty}\sum_{n=0}^{\infty} C_{mn}(k^2 - k_{mn}^2)\cos\frac{m\pi x}{L}\cos\frac{n\pi y}{W} = j\omega\mu_0 J_z \tag{A.7}$$

with $\frac{\partial\psi_{mn}}{\partial n} = 0$ and

$$(\nabla_t^2 + k_{mn}^2)\psi_{mn} = 0$$

at the edges which are modelled as a magnetic wall. These mode functions for the ideal non-radiating patch satisfy the homogeneous wave equation and the eigenvalues satisfy the separation equation

$$\begin{aligned} k_{mn}^2 = \omega_{mn}^2\mu\epsilon &= \left(\frac{m\pi}{L}\right)^2 + \left(\frac{n\pi}{W}\right)^2 \\ &= k_m^2 + k_n^2 \end{aligned} \tag{A.8}$$

where k_{mn}^2 is real.

Eqn. (A.7) except for the factor $j\omega\mu_0$ is recognizable as the Fourier series expansion of the current J_z. As a result it is multiplied by

$$\cos(n'\pi x/L)\cos(m'\pi y/W)$$

anticipating the use of the completeness and orthonormality relations

$$\begin{aligned}\sum_{\alpha}\psi_{\alpha}(\mathbf{r})\psi_{\alpha}^{*}(\mathbf{r}') &= \delta(\mathbf{r}-\mathbf{r}')\\ \int_{v}\psi_{\alpha}(\mathbf{r})\psi_{\alpha}^{*}(\mathbf{r})d\mathbf{r} &= \delta_{\alpha\beta}\end{aligned}$$

Using the orthogonality of the mode functions, the amplitude coefficient reads

$$C_{mn}=\frac{\delta_{mm'}\delta_{nn'}}{LW}\int_{0}^{L}\int_{0}^{W}\frac{j\omega\mu_0 J_z(x,y)\cos(n'\pi x/L)\cos(m'\pi y/W)}{k^2-k_{mn}^2}dxdy \qquad \text{(A.9)}$$

where $\delta_{mm'}$ stands for the Kronecker symbol

$$\delta_{mn}=\begin{cases}1 & n=m\\ 0 & n\neq m \text{ and } n,m\geq 1.\end{cases}$$

The power fed into the patch is $\frac{1}{2}I_0^2 Z_{in}$ from which the input impedance may then be defined as

$$Z_{in}=-\frac{1}{I_0^2}\iiint_{V}\frac{\mathbf{E}\cdot\mathbf{J}}{k^2-k_{mn}^2}dV \qquad \text{(A.10)}$$

The amplitude coefficient becomes infinite as k approaches k_{mn}, the real resonant wave number of the mn^{th} mode. This situation does not set in because of the damping effect of losses. It does however underscore the resonant (cavity) nature of the patch. To treat the singularity, $k^2-k_{mn}^2$ is expressed as

$$\mu_0\epsilon\left[\omega^2-\frac{k_{mn}^2}{\mu_0(\epsilon'-\epsilon'')}\right]=\mu_0\epsilon\left[\omega^2-\frac{k_{mn}^2}{\mu_0\epsilon'}\left(1-\frac{j\epsilon''}{\epsilon'}\right)\right] \qquad \text{(A.11)}$$

where clearly the dependence on the loss tangent $\tan\delta=\frac{\epsilon''}{\epsilon'}$ of the substrate is apparent.

The eigenvalues become complex, corresponding to complex resonant frequencies, so that k_n is slightly less than $\frac{n\pi}{W}$ and k_m is slightly less than $\frac{m\pi}{L}$ making radiation from the cavity possible. Radiation and other losses from the cavity are represented in terms of an artificially increased loss tangent of the substrate. The tangential component magnetic field is then no longer zero on the cavity sidewalls. By lumping and radiative losses with the dielectric losses in an artificially augmented effective loss tangent instead of that of the dielectric substrate alone, Richards *et al.* [79] obtained good agreement between theory and experiment. By allowing the effective permittivity to take complex values, non-resonant modes are included in the calculation of the electric field at the radiating edges or slots. Thus the find for the electric field

$$E_z=j\omega\mu_0\sum_{m}\sum_{n}\frac{1}{k_{\mathit{eff}}^2-k_{mn}^2}\frac{<J_z\psi_{mn}^{*}>}{<\psi\psi_{mn}^{*}>}\psi_{mn} \qquad \text{(A.12)}$$

where $k_{\mathit{eff}}^2=\omega^2\mu\epsilon\left(1+\frac{\sigma_{\mathit{eff}}}{j\omega\epsilon}\right)=k_0^2\epsilon_r(1-j\delta_{\mathit{eff}})$ represents the effect of lumping losses in an augmented loss tangent.

The field and thus input impedance are proportional to the amplitude factor which on its own is dependent on patch dimensions as well as on both position and size of the feed, elements which are absent in the transmission line and single mode cavity models. Once the field distribution is obtained, the radiation can calculated.

Bibliography

[1] National Research Council. *The Evolution of Untethered Communications*. National Academy Press, Washington, D.C., 1997.

[2] Alford, A., and Sprague, R. M. A four Slot Cylindrical Antenna for VOR Service. *IRE National Convention Record* (March 1954), 12 – 24.

[3] Angwafo, N., and Mönich, G. An Integrated Microstrip Miniloop Antenna for Short Range Communications in Ubiquitous AVM. *IEEE - ICECom 18* (Oct. 2005), 189 – 192.

[4] Angwafo, N., Wittwer, M., von der Mark, S., and Mönich, G. Antenna Concepts for Ubiquitous Communication Networks: The Case of AVM. *Frequenz: Zeitschrift für Telekommunikation 58*, 3 - 4 (Jan./Feb. 2004), 80 – 86.

[5] Arai, H. *Handbook of Antennas in Wireless Communications*. The Electrical Engineering and Applied Signal Processing Series. CRC Press, Boca Raton, 2002.

[6] Arfken, G. B., and Weber, H.-J. *Mathematical Methods for Physicists*, 4th ed. Academic Press, San Diego, Ca., 1996.

[7] Berenger, J.-P. A perfectly matched layer for the absorption of electromagnetic waves. *J. Comput. Phys. 114*, 2 (Oct. 1994), 185 – 200.

[8] Booker, H. Babinet's Principle and the Theory of Resonant Slots. *TRE (Great Britain) Report No. 29* (Dec. 1941).

[9] Booker, H. Slot aerials and their relation to complementary wire aerials (Babinet's Principle). *J. Inst. Electr. Eng. 93* (1946), 620 – 626.

[10] Bryant, J. H. The First Century of Microwaves 1886 - 1986. *IEEE Trans. MTT 36* (May 1988), 830 – 858.

[11] Carver, K. R., and Mink, J. W. Microstrip Antenna Technology. *IEEE Trans. Antennas Propagat. 29*, 1 (Jan. 1981), 2 – 24.

[12] Chen, C., McKinzie, W., and Alexopoulos, N. G. Spectral domain analysis of microstripline fed arbitrarily-shaped aperture antennas. *APS Int. Symposium Digest 1* (20 - 24 June 1994), 158 – 161.

[13] Chu, L. J. Physical Limitations of Omni-directional Antennas. *J. Appl. Phys. 19* (Dec. 1948), 1163 – 1175.

[14] Collin, R. E. *Foundations for Microwave Engineering*, 2nd ed. IEEE Press Series on Electromagnetic Wave Theory. IEEE/Wiley Interscience, 2001.

[15] Collin, R. E., and Rothschild, S. Evaluation of antenna Q. *Antennas and Propagation, IEEE Transactions on 12*, 1 (Jan. 1964), 23 – 27.

[16] Debski, T. R., and Hannan, P. W. Complex Mutual Coupling Measurements in a Large Phased Array Antenna. *Microwave Journal 8* (June 1965), 93 – 96.

[17] Derneryd, A. G. A Theoretical Investigation of the Rectangular Microstrip Antenna Element. *IEEE Trans. Antennas Propagat. 26*, 4 (July 1978), 532 – 535.

[18] Deschamps, G. A. Microstrip Microwave Antennas. *The Third Symposium on The USAF Antenna R & D Program, Monticello, Illinois* (1953), 18 – 22.

[19] Devoret, M. H., and Schoelkopf, R. J. Amplifying Quantum Signals with the Single - Electron Transistor. *Nature 406* (Aug. 2000), 1039 – 1046.

[20] Dunlavy, Jr., J. H. Wide-range tunable transmitting antenna. U.S. Patent 3 588 905, June 1971.

[21] Evans, H., Gale, P., and Sambell, A. Performance of 4 X 4 sequentially rotated patch antenna array using series feed. *Electronics Letters 39*, 6 (March 2003), 493 – 494.

[22] Finkenzeller, K. *RFID Handbook: Fundamentals and Applications in Contactless Smart Card and Identification*, 2nd ed. John Wiley & Sons Ltd, 2003.

[23] Foschini, G., and Gans, M. On Limits of Wireless Communications in a Fading Environment when Using Multiple Antennas. *Wireless Personal Communications 6* (1998), 311 – 335.

[24] Fujimoto, K., Henderson, A., Hirasawa, K., and James, J. R. *Small Antennas*. Antennas. Research Studies Press Ltd. John Wiley & Sons Inc., 1987.

[25] Gedney, S., and Roden, J. A. Well posed non-orthogonal FDTD methods. *IEEE APS Int. Symposium 1*, 1 (June 1998), 596 – 599.

[26] Goubau, G. Multi-element monopole antennas. *Proc. Workshop on Electrically Small Antennas -* (May 1976), 63 – 67.

[27] Grieg, D., and Engelmann, H. Microstrip Ű A New Transmission Technique for the Kilomegacycle Range. *Proc. IRE 40* (Dec. 1952), 1651 – 1657.

[28] Gupta, P., and Kumar, P. R. The capacity of wireless networks. *Information Theory, IEEE Trans. 46*, 2 (March 2000), 388 – 404.

[29] Gutton, H., and Baissinot, G. Flat Aerial for Ultra High Frequencies. *French Patent no. 703113* (1955), –.

[30] Hammerstad, E. O. Equations for Microstrip Circuit Design. *Proc. Fifth European Microwave Conf.* (Sept. 1975), 268 – 272.

[31] Hammerstad, E. O., and Jensen, O. Accurate Models for Microstrip Computer-Aided Design. *Microwave Symposium Digest, 1980 MTT-S Int. 80*, 1 (May 1980), 407 – 409.

[32] Haneishi, M., and Suzuki, Y. *Handbook of Microstrip Antennas*, vol. 1 of *IEE Electromagnetic Waves*. Peter Peregrinius, 1989, ch. 4, pp. 219 –274. Circular Polarisation and Bandwidth.

[33] Hannan, P. W. The Ultimate Decay of Mutual Coupling in a Planar Array Antenna. *IEEE Trans. Antennas Propagat. 14* (March 1966), 246 – 248.

[34] Hansen, W. W., and Woodyard, I. R. A New Principle in Directional Antenna Design. *Proc. IRE 26*, 3 (March 1938), 333 – 345.

[35] Harrington, R. F. Effect of Antenna Size on Gain, Bandwidth, and Efficiency. *J. Research NBS 64D* (Jan. 1960), 1 – 12.

[36] Harrington, R. F. *Field Computation by Moment Method*. Macmillan, New York, 1968.

[37] Harrington, R. F. *Time Harmonic Electromagnetic Fields*. IEEE Press Wiley Interscience, New York, N.Y., 2001.

[38] Harrington, R. F. *Introduction to Electromagnetic Engineering*. Dover Publications, Inc. NY, 2003.

[39] Hori, T., Terada, N., and Kagoshima, K. Electronically Steerable spherical array antenna for mobile earth station. *IEE Conf . on Ant. and Prop. ICAP 87 York* (March 30 - Apr. 2 1987), 55 – 58.

[40] Horner, F. Scattering of Radio Waves by Metal Wires and Sheets. *Proc. of the IEE 96*, Part III (1949), 333 – 339.

[41] Howeth, S. L. History of Communications - Electronics in the "United States Navy". *Bureau of Ships and Office of Naval History 64-62870, Government Printing Office, Washington* - (1963), 15 – 23.

[42] Huang, J. The Finite Ground Plane Effect on the Microstrip Antenna Radiation Patterns. *IEEE Trans. Antennas Propagat. 31*, 7 (July 1983), 649 – 653.

[43] Huber, M., v[on] d[er] Mark, S., Angwafo, N., and Böck, G. System Architecture for Low Power 24 GHz Front-End. *Frequenz -Zeitschrift für Telekommunikation 58*, 58 (March/April 2004), 74 – 79.

[44] Huber, M., von der Mark, S., Angwafo, N., and Boeck, G. Ultra low power wakeup circuits for pico cell networks, a conceptional view. *Technical Report of the 1st European Workshop on Wireless Sensor Networks (EWSN)* (Jan. 2004), 30 – 32.

[45] IEEE. Grand Challenges of Electrotechnology for the Twenty-first Century. The New Technology Directions Committee: `www.hitl.washington.edu/publications/p-95-17/p-95-17.pdf`.

[46] Ito, K., Teshirogi, T., and Nishimura, S. *Handbook of Microstrip Antennas*, vol. 1 of *IEE Electromagnetic Waves*. Peter Peregrinius, 1989.

[47] James, J., and Hall, P., Eds. *Handbook of Microstrip Antennas*. IEE Electromagnetic Waves. Peter Peregrinius, 1989.

[48] Keller, J. B. Geometrical theory of diffraction. *J. Opt. Soc. Amer. 52* (1962), 116 – 130.

[49] King, R. W. *Antenna Theory*, vol. 7 of *Inter-University Electronics Series*. McGraw-Hill Book Company, 1969.

[50] Kishk, A. A., and Shafai, L. Effect of various Parameters of Circular Microstrip Antennas on their radiation efficiency and the mode excitation. *IEEE Trans. on Antennas and Propagat. 34* (Aug. 1986), 969 – 977.

[51] Kline, M. An asymptotic solution of Maxwell's equations. *Commun. Pure Appl. Math. 4* (1951), 225 – 262.

[52] Kohno, R., Meidan, R., and Milstein, L. B. Spread spectrum access methods for wireless communications. *IEEE Communications Magazine 33*, 1 (Jan. 1995), 58 – 67.

[53] Kong, J. A. *The Electrical Engineering Handbook*. CRC Press LLC, Boca Raton, 2000, ch. 35 Electromagnetic Fields, pp. 930 – 938.

[54] Korn, G. A., and Korn, T. M. *Mathematical Handbook for Scientists and Engineers: Definitions, Theorems, and Formulas for Reference and Review*. Dover Publications, Inc. Mineola N.Y., 2000.

[55] Kouyoumjian, R. G., and Pathak, P. H. A Uniform Geometrical Theory of Diffraction for an Edge in a Perfectly Conducting Surface. *Proc. IEEE 62*, 11 (Nov. 1974), 1448 –1461.

[56] Kraus, J. D., and Marhefka, R. J. *Antennas: For All Applications*, 3rd ed. McGraw-Hill, New York, 2002.

[57] Kunz, K. S., and Luebbers, R. J. *The Finite Difference Time Domain Method for Electromagnetics*. CRC Press LLC, Boca Raton, 1993.

[58] Kurokawa, K. The Expansions of Electromagnetic Fields in Cavities. *IRE Trans. Microwave Theory Tech. 1* (April 1958), 178 – 187.

[59] Kwankam, S. Y., and Ningo, N. N. Information Technology in Africa A Proactive Approach and the Prospects of Leapfrogging Decades in the Development Process. `http://www.isoc.org/isoc/whatis/conferences/inet/97/proceedings/B7/B7_1.HTM`.

[60] Law, P. E. *Shipboard Antennas*, 2nd ed. Artech House Publishers, April 1986.

[61] Lo, Y. T., Solomon, D., and Richards, W. F. Theory and Experiment on Microstrip Antennas. *IEEE Trans. Antennas Propagat. 27*, 3 (March 1979), 137 – 145.

[62] Marcuvitz, N. Guided Wave Concept in Electromagnetic Theory. *IRE Trans. Antennas Propagat. 3* (Aug. 1952), 231 – 239.

[63] Maxwell, J. C. A Dynamical Theory of the Electromagnetic Field. *Phil. Trans. Royal Society (London) 155* (1865), 459 – 512.

[64] Maxwell, J. C. *A Treatise on Electricity and Magnetism*. Dover Publications, Inc., New York, NY, 1954.

[65] McLean, J. S. A Re-Examination of the Fundamental Limits on the Radiation Q of Electrically Small Antennas. *IEEE Trans. Antennas Propagat. 44*, 5 (May 1996), 672 – 672.

[66] Mönich, G. Handformeln zur Erfassung radialsymmetrisch rückstrahlender Streukörper im elektromagnetischen Wellenfeld. *Nachrichten Elektronik 6* (1980).

[67] Mönich, G., Angwafo, N., and Böck, G. A Concept for Wattless Reception in Wireless Communication between Pico Cells. *Int. ITG Conf. on Antennas 178* (Sept. 2003), 21 – 24.

[68] Munson, R. E. Conformal Microstrip Antennas and Microstrip Phased Arrays. *IEEE Trans. Antennas Propagat. 22*, 1 (Jan. 1975), 74 – 78.

[69] Mur, G. Absorbing boundary condition for the finite-difference approximation of the time-domain electromagnetic-field equations. *IEEE Trans. Electromag. Compat 23*, 4 (Nov. 1981), 377 – 382.

[70] Nishizawa, S., Angwafo, N., Ruoss, H.-O., Spreitzer, W., Landstorfer, F., and Hashimoto, O. Calculation of current densities induced in an anatomical model of the human body caused by emission from household appliances in the low frequency range. In *6th Int. Congress of the European Bioelectromagnetics Association* (Nov. 2003), vol. 11, EBEA, p. 75.

[71] Noam, E. M. An unfettered internet? keep dreaming. The New York Times, July 1997. Section A: Page 27.

[72] Peercy, P. The Drive to Miniaturization. *Nature 406* (Aug. 2000), 1024 – 1026.

[73] Perlmutter, P., Shtrikman, S., and Treves, D. Electric surface current model for the analysis of a microstrip rectangular element. *APS Int. Symposium 22* (June 1984), 577 – 580.

[74] Pozar, D. M. Microstrip Antenna Aperture-coupled to a Microstripline. *Electron. Lett. 21*, 2 (Jan. 1985), 49 – 50.

[75] Pozar, D. M. *Handbook of Microstrip Antennas*. No. 28 in IEE Electromagnetic Waves Series. Peter Peregrinus Ltd. London, 1989, ch. 12 Analysis and design considerations for phased-array antennas, pp. 693 – 753.

[76] Pozar, D. M. Microstrip Antennas. *Proc. IEEE 80* (Jan. 1992), 79 – 91.

[77] Pucel, R. A., Massé, D. J., and Hartwig, C. P. Losses in Microstrip. *IEEE Trans. on MTT 16* (June 1968), 342 – 350.

[78] Rappaport, T. S. *Wireless Communications: Principles and Practice*, 1st ed. IEEE Press Piscataway, NJ, 1996.

[79] Richards, W. F., Lo, Y. T., and Harrison, D. D. An Improved Theory for Microstrip Antennas and Applications. *IEEE Trans. Antennas Propagat. 29*, 1 (Jan. 1981), 38 – 46.

[80] Rogers Corporation. How is the dielectric constant of the different high frequency materials affected by changes in temperature? `http://www.rogerscorporation.com/mwu/tip13.htm`, Advanced Circuit Materials Division.

[81] Rudge, A., Milne, K., Oliver, A., and Knight, P. *Handbook of Antenna Design*. IEE Peter Peregrinus, 1982.

[82] Schantz, H. G. A brief history of UWB antennas. *IEEE Conf. on Ultra Wideband Systems and Technologies* (Nov. 2003), 209 – 213.

[83] Schelkunoff, S. A. *Electromagnetic Waves*. D. Van Nostrand Company, Inc., 1951.

[84] Schelkunoff, S. A. Microwaves and Mathematics. *IRE Trans. on MTT* (1957), 173.

[85] Schneider, M. V. Microstrip Dispersion. *Proc. IEEE 60* (Jan. 1972), 144 – 146.

[86] Schuhmann, R., and Weiland, T. A Stable Interpolation Technique for FDTD on Non-Orthogonal Grids. *Int. J. of Numerical Modelling: Electronic Networks, Devices and Fields 11*, 6 (Nov. – Dec. 1998), 299 – 306.

[87] Schuhmann, R., and Weiland, T. Conservation of Discrete Energy and Related Laws in the Finite Integration Technique. *Progress In Electromagnetics Research 32* (2001), 301 – 316.

[88] Schurgers, C., Raghunathan, V., and Srivastava, M. B. Power Management for Energy-Aware Communication Systems. *ACM Trans. on Embedded Computing Systems 2*, 3 (Aug. 2003), 431 – 447.

[89] Schwinger, J. S., Lester L. DeRaad, J., Milton, K. A., and yang Tsai, W. *Classical Electrodynamics*. Perseus books, Massachusetts, 1998.

[90] Shannon, C. A mathematical theory of communication. *Bell System Technical Journal 27* (July 1948), 379 – 623.

[91] Smith, H. K., and Mayes, P. E. Aperture Coupling to Increase the Bandwidth of Thin Cavity Antennas. *AP-S. Digest 2* (June 1989), 1138 – 1141.

[92] Stutzman, W. L., and Thiele, G. A. *Antenna Theory and Design*, 2nd ed. John Wiley and Sons, Inc., 1981.

[93] Taflove, A., and Hagness, S. C. *Computational Electrodynamics: The Finite-Difference Time-Domain Method*, 2nd ed. Artech House, Norwood, MA, 2000.

[94] Taga, T., and Tsunekawa, K. Performance analysis of a built-in planar inverted F antenna for 800 MHz band portable radio units. *IEEE J. on Selected Areas in Communications 5* (June 1987), 921 – 929.

[95] Teshirogi, T., Tanaka, M., and Chujo, W. Wideband Circularly Polarized array with Sequential Rotation. *Proc. ISAP, Tokyo Japan* (Aug. 1985), 117 – 120.

[96] The Economist. Mr. PC goes to Washington. print edition, May 2002. `http://www.economist.com/business/displayStory.cfm?story_id=1154551`.

[97] Toumpis, S., and Goldsmith, A. J. Capacity regions for wireless ad hoc networks. *Wireless Communications, IEEE Trans. 2*, 4 (July 2003), 736 – 748.

[98] Waterhouse, R. A Broadband Stacked Shorted Patch. *Electron. Lett. 35* (Jan. 1999), 98 – 100.

[99] Waterhouse, R., Targonski, S., and Kokotoff, D. Design and Performance of Small Printed Antennas. *IEEE Trans.Antennas and Propagat. 46* (Nov. 1998), 1629 – 1633.

[100] Weiland, T. A discretization method for the solution of maxwell's equations for six-component field. *Electronics and Communication, (AEU) 31* (1977), 116 – 120.

[101] Weiland, T. Time domain electromagnetic field computation with finite difference methods. *Int. J. of Numerical Modelling: Electronic Networks, Devices and Fields 9* (1996), 259 – 319.

[102] Wheeler, H. A. Fundamental Limitations of Small Antennas. *Proc. IEE 35* (Dec. 1947), 1479 – 1484.

[103] Wheeler, H. A. Transmission Line Properties of Parallel Strips Separated by a Dielectric Sheet. *IEEE Trans. on MTT MTT-13* (March 1965), 172 – 185.

[104] Wheeler, H. A. The grating-lobe series for the impedance variation in a planar phased-array antenna. *IEEE Trans. Antennas Propagat. 14* (Nov. 1966), 707 – 714.

[105] White, M. J., Yun, Z., and Iskander, M. F. A New 3-D FDTD Multigrid Technique with Dielectric Traverse Capabilities. *IEEE Trans. MTT 49*, 3 (March 2001), 422 – 430.

[106] Wong, K.-L., and Lin, Y.-F. Small broadband rectangular microstrip antenna with chip-resistor loading. *IEE Electron. Lett. 33*, 19 (Sept. 1997), 1593 Ű 1594.

[107] Yang, S. C. *CDMA RF System Engineering*. Artech House, Inc. Norwood, MA, 1998.

[108] Yaru, N. A Note on Super-Gain Arrays. *Proc. IRE 39* (1951), 1081 – 1085.

[109] Yee, K. S. Numerical Solution of Initial Boundary Value Problems Involving Maxwell's Equations in Isotropic Media. *IEEE Trans. Antennas Propagat. 14* (May 1966), 302 – 307.

[110] Zhao, L., and Cangellaris, A. C. GT-PML: Generalized Theory of Perfectly Matched Layers and Its Application to the Reflectionless Truncation of Finite-Difference Time-Domain Grids. *IEEE Trans. MTT 44*, 12 (Dec. 1996), 2555 – 2563.

[111] Zinke, O., and Brunswig, H. *Lehrbuch der Hochfrequenztechnik: Band I*. Springer Verlag, Berlin, 1986.